ADVANTICA
A Germanischer Lloyd Company

Report Number: R9247 *February 2009*

PROJECT #153L

THE REMAINING STRENGTH OF CORRODED LOW TOUGHNESS PIPE

Advantica Restricted

Restricted to :US Dept of Transportation ,PRCI & Advantica

Prepared for:

R Smith

US Dept of Transportation

Pipeline and Hazardous Materials Safety Administration

1200 New Jersey Avenue
SE Building, Second Floor
Washington DC 20590
USA

Prepared by:

M Martin, R M Andrews and V Chauhan

Advantica

Holywell Park
Ashby Road
Loughborough Leicestershire
LE11 3GR
United Kingdom

Tel: +44 (0)1509 282363
Fax: +44 (0)1509 283119

E-mail: vinod.chauhan@advanticagroup.com

Website: www.advanticagroup.com

Customer Reference: DTPH56-05-T0003 - Project 153

ISO 9001
FS 45127

This Report is protected by copyright and may not be reproduced in whole or in part by any means without the approval in writing of Advantica Ltd. No Person, other than the Customer for whom it has been prepared may place reliance on its contents and no duty of care is assumed by Advantica toward any Person other than the Customer.
This Report must be read in its entirety and is subject to any assumptions and qualifications expressed therein. Elements of this Report contain detailed technical data which is intended for analysis only by persons possessing requisite expertise in its subject matter.

Registered in England and Wales No. 3294136.
REGISTERED OFFICE: HOLYWELL PARK, NEW ASHBY ROAD, LOUGHBOROUGH, LEICESTERSHIRE, LE11 3GR, UK

REPORT ISSUE / AMENDMENT RECORD

Report Title: Project #153L The Remaining Strength of Corroded Low Toughness Pipe	
Report Number: R9247	**Project Title:** Project #153L The Remaining Strength of Corroded Low Toughness Pipe **Project SAP Code:** 1/12461

Amendment details

Issue	Description of Amendment	Originator/Author
1.0	Interim Report	M Martin
		R M Andrews
2.0	Report modified to address PRCI comments	M Martin
		R M Andrews
3.0	Report modified to address further PRCI comments	V Chauhan

Report approval

Issue	Checked by	Approved by	Date
1.0	R M Andrews	C Ward	Sept 2006
2.0	V Chauhan	P Ingham	June 2008
3.0	V Chauhan	P Ingham	February 2009

Previous issues of this document shall be destroyed or marked SUPERSEDED

Project Code: 1/12461

DISTRIBUTION

Name	Company
R Smith A Mayberry S Nanney J Merritt	**Error! Reference source not found.**
M Piazza D Johnson R Owen R Espiner	PRCI
I Wood B Dudley	Electricore, Inc.

DISCLAIMER

This report is furnished to the U.S. Department of Transportation (DOT), Electricore, Inc. (Electricore) and Pipeline Research Council International, Inc. (PRCI) under the terms of DOT contract DTPH56-05-T-0003 between DOT and Electricore, Electricore agreement DTPH56-05-T-0003 between Electricore and Advantica, Inc. (Advantica), and PRCI contract PR-273-0323 between PRCI and Advantica. The contents of this report are published as received from Advantica. The opinions, findings and conclusions expressed in this report are those of the authors and not necessarily those of DOT, Electricore or PRCI, including PRCI's member companies or their representatives. Publication of this report by Electricore or PRCI should not be considered an endorsement by Electricore, PRCI or Advantica, or the accuracy or validity of any opinions, findings or conclusions expressed herein.

In publishing this report, Electricore, PRCI and Advantica make no warranty or representation, expressed or implied, with respect to the accuracy, completeness, usefulness, or fitness for purpose of the information contained herein, or that the use of any information, method, process, or apparatus disclosed in this report may not infringe on privately owned rights. Electricore, PRCI and Advantica assume no liability with respect to the use of, or for damages resulting from the use of, any information method, process, or apparatus described in this report. The text of this publication, or any part thereof, may not be reproduced or transmitted in any form by any means, electronic or mechanical, including photocopying, recording, storage in an information retrieval system, or otherwise, without written approval of Electricore, Advantica and PRCI.

EXECUTIVE SUMMARY

Corrosion metal loss is one of the major damage mechanisms to transmission pipelines worldwide. The remaining strength of corroded pipe subjected to internal pressure loading has been extensively researched and guidelines for assessing corrosion are well defined. Methods including ASME B31G, Modified ASME B31G and RSTRENG and LPC have been developed, validated and matured to the extent that they are now incorporated in standards and regulatory requirements. However, these methods are based on the assumption that the pipe fails via a ductile mechanism, i.e., the line pipe material has sufficient toughness to prevent a toughness dependent failure. This limits the application of the existing methods to materials that have sufficient toughness.

It is possible that some older pipelines operate with the material in the ductile / brittle transition region of the Charpy transition curve, or even on the lower shelf. It is also possible that under fault conditions, a pipeline normally operating on the upper shelf could be temporarily in the transition region. In these circumstances, existing assessment criteria may be non-conservative. At present there are no rigorous criteria available for assessing corrosion defects in low toughness pipe.

Previous experimental work carried out by Advantica has tested a range of corrosion defect geometries in two low toughness materials. The results were inconclusive due to the limited number of tests carried out at each condition and the scatter found in the transition region. However, they suggested that existing assessment criteria may be applicable to some low toughness materials, and that the occurrence of brittle fracture was influenced by the defect geometry. The present project has extended the previous work using a modelling approach. This is based on the Beremin approach to brittle cleavage fracture. Comparison of the Beremin results with existing assessment methods allows an ‘effective’ transition temperature’ to be defined as the temperature at which current assessment methods such as LPC-1 are no longer conservative. The results suggest that, for the corrosion defects investigated, the effective transition temperature is sufficiently low that existing assessment methods will remain conservative.

CONTENTS

1 INTRODUCTION 1
2 BACKGROUND 2
3 APPROACH 2
4 NOMENCLATURE AND UNITS 4
5 THE BEREMIN APPROACH 5
6 MATERIAL PROPERTIES 6
7 NOTCHED TENSILE TESTS 9
8 DETERMINATION OF WEIBULL PARAMETERS 10
9 APPLICATION TO CORROSION DEFECTS 14
9.1 Corrosion defect geometries considered 15
9.2 FEA procedure 16
9.3 Post-processing procedure 21
10 PRINCIPAL RESULTS 22
10.1 Hoop Stress Temperature Transition Curves 22
10.2 Geometrical Dependence of Effective Transition Temperature 26
10.3 Development of Plasticity 30
11 DISCUSSION 34
11.1 Plasticity Development 34
11.2 Defect Geometry 37
11.3 Implications of Results 38
11.4 Complex loading and rate effects 38
12 CONCLUSIONS 40
13 RECOMMENDATIONS 40
14 ACKNOWLEDGEMENTS 41
15 REFERENCES 41
APPENDIX A LOW TEMPERATURE TEST PROGRAM A1
APPENDIX B TENSILE TEST SPECIMEN DETAILS B1
APPENDIX C DEFECT GEOMETRY SUMMARY C1
APPENDIX D WEIBULL DISTRIBUTION CALIBRATION DATA D1
APPENDIX E RING EXPANSION DEFECT RESULTS SUMMARY E1
APPENDIX F 5% / 95% FAILURE PROBABILITY GRAPHS F1
APPENDIX G PROCEDURE FLOWCHART G1
APPENDIX H THE MODIFIED ASME B31G AND LPC-1 METHODS H1

1 INTRODUCTION

The remaining strength of corroded pipe subjected to internal pressure loading has been extensively researched and guidelines for assessing volumetric corrosion defects are now well defined. Methods such as ASME B31G [1], RSTRENG [2][3] and LPC-1 [4] have been developed, validated and have matured to the extent that they are now incorporated in standards and regulatory requirements such as CFR 49 Parts 192 and 195. However, these methods are all based on the assumption that the pipe fails in a ductile manner. The test data used to validate the methods generally shows that the materials were on the upper shelf of the Charpy transition curve, where ductile behaviour is expected. In a few cases the material may have been in the upper part of the transition region, but the absorbed energy values were above typical acceptance levels in pressure vessel codes.

There are some pipelines, usually older, which operate with the material in the ductile / brittle transition region of the Charpy transition curve, or even on the lower shelf. It is also possible that under fault conditions, a pipeline which is normally operating on the upper shelf could be temporarily in the transition region. Under these conditions, the failure criteria which assume ductile behavior may not apply and could be non-conservative. At present there are no alternative criteria to use to assess corrosion defects in low toughness pipe.

Pipeline Research Council International, Inc (PRCI) project PR 273-0136 [10] investigated experimentally the failure pressures of corrosion defects in low toughness pipes at temperatures towards, or on, the lower shelf region of the Charpy transition curve. In this region the material is exhibiting predominantly brittle behaviour. These results showed that the predictions using methods such as the Modified ASME B31G method were generally acceptable even at the low toughness of the materials tested. However, the predictions were non-conservative in some cases, and the margins on other predictions were small. There was also a tendency for the failure mode to change to a brittle failure as the acuity of the defects increased.

Unfortunately, the costs involved in testing are such that the amount of data which could be generated by experiments is limited; for studies on low toughness material there is also a limit on the amount of material available for testing. The interpretation of the low toughness data is complicated by the increased scatter which is normally found in the transition region. The defect geometry would also be expected to influence the results, as it would be expected that the initiation of brittle fracture is more sensitive to local stresses than a ductile failure where local yielding relaxes locally high stresses. In addition, it is widely accepted that there is a statistical size effect in brittle failure, such that as the size of the component increases the probability of failure also increases. Thus it might be expected that a “large” corrosion feature would be at a greater risk of failure than a “small” feature with the same predicted failure pressure from current models because the large feature has a greater volume of high stressed material.

In order to resolve these issues and to generate additional predicted failures for other defect geometries, a modelling study has been undertaken in the present project. This has used the "local approach" to brittle fracture to predict failure probabilities for a range of corrosion defect geometries. The approach used is that of Beremin [5] where a failure probability is calculated from a "Weibull stress". The Weibull stress is defined by two parameters, obtained through a series of calibration tests on notched tensile specimens at low temperature to ensure that the cleavage mode is dominant in the failure mechanism. The Weibull stress and hence the failure probability is determined for the corroded pipe by processing the results of a non-linear finite element model of the defective pipe under increasing pressure. The failure probability is a function of the internal pressure, temperature and defect geometry.

2 BACKGROUND

It is important to establish material criteria for distinguishing toughness dependent and independent failure behaviour in corroded pipelines so that existing and possible new methods for low toughness pipes can be safely applied to ageing pipelines with reasonable confidence. The existing criteria and engineering methods for assessing corroded pipelines, including ASME B31G[1], Modified ASME B31G/RSTRENG[2][3] and LPC[4], are based on theoretical studies of toughness independent failure behavior of corroded linepipe and experimental testing on materials dominated by ductile, high toughness, linepipe.

The interpretation of the low toughness data is complicated by issues such as the influence of the defect geometry on the local stresses. It would be expected that the initiation of brittle fracture is more sensitive to local stresses than a ductile failure where local yielding relaxes locally high stresses. In addition, it is widely accepted that there is a statistical size effect in brittle failure, such that as the size of the component increases the probability of failure also increases. It follows that a larger corrosion feature would be expected to be at a greater risk of failure than a smaller feature with the same predicted failure pressure from current models because the large feature results in a greater volume of highly stressed material in the pipe wall. As a result a probabilistic approach, as presented in this report, is appropriate in the analysis of toughness dependent failures.

It should also be noted that the existing approaches are all based on burst tests and analysis carried out at low strain rates where rate effects would not have an effect. The existing codified approaches are also only able to predict the initiation of a failure, and cannot determine if the through-wall defect created by the failure will stay stable or extend to a greater length. These issues are discussed in more detail in Section 11.

3 APPROACH

This project provides an approach for removing the uncertainty in the use of existing methods for assessing corrosion defects in older, low toughness pipelines. A numerical method has been developed, based on the Beremin[5] local approach[5][6][7] to brittle

fracture in which the cumulative probability of cleavage failure is defined as a function of a "Weibull Stress". The Weibull stress characterizes the stress state in the loaded structure. The cumulative failure probability is defined by a two parameter Weibull distribution. Once obtained, this distribution uniquely characterizes the low toughness behavior of the material and can be used to determine the failure probability for any loaded structure constructed from the same material, at any temperature. The two Weibull parameters have been defined by undertaking a series of low temperature notched tensile tests and post processing the results in conjunction with the results from a non-linear finite element (FE) model of the test specimen.

Throughout this study, finite element geometry mesh and post processing has been carried out using MSC PATRAN[8] and finite element analysis has been carried out using ABAQUS/Standard[9]. The corrosion defects analyzed include notches, grooves, patches and slits of various depths machined in old low toughness linepipe material.

Non-linear FE models of various ring expansion tests and vessel specimens with machined corrosion defects from previous experimental test programmes have been constructed and analyzed in conjunction with a series of five additional low temperature ring expansion tests undertaken as part of this study. The test programmes were:

Test Program 1[10] – Investigation of:

(i) notch, groove and patch machined corrosion defects in ring expansion test specimens. Three test temperatures of –20°C (-4 °F), 0°C (+32 °F) and +20°C (+68 °F) for each defect geometry

(ii) notch corrosion defects in vessel specimens. Tested at ambient temperature of +9.5°C to +15°C (+49 °F to +59 °F).

All the materials tested in this programme had impact energies below 5 J (3.9 ft-lb) in a half sized specimen at 0 °C, and shear areas of less than 20% at this temperature.

Test Program 2[11] – Investigation of groove, patch and slit machined corrosion defects in ring expansion tests, test temperatures in the range -9.2 °C to –1.6 °C. This material was tested on the lower shelf, having less than 1 J absorbed energy and less than 5% shear area.

Test Program 3 – Investigation of notch corrosion defects in ring expansion tests, test temperatures of -20°C and -60°C. Five ring expansion tests were undertaken as part of this project with a lowest test temperature of –60°C. A description of the test configuration is provided in Reference [11].

A series of FE analyses was carried out for each geometry with the material stress-strain properties changed in each case to represent a range of operating temperatures between –60°C and +20°C. This approach allows the temperature dependent response, and hence a predicted transition curve, to be investigated for each defect. Beremin post processing of the temperature dependent FE results has allowed the cumulative failure probability to be obtained as a function of internal pressure and, for a

given failure probability, the maximum allowable pressure as a function of temperature. Comparison with existing assessment criteria allows an 'effective' transition temperature' to be defined as the temperature at which the existing method is no longer conservative. The effective transition temperature has been found to be dependent on defect geometry.

4 NOMENCLATURE AND UNITS

The work in this project was carried out in SI units, and has been reported in these units. The principal quantities used are listed below. Conversion factors for the units used are given below, and some conversions are given at key points in the text.

σ_1	Maximum principal stress	N/mm^2
σ_w	Weibull stress	N/mm^2
σ_u	Weibull distribution parameter	N/mm^2
$\sigma_{y0.2}$	0.2% yield strength	N/mm^2
σ_{uts}	Tensile strength	N/mm^2
$\bar{\sigma}_1$	Average maximum principal stress	N/mm^2
d	Defect depth	mm
D	Pipe diameter	mm
j	Element number	
k_t	Stress concentration factor	Dimensionless
L	Defect length	mm
m	Weibull distribution parameter	Dimensionless
P_f	Probability of brittle failure	%
t	Pipe wall thickness	mm
T_{tr}	Ductile / brittle transition temperature	°C
V_0	Characteristic material volume	mm^3
V_p	Plastic zone size	mm^3

ΔV_j	Elemental volume	mm^3

Useful conversions are:

1 ksi = 6.895 N/mm^2 °F = 9/5 * °C + 32

1 inch = 25.4 mm

5 THE BEREMIN APPROACH

The Beremin model[5], or local approach[5][6][7], to cleavage fracture, is a micro-mechanical model capable of predicting the brittle failure of a structure based on the concept of the weakest link. The Beremin model states that the cumulative probability of cleavage failure, for a particular magnitude of load applied to a structure, is provided by a two parameter Weibull statistical distribution, as demonstrated by Eq. (1).

$$Pf(\sigma_w) = 1 - \exp\left(-\left(\frac{\sigma_w}{\sigma_u}\right)^m\right) \qquad (1)$$

In Eq. (1), σ_w is the Weibull stress and σ_u and m are the Weibull parameters that are assumed to be uniquely characteristic of the material and independent of temperature. Parameter m controls the shape of the distribution; as m increases the distribution tends towards a step function. Parameter σ_u controls the position of the distribution in the σ_w axis.

The Weibull stress parameter, σ_w, is a function of the exponent m and represents a global or structure-wide parameter, characterizing the stress state in the loaded structure. For two different structures of the same material, loading producing an equal Weibull stress in the two structures indicates an equal probability of failure. The Weibull stress is defined by Eq. (2).

$$\sigma_w = \left[\frac{1}{V_0}\int_{V_P} \sigma_1^m dV_P\right]^{\frac{1}{m}} \qquad (2)$$

The integration of Eq. (2) is taken over the volume of the plastic zone V_p, usually associated with a stress raising feature such as a crack or corrosion defect. V_0 is an arbitrary material volume which is taken to be of the same scale of size as material grains, typically about $50^3 mm^3$ in steels. σ_1 is the maximum principal stress acting on the element volume dV_p.

Following calculation of the maximum principal stress using a finite element approach, the Weibull stress can be calculated using a discrete formulation of Eq. (2), as demonstrated by Eq. (3).

$$\sigma_w = \left[\sum_{j=1}^{n} \left(\sigma_{1,j} \right)^m \frac{\Delta V_j}{V_0} \right]^{\frac{1}{m}} \qquad (3)$$

Equation (3) is summed over n finite element integration stations within the instantaneous plastic zone. ΔV_j and $\sigma_{1,j}$ are the volume and maximum principal stress associated with integration station j.

In this project, the effects of load history have been accounted for in the calculation of Weibull stress by ensuring that at each point in the loading history the maximum value of stress experienced at all earlier points in the history is used in the calculation. This approach ensures that the probability of failure does not decrease as load increases. This approach is required to allow for the possibility that in some circumstances it is possible for certain geometries that local unloading occurs thus reducing the principal stresses in the plastic zone. Reducing the principal stresses would reduce the cumulative failure probability, but it is considered physically unrealistic for the failure probability to fall whilst the external load increases. By using the maximum stress value the contribution to the failure probability from the unloaded regions remains constant during the time it is unloaded.

A dedicated post processing routine has been developed as part of this project and used to determine the Weibull stress following finite element analysis by accessing the ABAQUS binary '.fil' file.

6 MATERIAL PROPERTIES

Geometrical and material properties of the vintage line-pipe used in these test programmes are summarized in Table 1, Table 2 and Table 3. Due to their age, the particular pipeline material grades were unknown – for comparison, the probable material grade properties are also listed.

Pipe ID	OD mm (in)	t mm (in)	Flattened Strap N/mm^2		E_{CVN} (half size specimen)	T_{tr} °C (°F)	X42 Comparison N/mm^2	
			$\sigma_{y0.2}$	σ_{uts}			$\sigma_{y0.2}$	σ_{uts}
HJKA	559 (22)	7.2 (0.28)	288	412	4 J at 0°C	37 (99)	290	414

Table 1 – Ring Expansion Test Material Properties

Pipe ID	OD mm (in)	t mm (in)	Flattened Strap N/mm^2		E_{CVN} (half size specimen)	T_{tr} °C (°F)	Grade B Comparison N/mm^2	
			$\sigma_{y0.2}$	σ_{uts}			$\sigma_{y0.2}$	σ_{uts}
HKR HLL*	559 (22)	7.2 (0.28)	267	399	4 J at 0°C	NA	241	414

Table 2 – Ring Expansion Test Material Properties

* Detailed material properties were not available for the HLL pipe material and therefore the HKR material properties have been used for all analysis work. Both materials were supplied by NV Nederlandse Gasunie (Gas Transport Services) and are believed to be from a similar source.

Pipe ID	OD mm (in)	t mm (in)	Flattened Strap N/mm^2		E_{CVN} (half size specimen)	T_{tr} °C (°F)	Grade B Comparison N/mm^2	
			$\sigma_{y0.2}$	σ_{uts}			$\sigma_{y0.2}$	σ_{uts}
HJKB	559 (22)	7.2 (0.28)	332	458	0.9J at 0°C	37 (99)	290	414

Table 3 – Vessel Burst Test Material Properties

To provide stress-strain curves for the subsequent analysis work, four waisted tensile specimens were machined from the HJKA pipe material identified in Table 1 in the transverse (hoop) orientation. The dimensions of the waisted tensile specimen gauge section were: 29.58 mm length, 6.575mm maximum nominal diameter, 4.575mm minimum nominal diameter with 45mm radius of curvature. The waisted tensile test specimen geometry is shown in Appendix B.

The specimens were tested to failure and the load and diametral contraction measured during the tests. Two monotonic tensile tests were carried out at –60°C and two at room temperature. The average true axial stress versus true axial strain characteristics were derived from the –60°C and room temperature tensile test results, as contained in Table 4 and illustrated in Figure 1.

Specimen	Test temperature (°C)	True stress (MPa)	Elastic true strain (mm/mm)	Plastic true strain (mm/mm)	Total true strain (mm/mm)
Average 5WR1E1 5WR1F1	Room temperature (approx. +20°C)	237.2	0.00115	0.00000	0.00115
		451.3	0.00218	0.10470	0.10688
		784.0	0.00379	0.80000	0.80379
Average 5WR1G1 5WR1H1	-60°C	444.5	0.00215	0.00000	0.00215
		717.3	0.00347	0.25277	0.25624
		932.5	0.00450	0.80000	0.80450

Table 4 – True Stress / True Strain Results from Tensile Tests

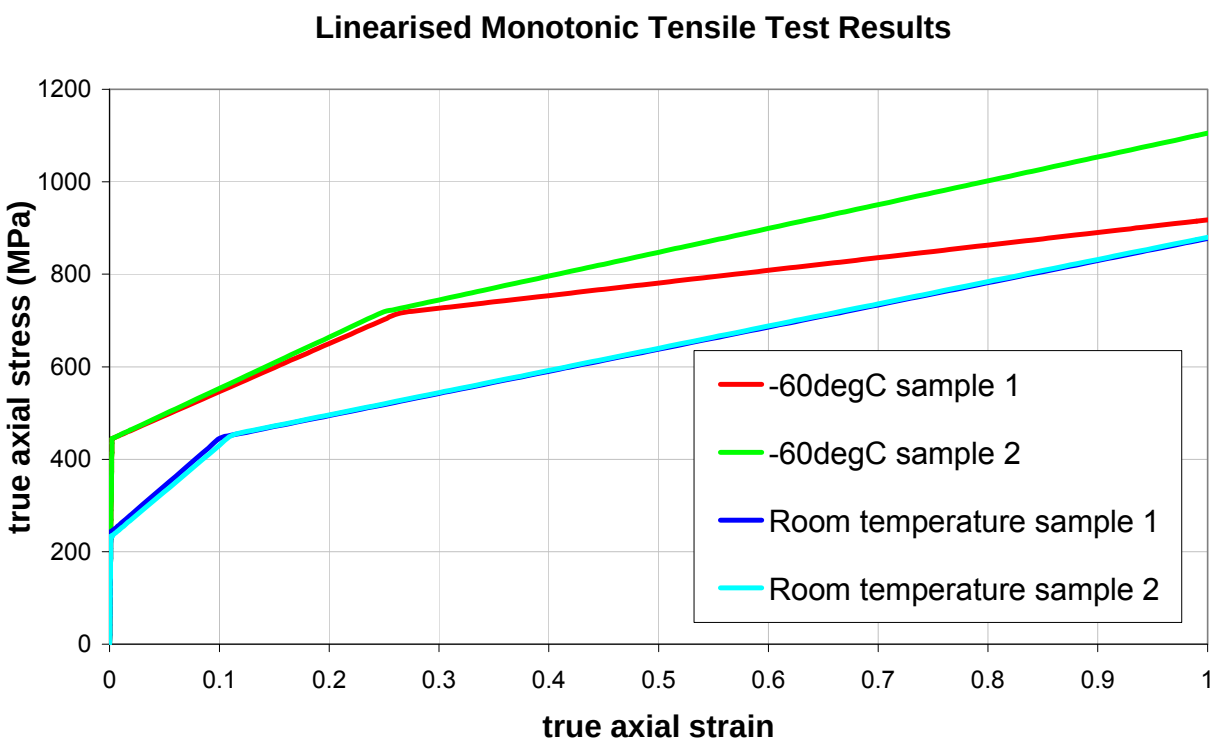

Figure 1 – Linearised True Stress / True Strain Monotonic Tensile Test Results

7 NOTCHED TENSILE TESTS

To enable calibration of the Weibull parameters specific to the HJKA low toughness material, a series of 26 notched tensile tests were carried out using the same material at a temperature of –60 °C to ensure brittle failure. The dimensions of the notched tensile specimen notch were: 1.25 mm full radius, 6.575 mm maximum nominal diameter and 4.575 mm minimum nominal diameter at the notch root. The notched tensile test specimen geometry is shown in Appendix B.

The specimens were tested to failure in a tensile test machine and the load and diametral contraction measured during the tests. Figure 2 shows the applied axial load versus diametral contraction (measured by a clip gauge) for a selection of the notched tensile tests and clearly displays a distribution in failure loads and strain to failure. The ranked numerical values of radial contraction of the notch root at failure for each of the 26 specimens are shown in Table 5.

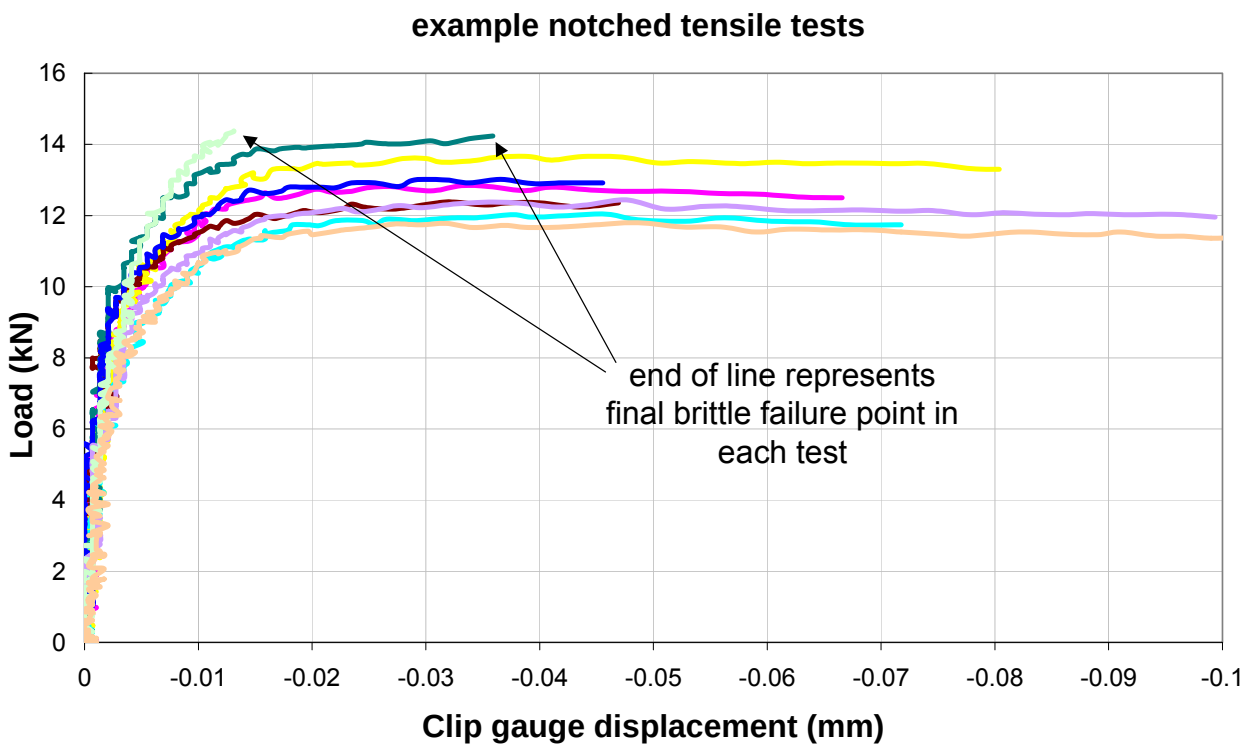

Figure 2 – -60°C Notched Tensile Tests, Variation in Load with Clip Gauge Displacement

Test Rank Position	Notch Root Diametral Reduction at Failure (mm)
1	0.00044
2	0.00283
3	0.00587
4	0.00603
5	0.00763
6	0.00784
7	0.00925
8	0.01000
9	0.01022
10	0.01261
11	0.01264
12	0.01315
13	0.01460
14	0.01569
15	0.01739
16	0.02074
17	0.02162
18	0.02208
19	0.02440
20	0.02440
21	0.02565
22	0.03668
23	0.09242
24	0.09459
25	0.09521
26	0.26419

Table 5 – Ranked Notch Diametral Reduction at Failure

8 DETERMINATION OF WEIBULL PARAMETERS

To derive the Weibull parameters from the notched tensile test data, a half symmetry axisymmetric finite element model of the specimen was constructed and meshed using MSC PATRAN [8]. The model was subsequently analysed using ABAQUS / Standard [9]. The model was loaded by applying a 50 step incremental axial displacement such that the maximum displacement achieved was in excess of the actual value experienced during the –60°C testing. The material stress-strain behaviour was specified using the data in Table 4. The axisymmetric mesh and contours of maximum principal stress at 30% of maximum load are shown in Figure 3 and Figure 4 respectively.

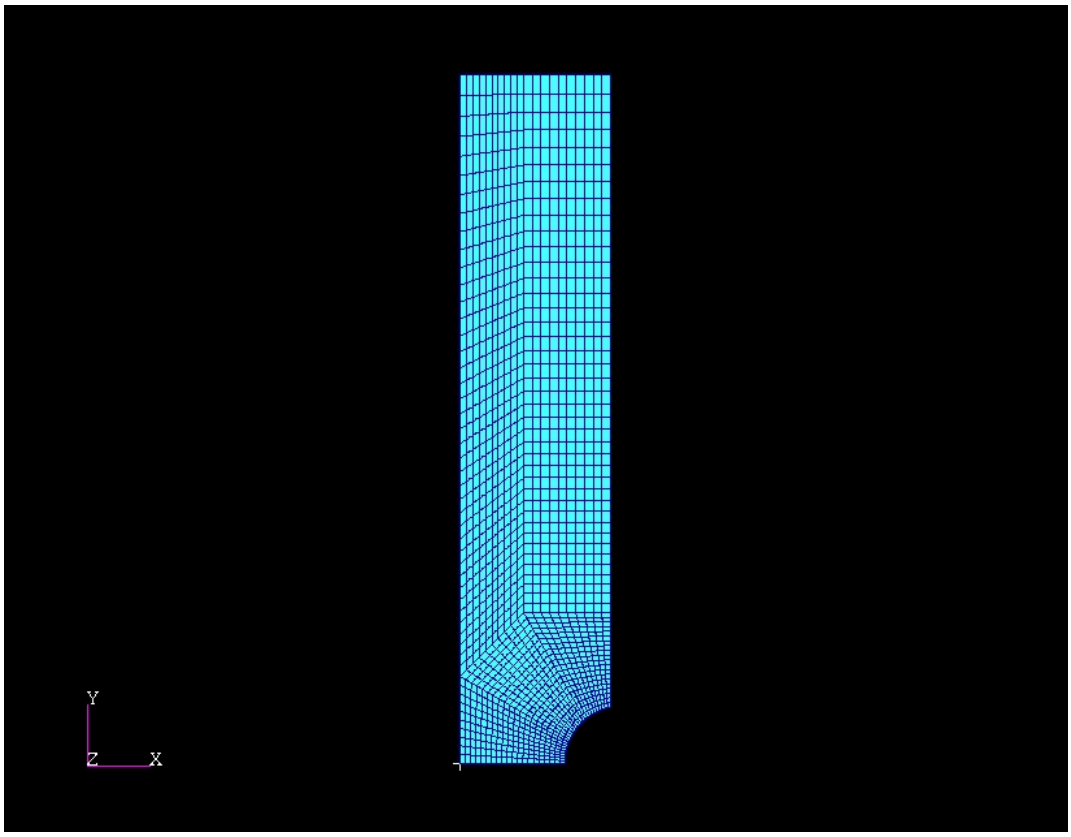

Figure 3 – Notched Tensile Axisymmetric Half Symmetry Mesh

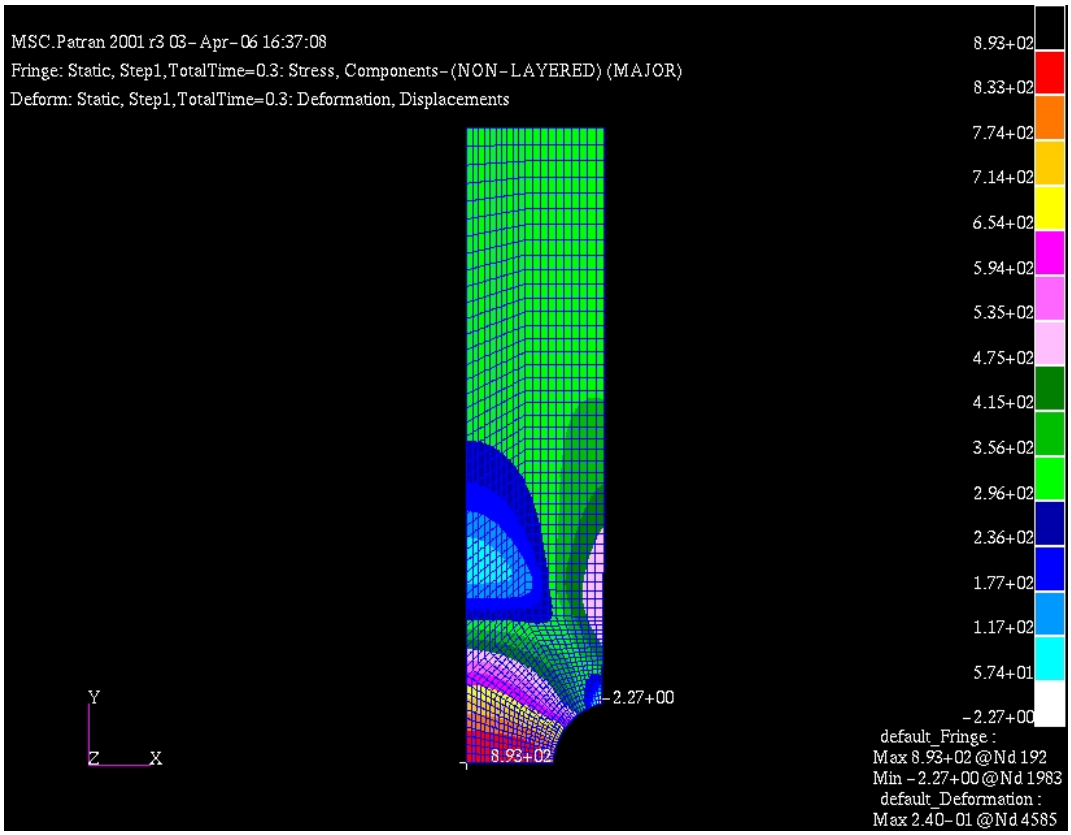

Figure 4 – Notched Tensile Specimen, Contours of Maximum Principal Stress at 30% Load

The following output data were requested from ABAQUS/Standard at each increment in the load history to enable calculation of the Weibull stress using Eq. (3).

i. Maximum principal stress for each element within the plastic zone

ii. Volume for each element within the plastic zone

In addition, the radial displacement at the notch root node was requested to provide a comparative 'linking parameter' with the experimental results. A dedicated ABAQUS/Standard processing routine has been developed to automate calculation of Weibull stress using Eq. (3) in conjunction with the FE output file. Using this routine to post-process the output from the axisymmetric notched tensile analysis results in the calculation of a Weibull stress value for a range of trial values of the parameter m at each load increment. The result is a table of Weibull stress values calculated at each load increment, for each trial value of m as shown in Table 6. The full results for all 50 load increments are provided in Appendix D.

At each load increment, the stress state and plastic zone is characterized by a value of Weibull stress, which is dependent on the exponent m. Further analysis is required to deduce the most appropriate value of m by considering the cumulative failure distribution to be approximated by a two parameter Weibull distribution defined by m and σ_u. The Weibull parameter m controls the gradient of the central section of the distribution. Increasing m increases the gradient of the central section and causes the low and high probability inflection points to tend towards a sharp corner. Weibull parameter σ_u shifts the distribution parallel to the σ_w axis and is equivalent to the value of σ_w at which the cumulative failure probability is equal to 63%.

Load inc.	Step Time	Notch Root (mm)	Weibull Stress				
			m=20	m=21	m=22	m=23	m=24
1	0.02	0.0008	790.5	776.0	763.1	751.4	741.0
2	0.04	0.0100	1087.0	1061.8	1039.4	1019.5	1001.7
3	0.06	0.0269	1186.7	1159.7	1135.8	1114.5	1095.4
4	0.08	0.0434	1216.0	1188.3	1163.9	1142.1	1122.6
-	-	-	-	-	-	-	-
-	-	-	-	-	-	-	-
50	1.00	0.7758	2162.2	2121.0	2084.4	2051.9	2022.8

Table 6 – Variation in Weibull Stress with m Resulting from Notched Tensile FEA, Selected Results

Using a Marquardt-Levenberg numerical curve fitting approach[12], the two Weibull parameters m and σ_u have been optimised to give best fit of the notched tensile experimental data points to the Weibull distribution. For each trial value of m and σ_u, the Weibull statistical distribution of failure probability is calculated using Eq. (1). Using the radial contraction of the notch root as the linking parameter between the experimental and finite element results, the Weibull stress for each experimental data point can be obtained, by interpolation if necessary, for each trial value of m using Table 6. Each experimental data point can then be positioned on the Weibull distribution using the calculated Weibull stress and cumulative failure ranking. This process has been implemented using a spreadsheet based iterative approach. The best fit values of m and σ_u were found to be as follows:

m = 22.6

σ_u = 1161.3

The resulting optimized Weibull distribution and experimental data points are shown in Figure 5. It can be observed that the resulting curve fit is good for the majority of the experimental data points, with the exception of a few points in the region of 5% and 95% failure probability. This may result from the assumption that the data will follow a Weibull distribution when a modified form of the distribution may be more appropriate.

Note that it is assumed in this project that the Weibull parameters are independent of temperature [5][6][7]. Thus the parameters derived above have been used to predict the probability of failure over the whole range of temperatures of interest. The effects of temperature have been included through the variation of the stress-strain curve with temperature, as discussed in Section 9.2.

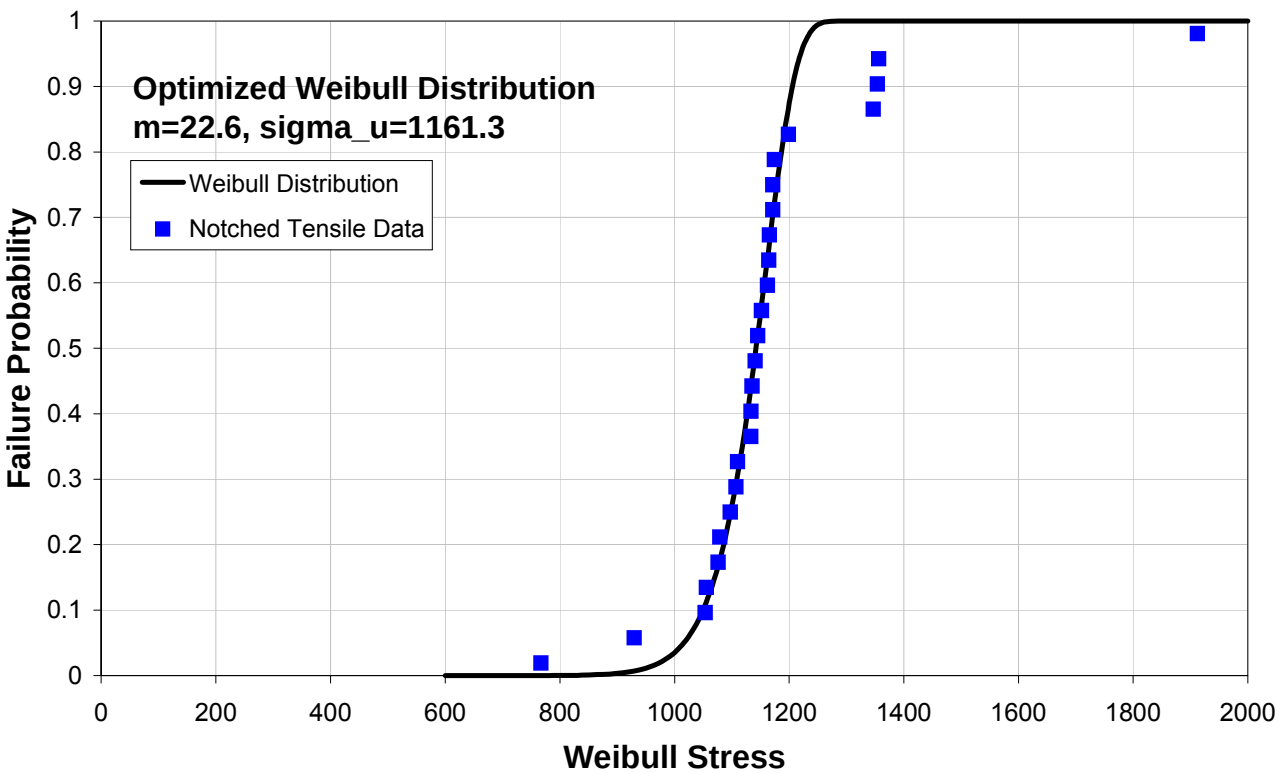

Figure 5 – Optimised Weibull Distribution, Variation in Cumulative Failure Probability with Weibull Stress

9 APPLICATION TO CORROSION DEFECTS

This section describes the application of the Beremin approach to a wide range of corrosion defects investigated in previous experimental programmes.

9.1 Corrosion defect geometries considered

Following calculation of Weibull parameters m and σ_u, the low toughness behaviour of the material is uniquely characterized and therefore the cumulative failure probability of any structure of the same material is governed by Eq. (1). It is therefore possible to construct a finite element model of any structure of the same material, calculate the Weibull stress for a given load condition and establish the resulting probability of failure. Using 2D / 3D non-linear finite element analysis, corrosion defects tested to failure in previous test programmes have been analysed and the results post-processed to provide failure probability predictions. Corrosion defects of the following types have been investigated:-

i. Notches (square and round cornered), patch, groove and slit defects of various depths in ring expansion test specimens
ii. Vessel defects of various depths and lengths

A definition of the various defect types is included in Table 7. Further details of the defect geometry are available in Appendix C.

Defect Type	Description
Notch	Constant notch root radius = 3mm, notch width = 6mm
Groove	Groove radius = groove depth
Patch	Patch width = constant
Square Groove	Constant notch width = 6mm
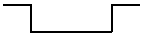 Square Patch	Patch width = constant
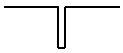 Slit	Slit width ~ 0.15mm

Table 7 – Defect Type Schematic Description

9.2 FEA procedure

The ring expansion specimens (HJKA, HKR and HLL) were modelled using a half symmetry 2D geometry with 8 node quadrilateral plane strain elements and loaded with internal pressure. The element depth was set to the length of the ring expansion specimens so that the volume of the plastic zone was correctly captured during post-processing to derive the Weibull stress. This approach represents an infinitely long defect in a buried pipe. The vessels (HJKB) were modelled using quarter symmetry 3D solid geometry with 20 node hexahedral elements and loaded with internal pressure. An end load was applied to the model to represent the effect of pressure loading on the vessel end closures. The load was applied incrementally up to a load 20% above the experimental failure load. In the case of the ring expansion geometry, the maximum load was applied in 50 increments and in the case of the vessels, the maximum load was applied in 10 increments.

Five separate non-linear analyses were undertaken for each geometry with elastic - plastic material properties selected to represent the following temperatures:

Temperature 1. –60 °C
Temperature 2. –40 °C

Temperature 3. –20 °C
Temperature 4. 0 °C
Temperature 5. +20 °C

A four stage linear model of the true stress / strain response was calculated for each temperature by interpolation between the waisted tensile results at –60 °C and room temperature. An example interpolated and linearized true stress / strain response at –20°C is shown in Figure 6. The numerical data generated by this interpolation of the true stress / true strain behaviour is shown in Table 8.

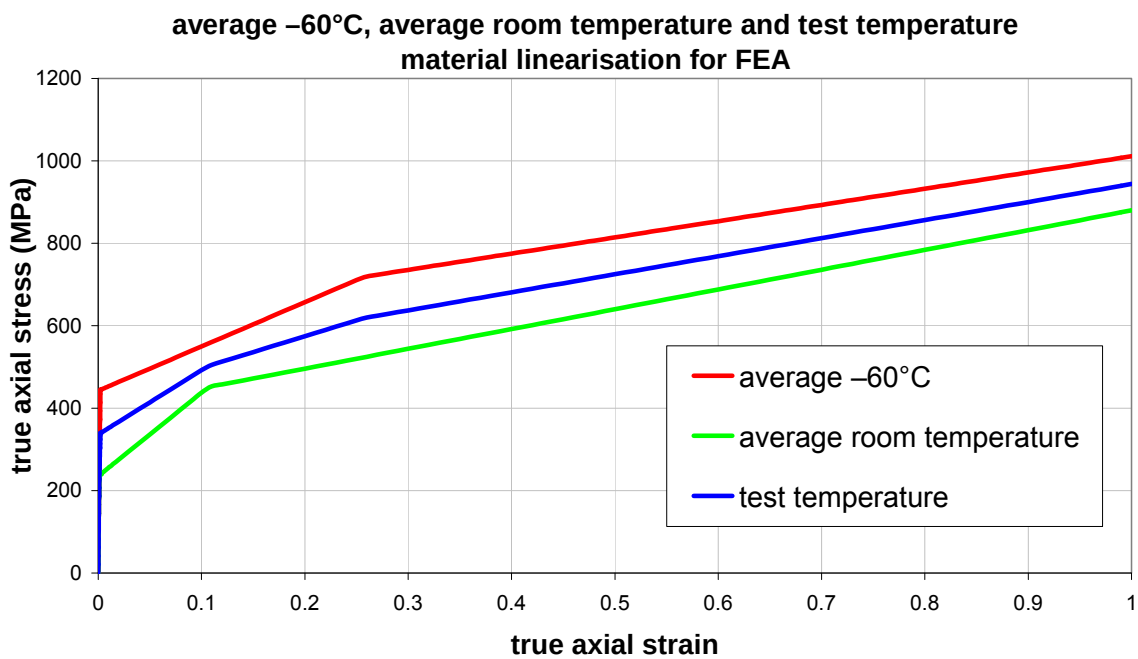

Figure 6 – Linearized True Stress / Strain Response at -20°C Used to Define FEA Material Model

Analysis temperature (°C)	True stress (MPa)	Elastic true strain (mm/mm)	Plastic true strain (mm/mm)	Total true strain (mm/mm)
-60°C	444.5	0.00215	0.00000	0.00215
	557.0	0.00270	0.10201	0.10471
	717.6	0.00347	0.25025	0.25372
	932.5	0.00451	0.79171	0.79622
-40°C	391.9	0.00189	0.00000	0.00189
	530.0	0.00256	0.10214	0.10470
	667.7	0.00323	0.25049	0.25372
	894.4	0.00432	0.79189	0.79621
-20°C	339.3	0.00164	0.00000	0.00164
	502.9	0.00243	0.10227	0.10470
	617.8	0.00299	0.25073	0.25372
	856.4	0.00414	0.79208	0.79622
0°C	286.7	0.00139	0.00000	0.00139
	475.8	0.00230	0.10240	0.10470
	567.9	0.00274	0.25097	0.25371
	818.3	0.00395	0.79226	0.79621
+20°C	234.1	0.00113	0.00000	0.00113
	448.7	0.00217	0.10253	0.10470
	517.0	0.00250	0.25121	0.25371
	780.2	0.00377	0.79244	0.79621

Table 8 – Numerical Data Required for True Stress / True Strain Interpolation

Figure 7 and Figure 8 show the half symmetry 2D mesh and maximum principal stress distribution at 30% of the final load for a 50% wall thickness notch defect in ring expansion specimen HJK R4 at -20ºC. Figure 9 and Figure 10 show the quarter symmetry 3D mesh and maximum principal stress at 30% of the final load for the 57% notch defect in vessel specimen HJK V1.

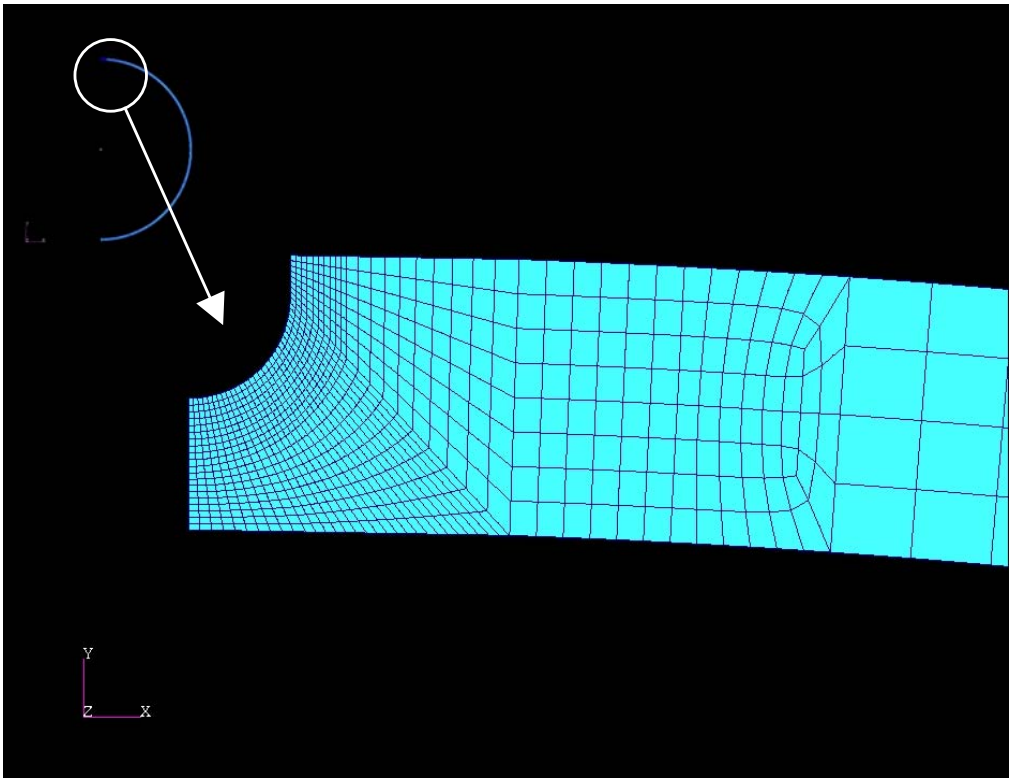

Figure 7 – HJK R4 50% Ring Expansion Notch Defect Half Symmetry Mesh, Local to Defect

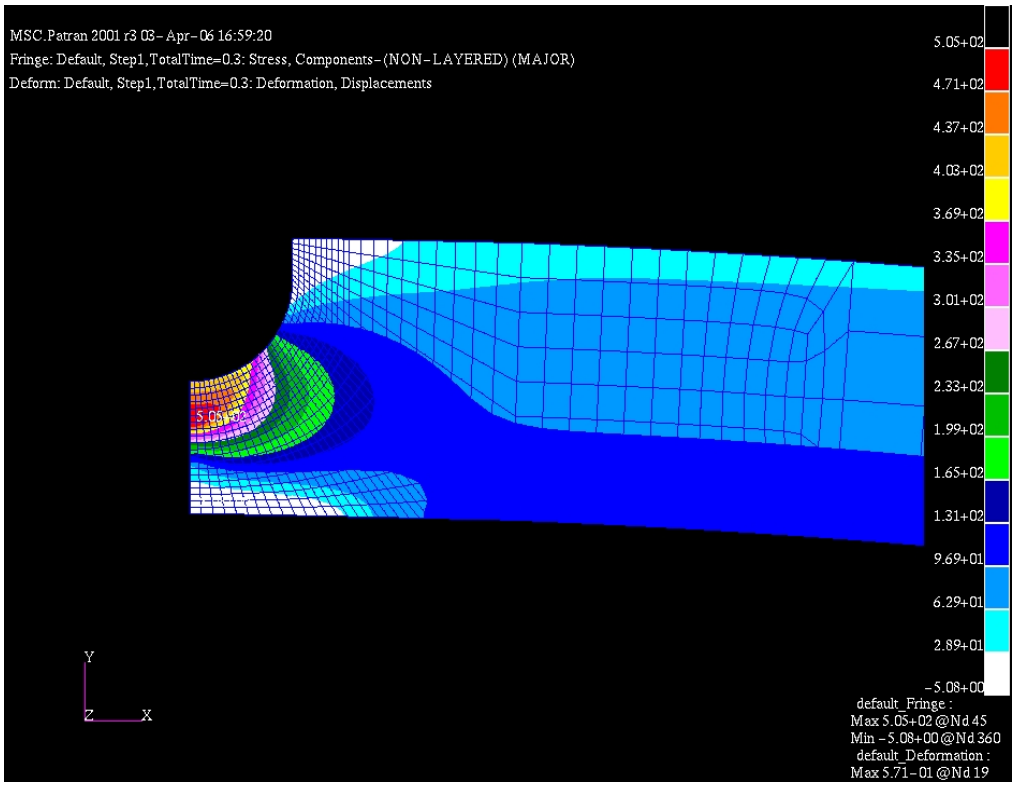

Figure 8 – HJK R4 50% Ring Expansion Notch Defect, Contours of Maximum Principal Stress

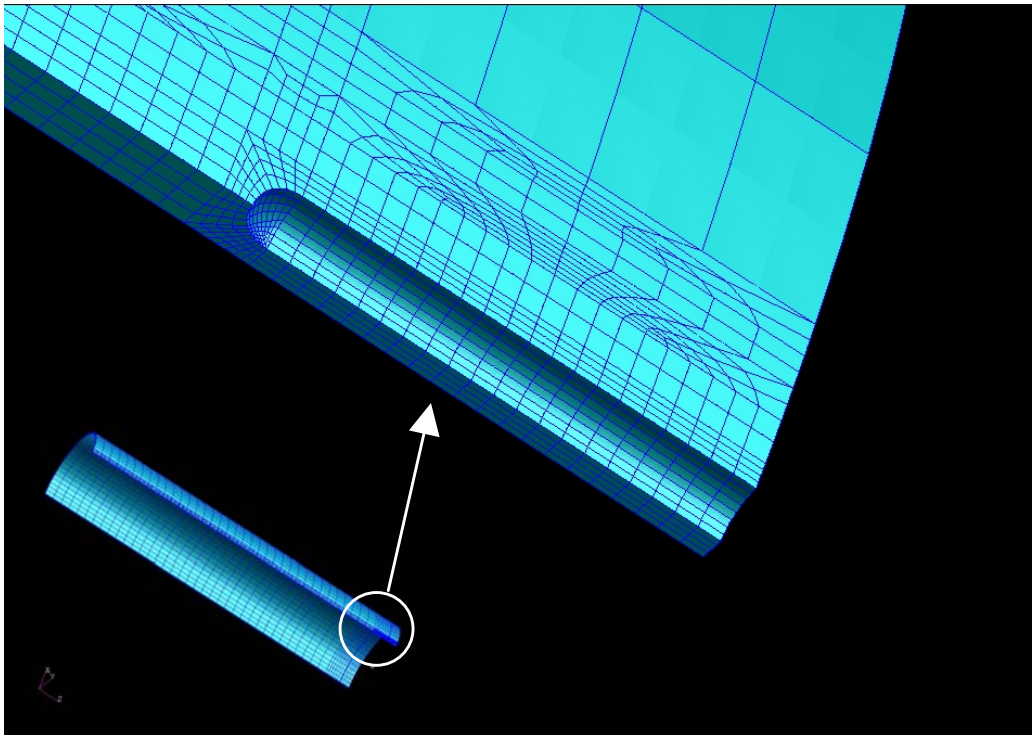

Figure 9 – HJK V1 Vessel Notch Defect Mesh, Local to Defect

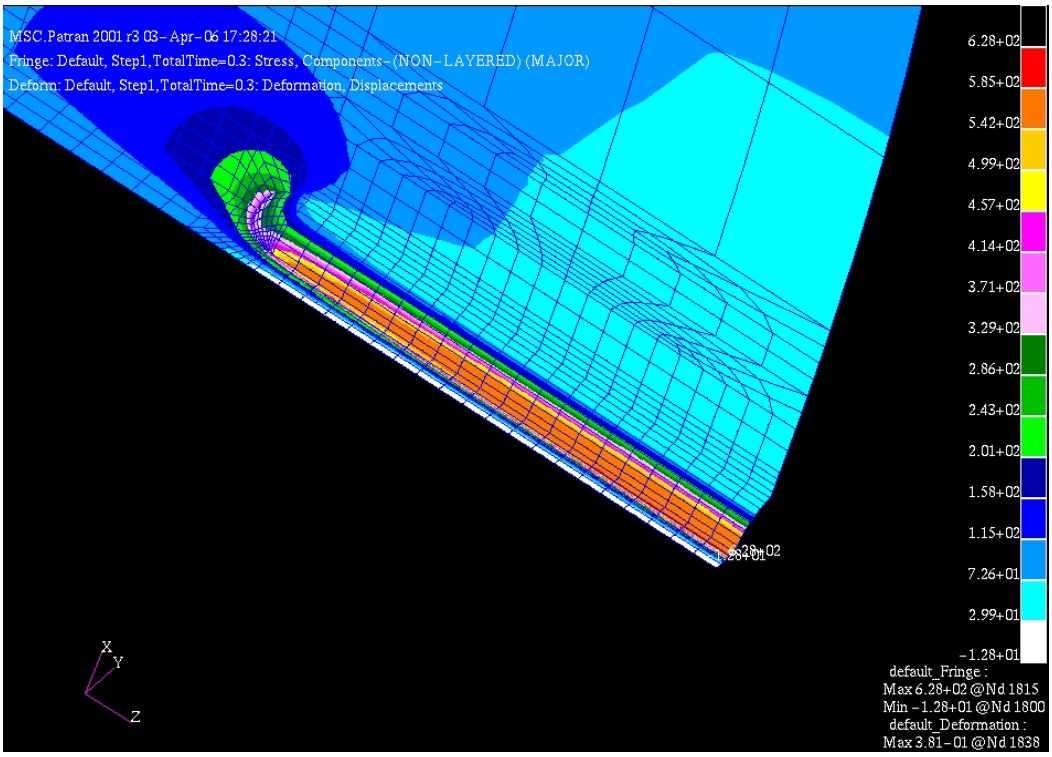

Figure 10 – HJK V1 Vessel Notch Defect, Contours of Maximum Principal Stress

9.3 Post-processing procedure

Following the finite element analysis of each geometry, the numerical data at each increment were post processed to give the variation in cumulative failure probability with internal pressure. As a result, the internal pressure and nominal hoop stress corresponding to failure probabilities of 5% and 95% have been obtained at each of the five temperatures analysed. The 5% failure probability to 95% failure probability Weibull stress range gives an indication of the sensitivity of the material to increasing load. The failure hoop stress can therefore be defined as a function of temperature and failure probability as shown in Eq. (4). An example plot of the change in failure hoop stress with temperature obtained for ring expansion test HJK R4 with 52% notch defect is shown in Figure 11. Similar plots for each of the defects analysed are contained in Appendix E. Sufficient load increments were required to ensure adequate resolution of the 5% and 95% probability loads.

$$\sigma_{h_fail} = f\left(T, p_{fail}\right) \qquad (4)$$

Comparison of the failure hoop stress results with predictions from standard corrosion defect assessment methods allows an 'effective transition temperature' to be defined as the temperature at which the existing method is no longer conservative. Effective transition temperatures were evaluated for 5% failure probability for each of the defect geometries analysed by comparison with the Modified ASME B31G and LPC-1 predictions. In the case of 52.4% notch specimen HJK R4, Figure 11 demonstrates the Modified ASME B31G and LPC-1 5% failure probability effective transition temperatures to be –27.6 °C and –25.3 °C respectively. The Modified ASME B31G and LPC-1 95% failure probability effective transition temperatures are lower, –56.3 °C and –58.0 °C respectively.

In the majority of cases, it was not possible to establish a 95% brittle failure probability effective transition temperature as no intersection between the Modified ASME B31G / LPC-1 lines and the 95% line occurred in the range –60°C to +20°C. As a result, in the cases in which no intersection with the 95% line occurs, the effective transition temperature can be assumed to be below -60°C. More details of the overall analysis and post processing procedure are provided in Appendix F. The Modified ASME B31G and LPC-1 calculations have been based on the measured yield and tensile strengths as the actual material grades are unknown. Further details of the Modified ASME B31G and LPC-1 methods, including failure pressure predictions, are included in Appendix G.

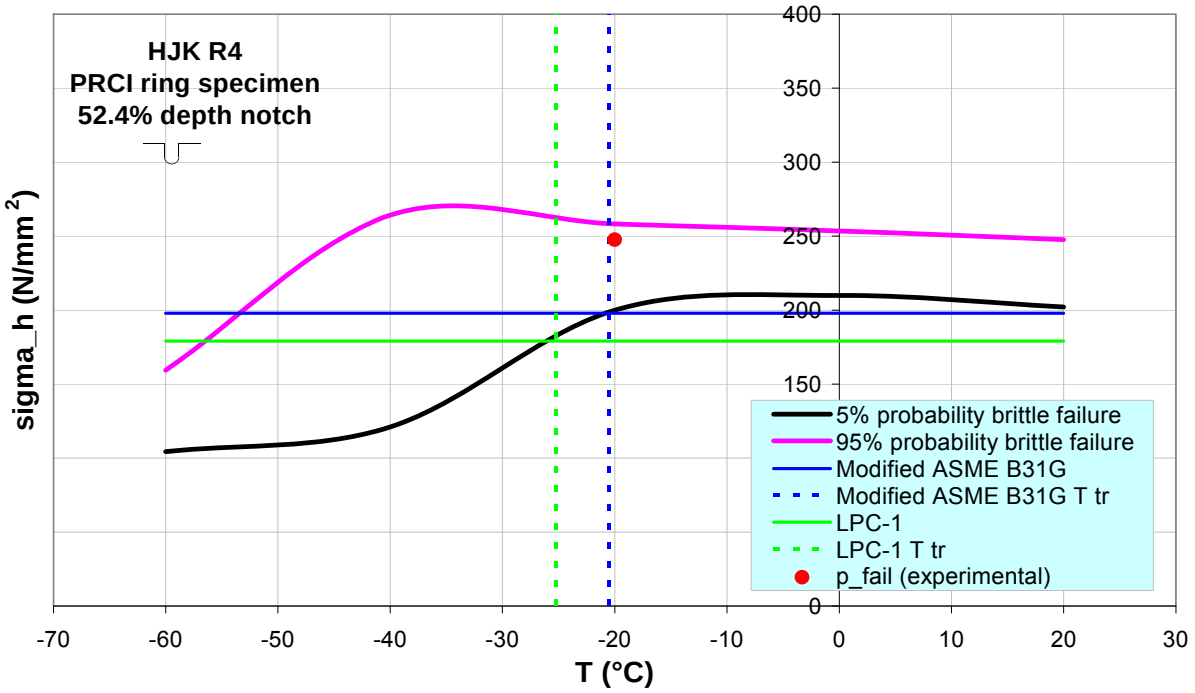

Figure 11 – HJK R4 50% Ring Expansion Notch Defect, Variation of Failure Hoop Stress with Temperature Based on 5% and 95% Failure Probability. Modified ASME B31G and LPC-1 Effective Transition Temperatures Shown in Blue and Green Respectively

10 PRINCIPAL RESULTS

10.1 Hoop Stress Temperature Transition Curves

Figure 12, Figure 13 and Figure 14 show the variation in failure hoop stress with temperature for the various HJKA ring expansion notch, groove and patch defects respectively. Figure 15 and Figure 16 show the variation in failure hoop stress for the HJKB vessel groove defects and HKR ring expansion defects respectively. Figure 17 shows the variation in failure hoop stress for the HLL ring expansion notch defects. An additional analysis was carried out for each of the vessel defects using a hypothetical defect length to investigate the influence of defect length on the failure behaviour. The original vessel defects tested experimentally were HJK V1 (57% notch × 125mm length) and HJK V2 (76% notch × 70mm length). To provide comparisons with the original vessel defects, modified versions of HJK V1 and HJK V2 were modelled and analysed with defect lengths of 70mm and 125mm respectively.

These curves are effective temperature transition curves, analogous to a Charpy transition curve. The general shape is similar to the classic Charpy transition curve, although the lower end of the corrosion defect curves does not drop down to zero failure

stress. In the Charpy curve the lower shelf can be at levels of essentially zero energy. This suggests that relatively smooth defects will have some residual strength even at very low temperatures. At the high temperature end, the predicted failure stresses fall with increasing temperature. This effect occurs in the Charpy transition for some materials, where it is usually attributed to the drop in yield strength with temperature. In the present case the reason for this phenomenon is not clear, but may be due to the lower post-yield strength of the material at higher temperature. This will allow more extensive yielding and so increase the volume of material in the plastic zone, and hence the amount of material contributing to the calculation of the Weibull stress. This increased volume of material may offset the slightly lower stresses due to the lower stress-strain curve.

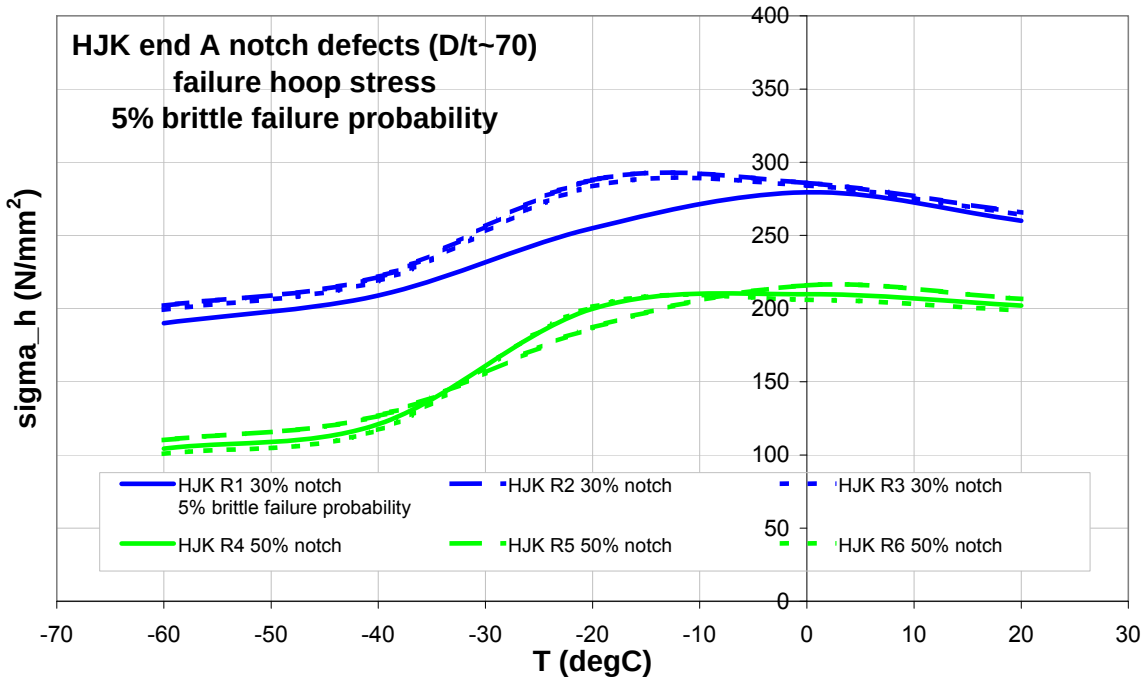

Figure 12 – HJKA Ring Expansion Notch Defects, Variation of Hoop Stress with Temperature

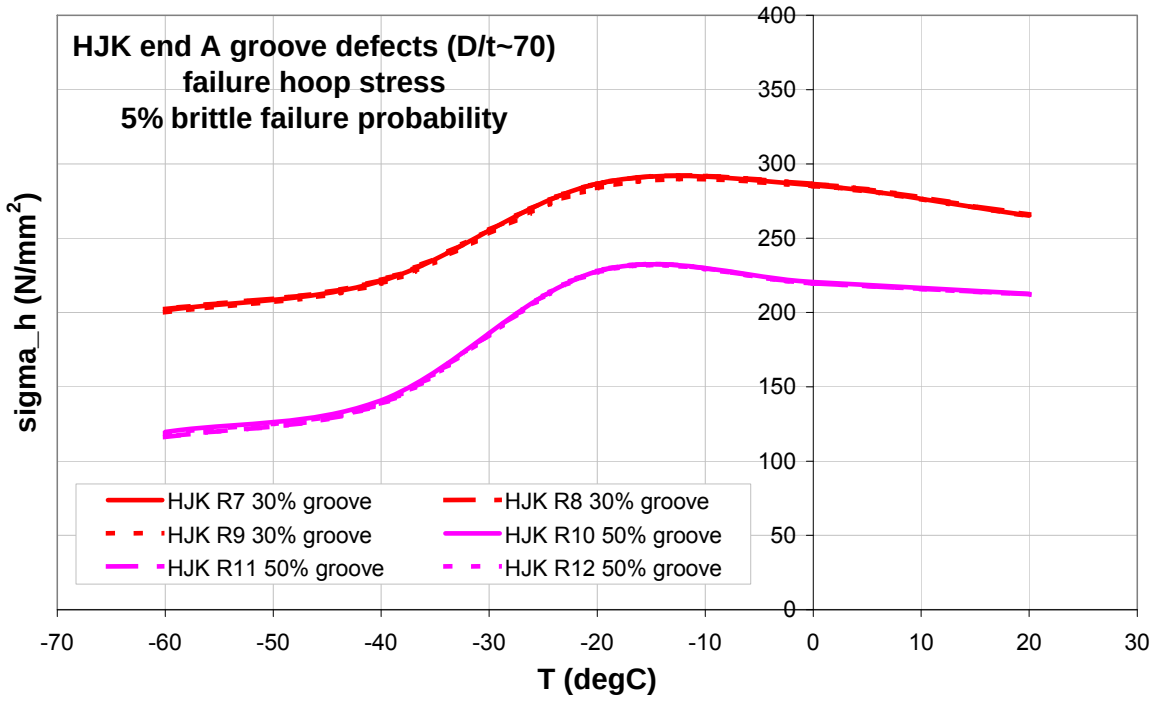

Figure 13 – HJKA Ring Expansion Groove Defects, Variation of Hoop Stress with Temperature

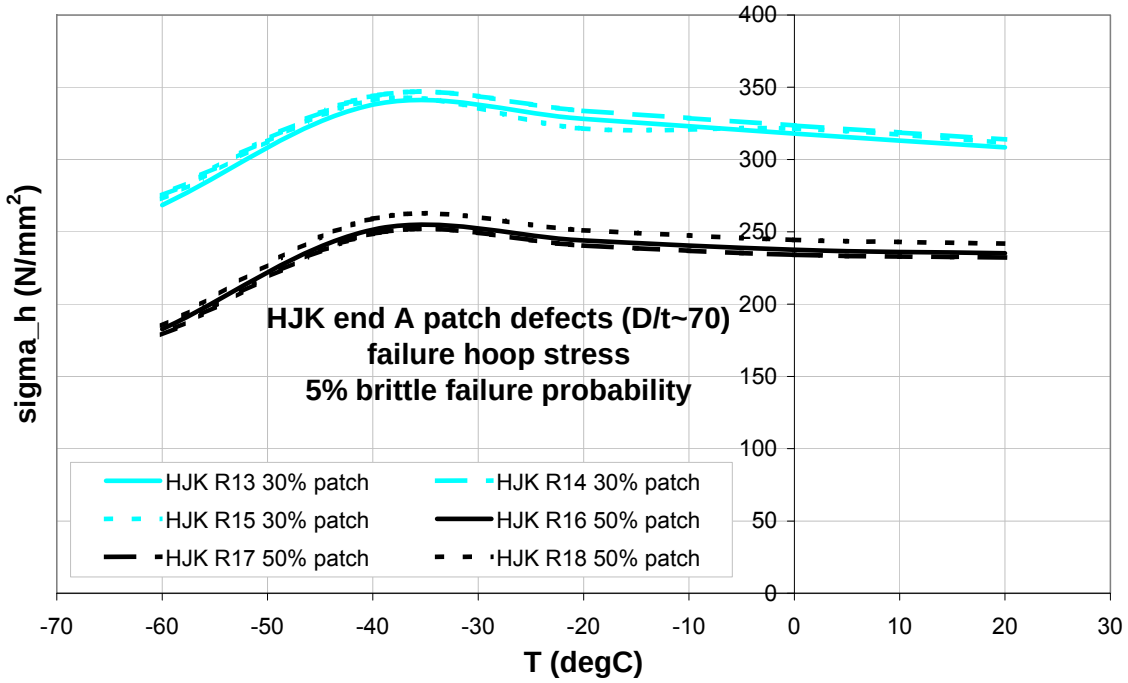

Figure 14 – HJKA Ring Expansion Patch Defects, Variation of Hoop Stress with Temperature

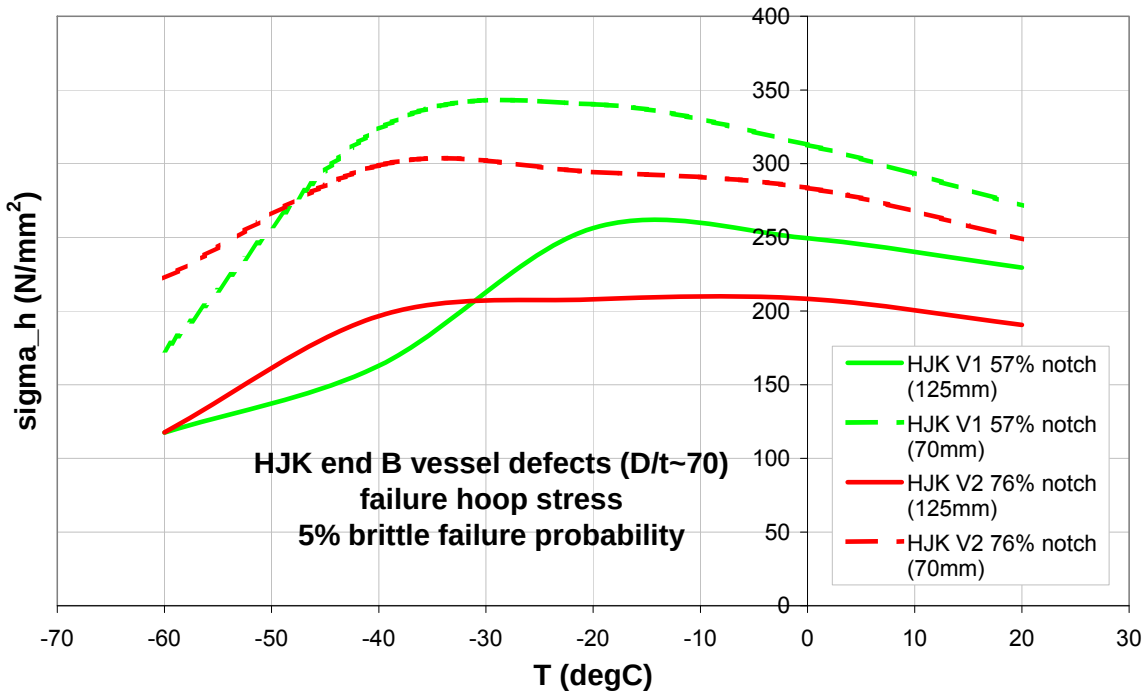

Figure 15 – HJKB Vessel Defects, Variation of Hoop Stress with Temperature

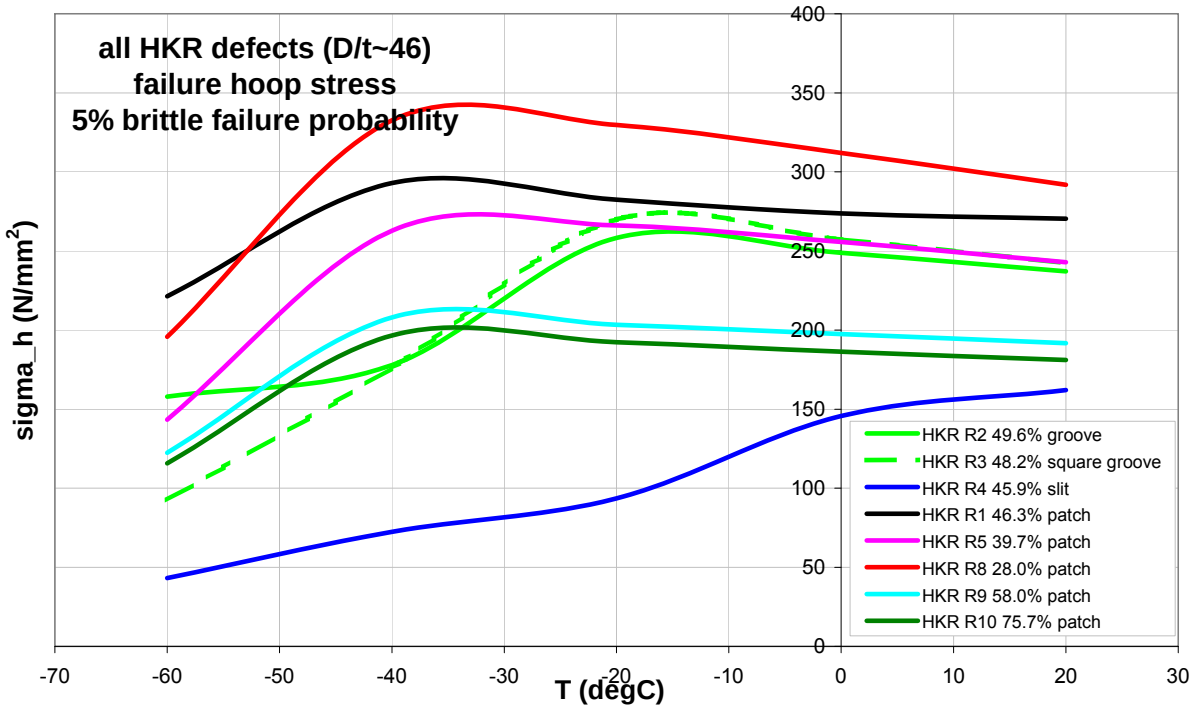

Figure 16 – HKR Ring Expansion Groove and Patch Defects, Variation of 5% Failure Probability Hoop Stress with Temperature

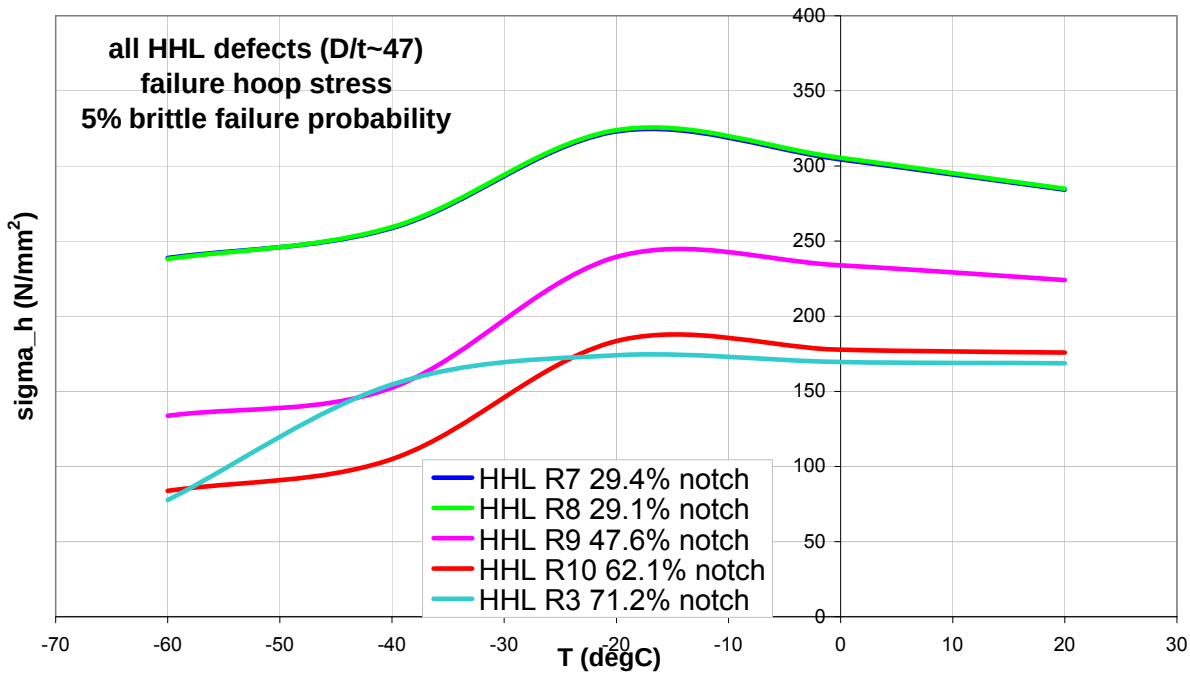

Figure 17 – HLL Ring Expansion Notch Defects, Variation of 5% Failure Probability Hoop Stress with Temperature

The 5% (and 95% where calculation was possible) brittle failure probability effective transition temperatures from each of the defects considered are listed in Appendix D. As expected, the sharper defect types such as notches and grooves display a higher effective transition temperature than the shallower patches. The slit defects have the highest transition temperature of all of the geometries analysed. For several geometries, mainly patches, the transition temperature is below –60°C, the lowest temperature considered. In these cases it is not possible to establish a value without extrapolation.

10.2 Geometrical Dependence of Effective Transition Temperature

To investigate in more detail the geometrical dependence of the 5% failure probability effective transition temperature predicted for each of the ring expansion defects, a stress concentration factor for each of the defect geometries has been calculated. The stress concentration factor was calculated from the ratio of maximum hoop stress at the defect, obtained from FEA, to the nominal hoop stress in the remaining ligament, as described by Eq. (5). The calculation is carried out at a load equivalent to 12% of the experimental burst pressure. The stress concentration factors for each of the ring expansion defects analysed are included in Appendix D.

$$k_t = \frac{2(t-d)\sigma_{h_\max}}{pD} \qquad (5)$$

The stress concentration factor was plotted against the Modified ASME B31G and LPC-1 effective transition temperatures, as shown in Figure 18 and Figure 19 respectively. Defects with a predicted effective transition temperature below -60 ºC are highlighted. As expected, the results show a general trend for an increase in the effective transition temperature as the stress concentration factor rises. It should be noted that a deeper defect does not correspond to a higher stress concentration factor in all cases, as demonstrated by HLL R10 (62.1% defect depth, k_t = 2.93) and HLL R3 (71.2% defect depth, k_t = 2.82). This can be explained by the loss of constraint provided by the material surrounding the defect as the remaining ligament becomes very thin. In this case plasticity can break through to internal face of the ring, allowing a transition to net section yielding of the remaining ligament. This is likely to limit the build up of stress compared with cases where the extent of plasticity is constrained by surrounding un-yielded material.

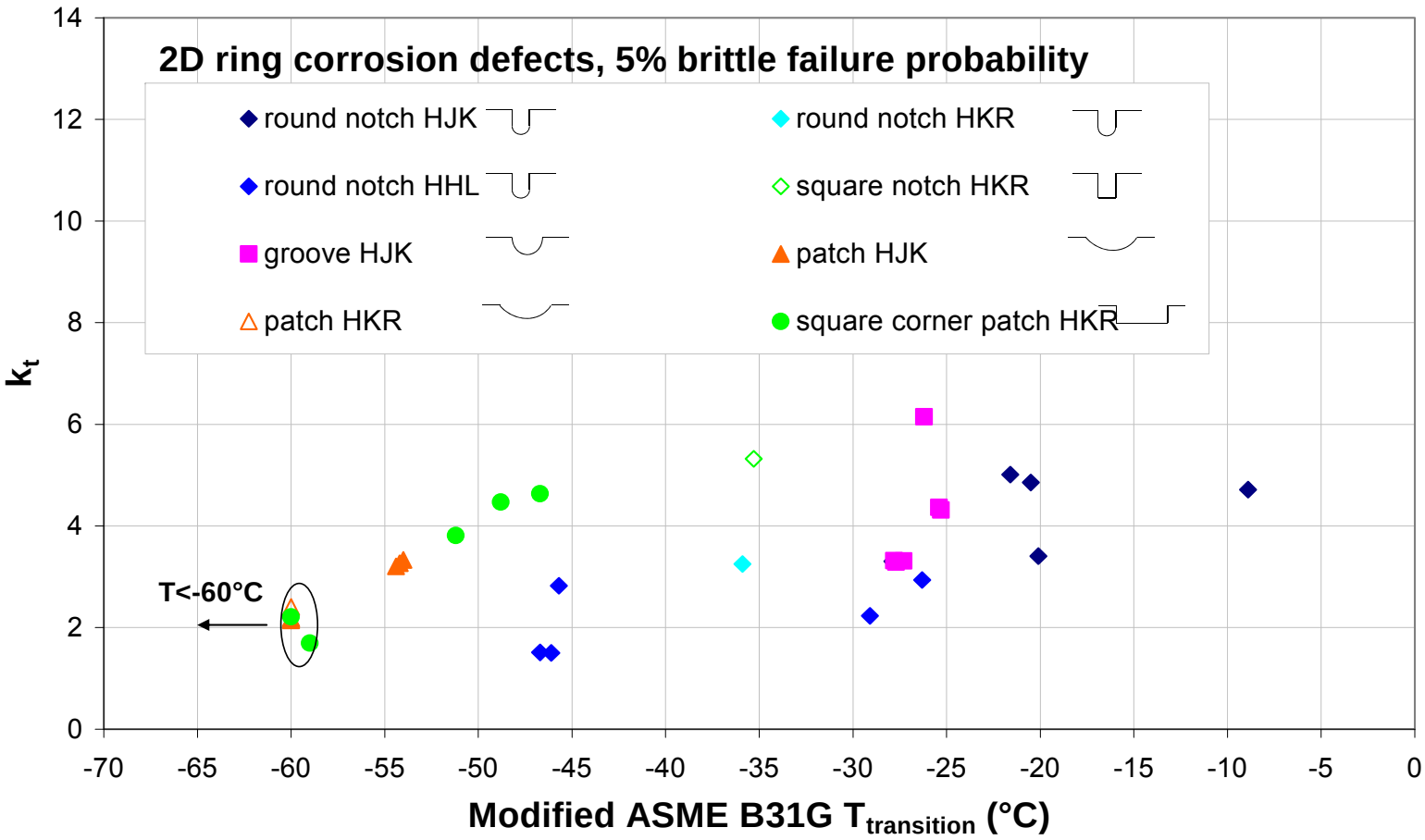

Figure 18 – Modified ASME B31G Effective Transition Temperature, Variation in Effective Transition Temperature with Stress Concentration Factor (Based on 5% Failure Probability)

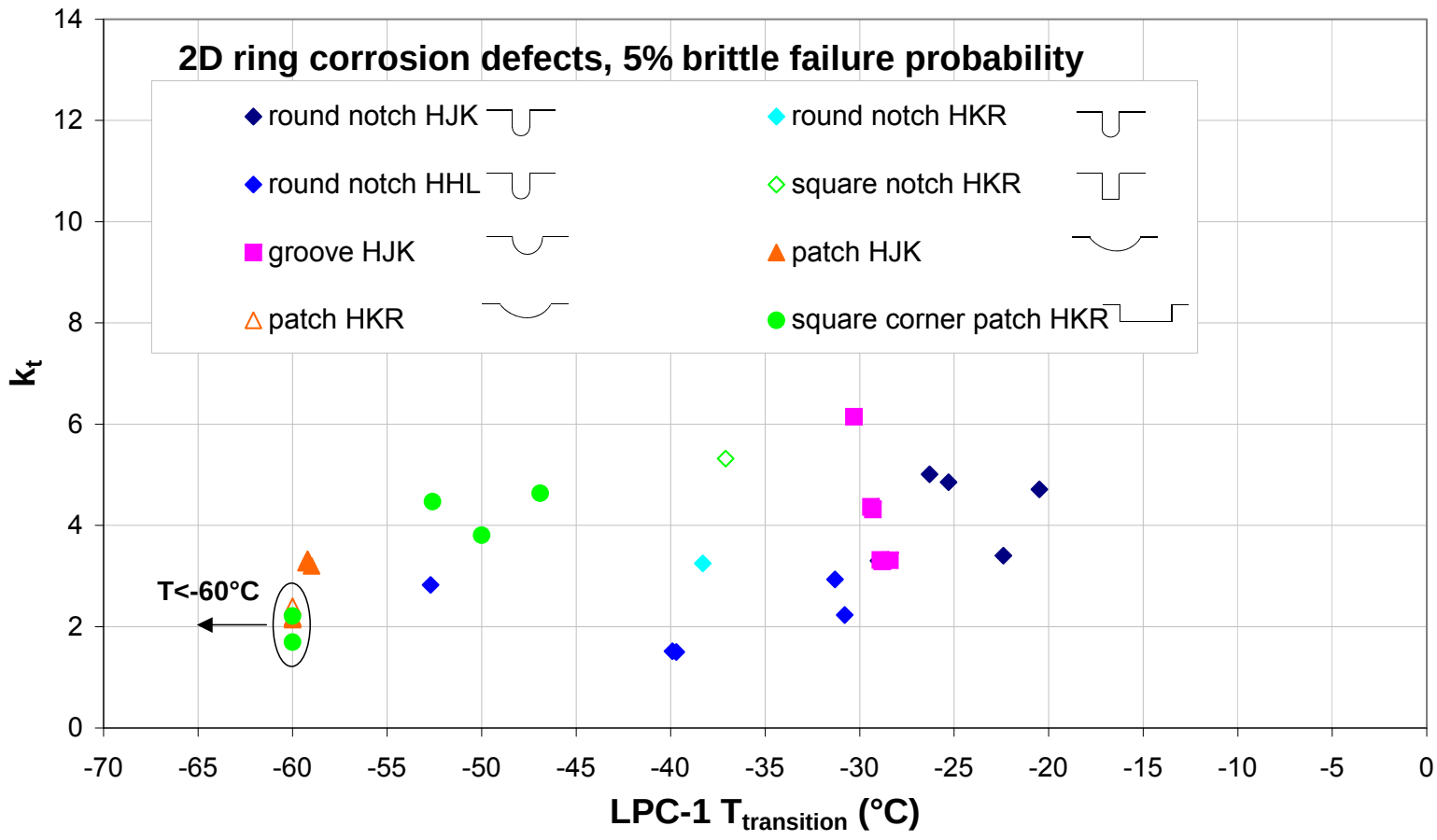

Figure 19 – LPC-1 Effective Transition Temperature, Variation in Effective Transition Temperature with Stress Concentration Factor (Based on 5% Failure Probability)

10.3 Development of Plasticity

The following series of plots shows contours of plastic strain magnitude for a sample of ring expansion defects at 24% and 96% of the measured burst pressure. Material properties are based on the curve for –20 °C. In the case of a round based notch, as shown in Figure 20 and Figure 21, plasticity develops in the root of the defect and gradually propagates inward through the wall thickness. The groove defect demonstrates similar behaviour to the notch defect, as shown in Figure 22 and Figure 23.

In the case of the square based notch, as shown in Figure 24 and Figure 25, plasticity first develops at the square corner and propagates inward through the wall thickness. The square corner patch defect shown in Figure 26 demonstrates similar behaviour to the square based notch with maximum plasticity occurring at the corner. The plastic strain remains approximately uniform throughout the central ligament region of the defect, remote from the corner. It should be noted that the plastic strain magnitude at 24% of the measured burst pressure was zero throughout.

The round based patch, shown in Figure 27, shows similar behaviour to the round based notch and groove but with a reduced contour gradient in the through thickness direction due to the reduced stress concentration factor.

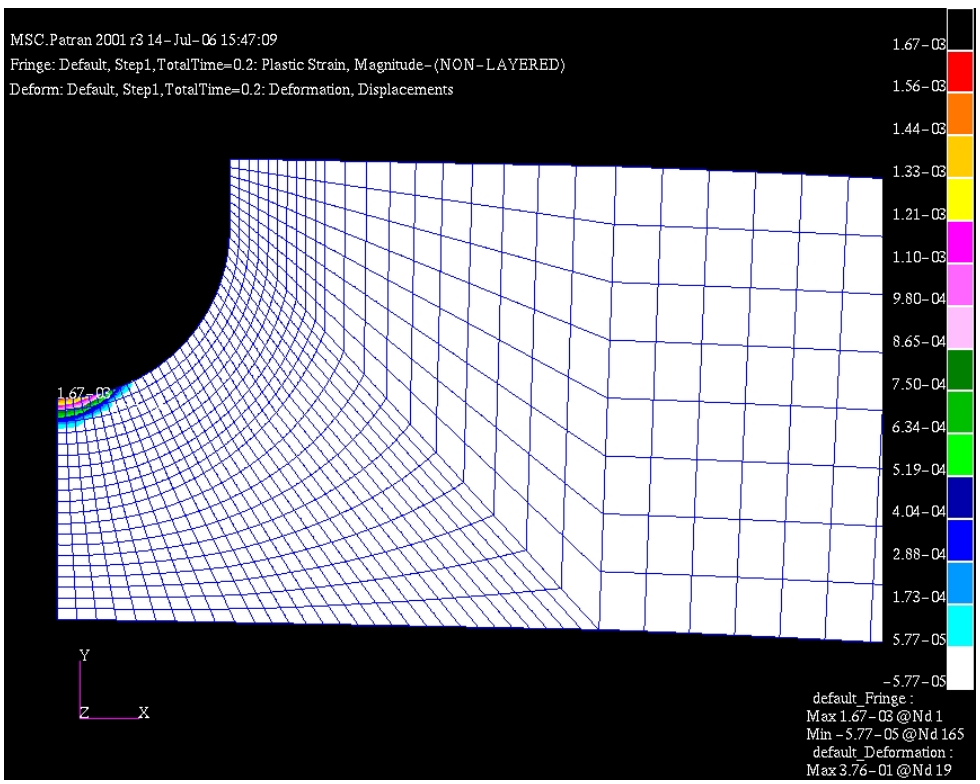

Figure 20 – HJK R4 52.4% Round Based Notch Defect, 24% Load

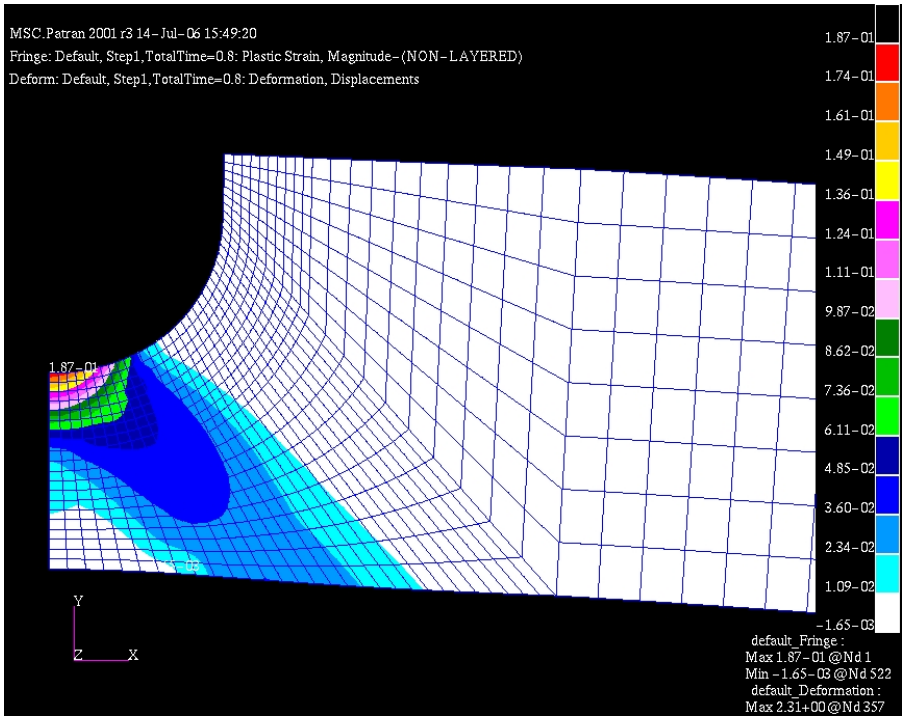

Figure 21 – HJK R4 52.4% Round Based Notch Defect, 96% Load

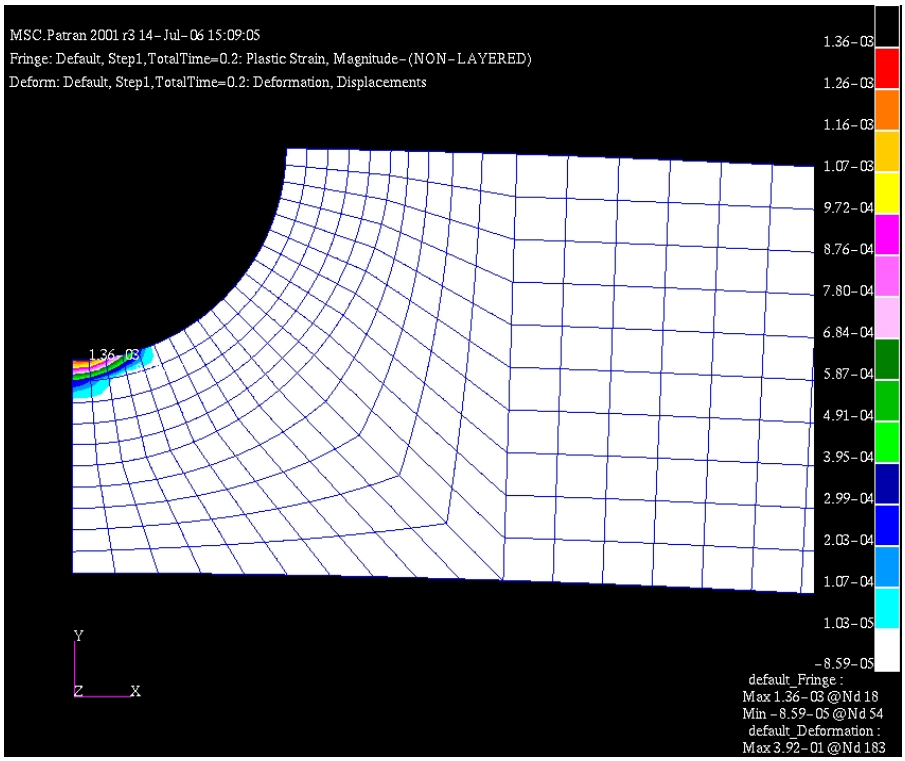

Figure 22 – HJK R10 50.2% Groove Defect, 24% Load

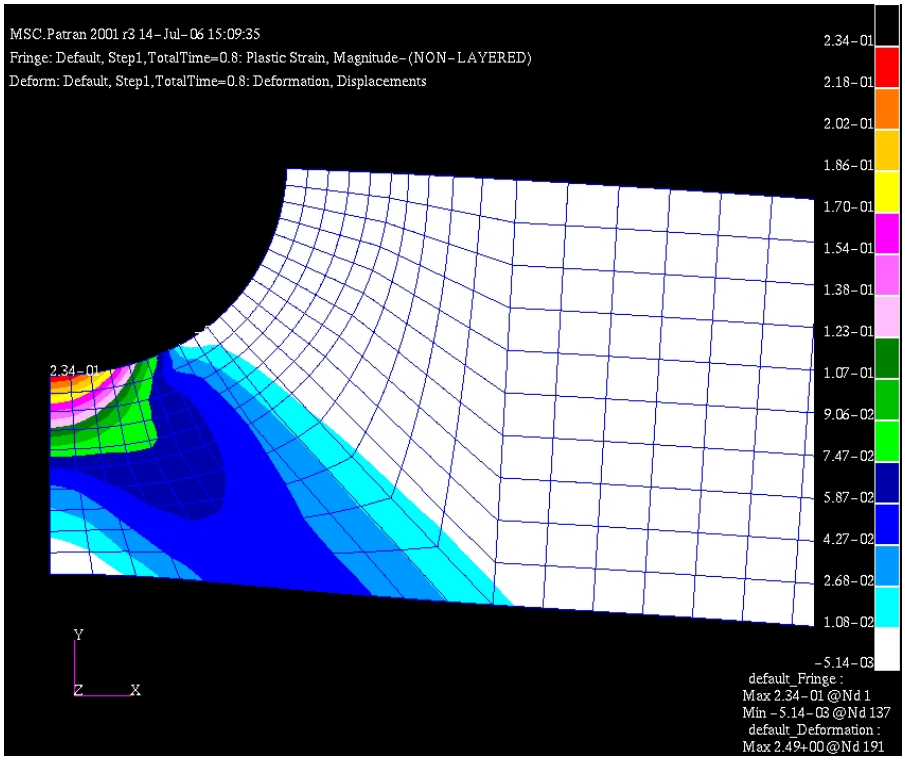

Figure 23 – HJK R4 50.2% Groove Defect, 96% Load

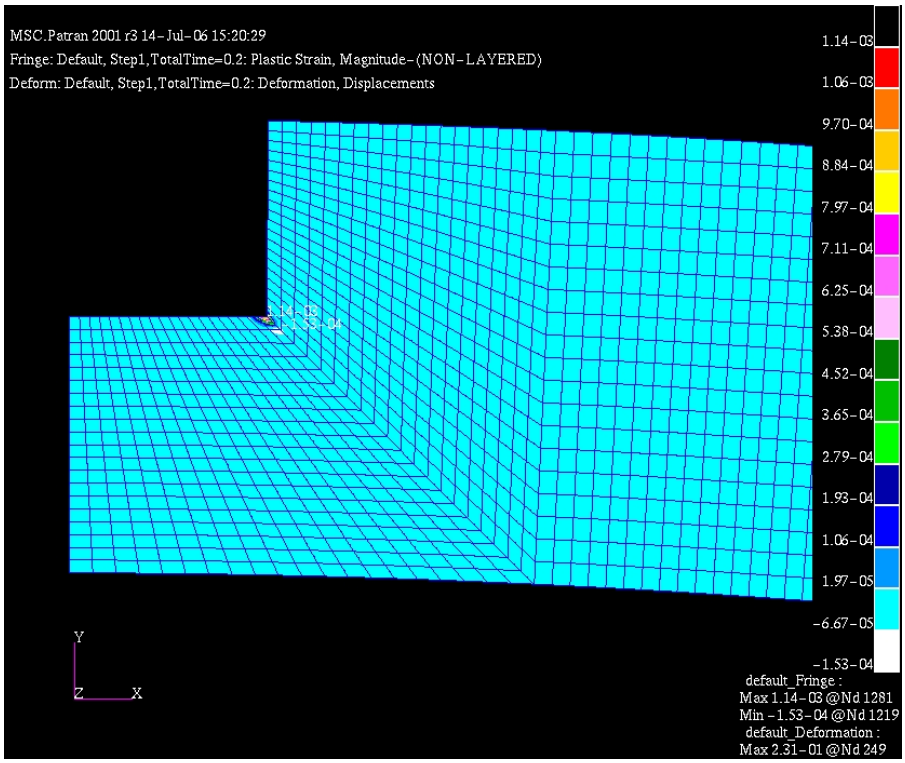

Figure 24 – HKR R3 48.2% Square Based Notch Defect, 24% Load

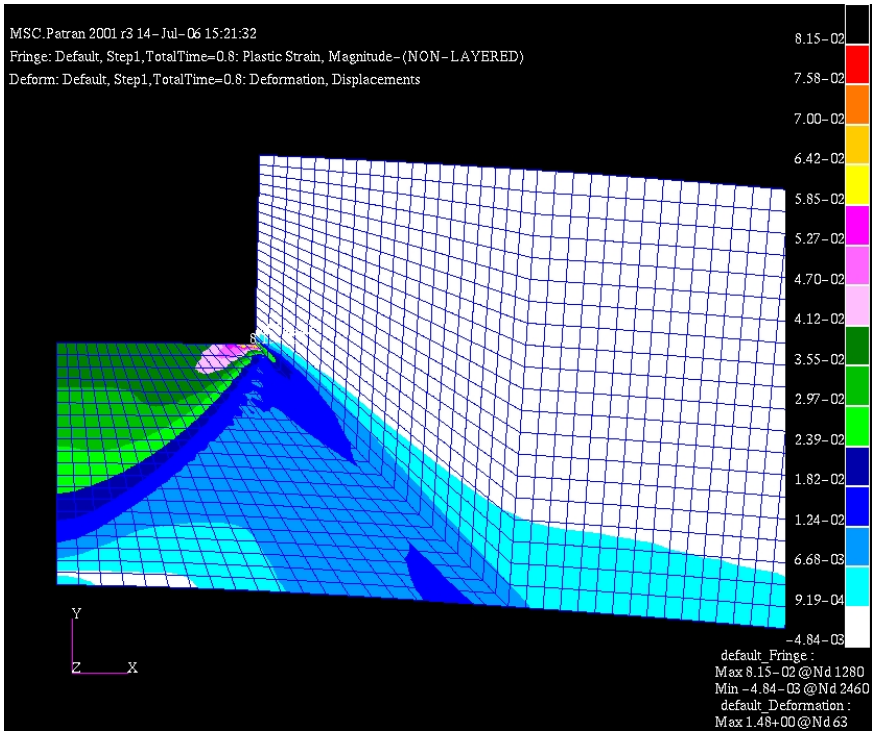

Figure 25 – HKR R3 48.2% Square Based Notch Defect, 96% Load

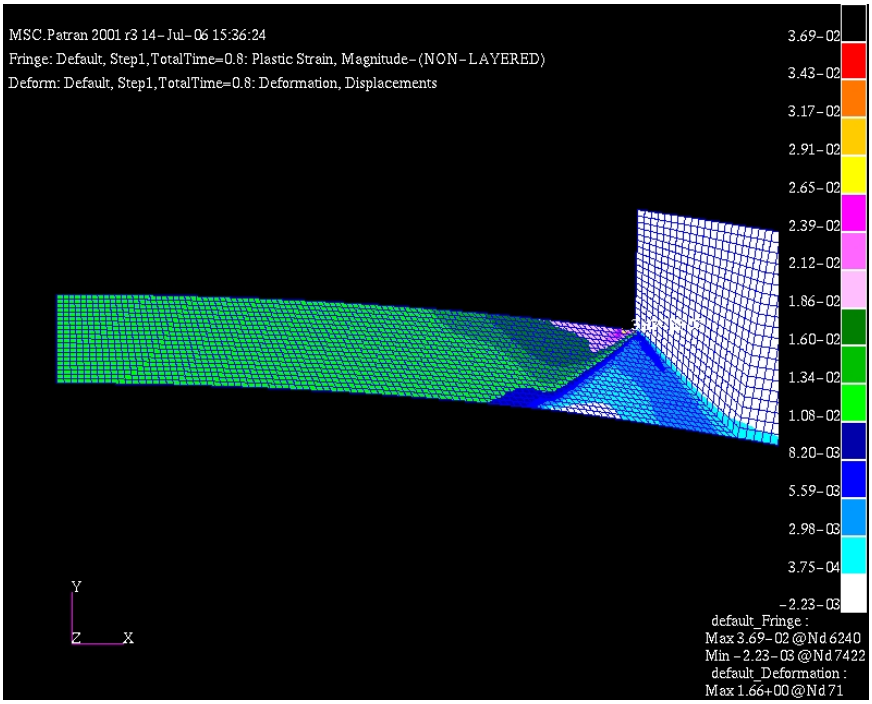

Figure 26 – HKR R9 58.0% Square Based Patch Defect, 96% Load

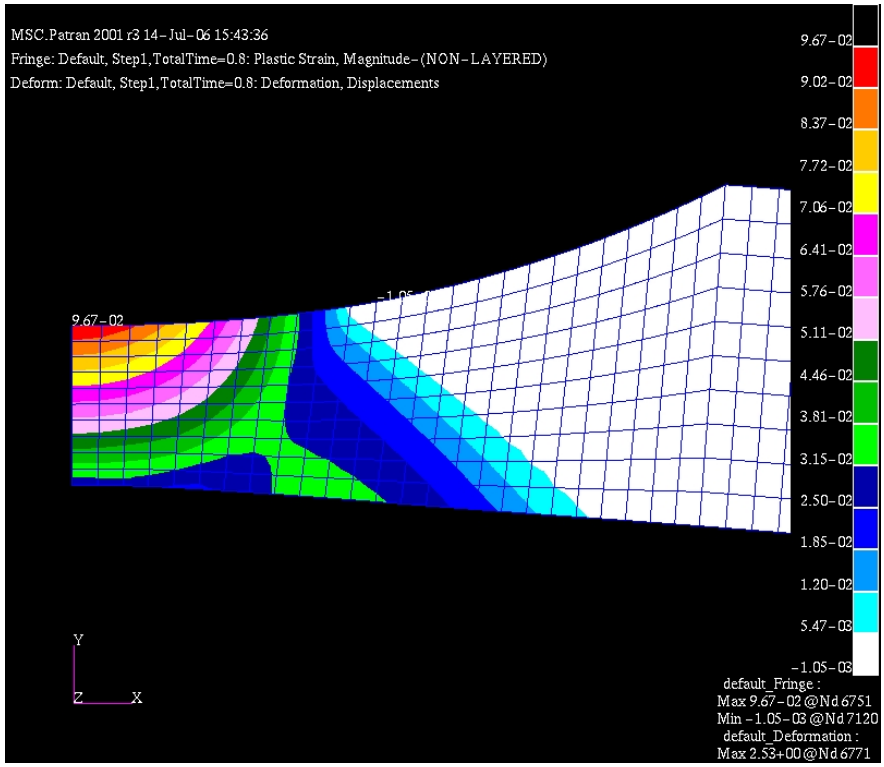

Figure 27 – HJK R16 50.8% Round Based Patch Defect, 96% Load

11 DISCUSSION

11.1 Plasticity Development

The figures in Appendix E generally demonstrate a reduction in failure hoop stress as the temperature increases from 0°C to +20ºC. This is due to the competing effects of plastic zone size and the principal stresses generated within the plastic zone. This effect appears to be most pronounced in the vessels, as shown in Figure 15. To investigate this phenomenon, the average maximum principal stress, $\overline{\sigma}$, has been calculated using Eq. (6) at several points in the load history from zero pressure to maximum pressure for ring HJK R1 at each of the five analysis temperatures. The summation is taken over all elements in the plastic zone.

$$\overline{\sigma} = \frac{\sum_j \sigma_{1j} V_j}{\sum_j V_j} \qquad (6)$$

Figure 28, Figure 29, Figure 30, Figure 31 and Figure 32 show how the average maximum principal stress (solid blue line) and plastic zone volume (dotted blue line) change with internal pressure and temperature for ring HJK R1. The vertical lines show the pressures equivalent to 5% and 95% probability of failure respectively. In

each case, the yield volume increases relatively slowly up to a point at which large scale yielding occurs. The onset of yield appears to reduce the average maximum principal stress within the plastic zone. At higher temperatures, large scale yielding has developed at the pressures equivalent to 5% and 95% probability of failure. This suggests ductile behaviour is now occurring and the Beremin approach is not valid in this region. When large scale yielding has developed, the constraint effect near the defect is reduced and the average maximum principal stress throughout the plastic zone is reduced.

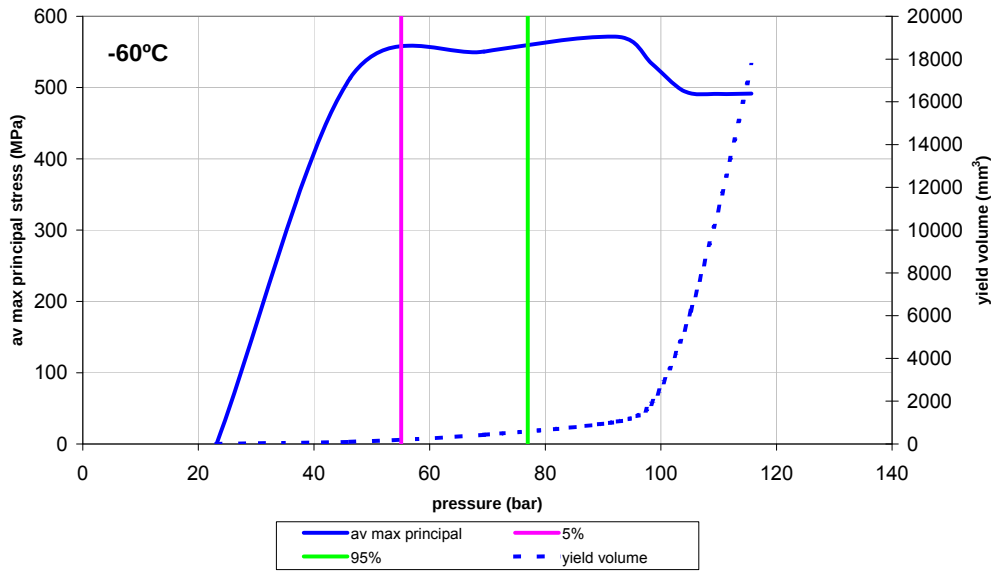

Figure 28 – Development of Average Maximum Principal Stress and Plastic Zone Size at –60ºC

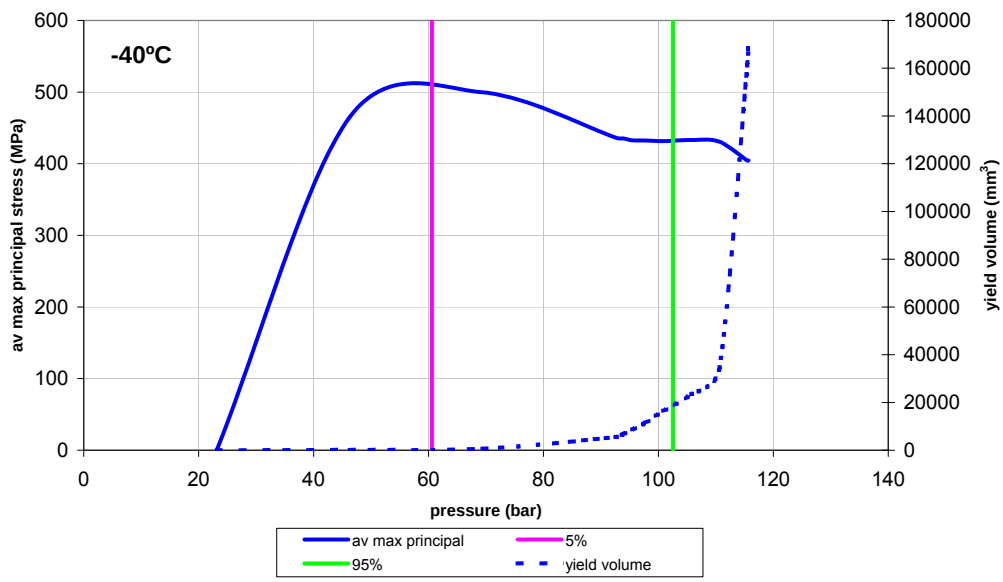

Figure 29 – Development of Average Maximum Principal Stress and Plastic Zone Size at –40ºC

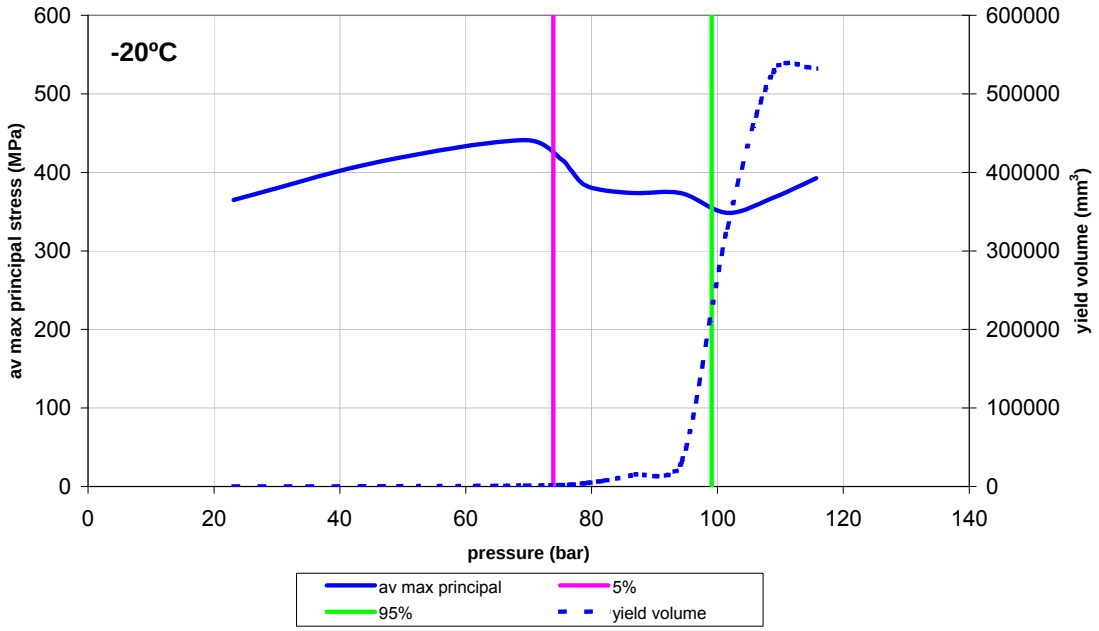

Figure 30 – Development of Average Maximum Principal Stress and Plastic Zone Size at –20ºC

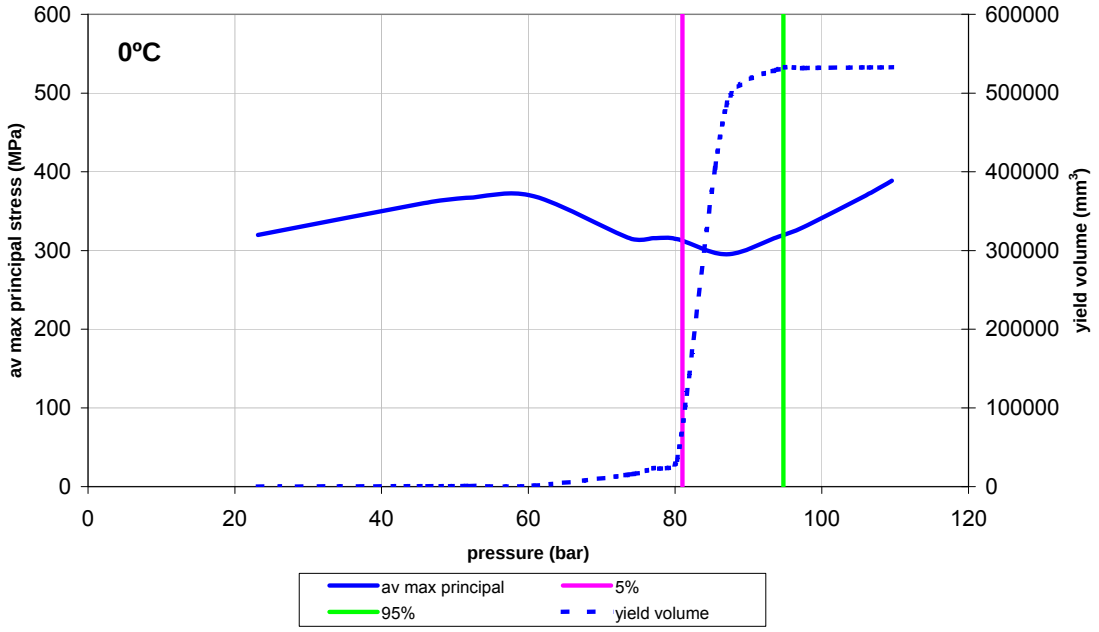

Figure 31 – Development of Average Maximum Principal Stress and Plastic Zone Size at 0ºC

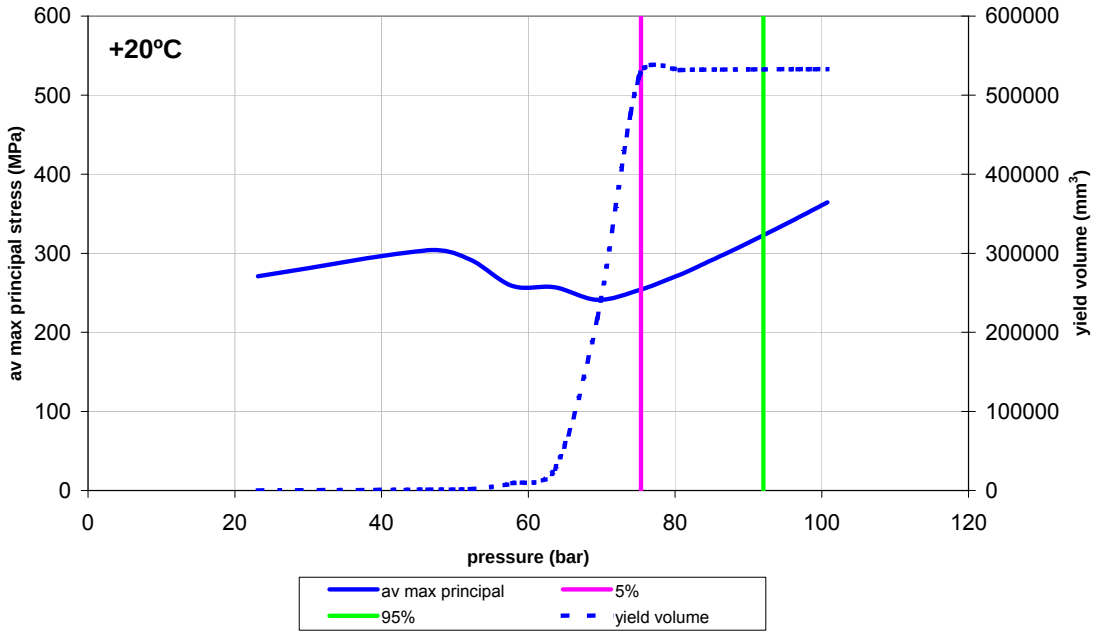

Figure 32 – Development of Average Maximum Principal Stress and Plastic Zone Size at +20ºC

11.2 Defect Geometry

The 5% brittle failure hoop stress variation with temperature in the case of both notch and groove defects is similar – this is to be expected as the material at the top of the defect near the outside diameter of the ring does not develop plasticity. The patches display different behaviour from notches and grooves, demonstrating only a small change in the 5% brittle failure hoop stress over the temperature range –20°C to +20°C. This result suggests that the patch geometry is unlikely to result in a brittle failure when tested at temperatures of –20°C or above. To maximise the probability of brittle failures, temperatures below those used in the HJK and HKR test programmes should be used.

The presence of a sharp corner at the base of the notch defects appears to increase the gradient of the 5% brittle failure hoop stress line in the range –60°C to –40°C when compared to a round notch base. This effect is illustrated by comparison of Figure 12, Figure 16 and Figure 17.

In the vessels, a region of plasticity is developed at each end of the defect in addition to the remaining ligament below the defect. Therefore, vessel behaviour is not directly comparable to the behaviour of 2D infinite defects. However, above a certain defect length, the contribution of the notch end plasticity will be small when compared to the plasticity developed in the ligament and the vessel behaviour will approach the 2D case. This effect can be observed in the response of vessel HJK V1 (125mm defect length) and the ring expansion tests HJK R10 to HJK R12.

The behaviour of the slit defect (HKR R4) is significantly different from all of the other defects investigated. The 5% brittle failure probability hoop stress line demonstrates

a positive gradient throughout the temperature range of –60 °C to +20 °C and does not intersect the Modified ASME B31G or LPC-1 failure prediction lines, indicating a transition temperature above +20 °C. This is due to the defect behaving more like a crack than a volumetric corrosion defect, generating a localized area of high stresses at the slit so that a cleavage fracture is triggered before any generalized yielding can occur. Figure 16 also shows that this defect has the lowest predicted failure stress at the 5% level of any of the defects tested.

11.3 Implications of Results

With the exception of the slit defect (HKR R4) and one of the nominal 50% notch defects (HJK R5), all of the 5% brittle failure probability effective transition temperatures deduced in this study are below –20 ºC. This is the case for both the LPC-1 and the Modified ASME B31G prediction methods. The slit defects can be neglected as this type of defect would not be considered as a corrosion defect. For the other high transition temperature prediction, ring HJK R5, it is only the Modified ASME B31G prediction which has the high transition temperature. The LPC-1 prediction is below -20 °C.

The low transition temperatures predicted for the corrosion defects should be compared with the Charpy 50% shear area transition temperature for these materials of about +25 °C. Hence it is considered that the corrosion defects exhibit a temperature shift of at least 40 °C from the Charpy impact transition temperature. In fact the less acute patch type defects exhibit a greater shift, at least 60 °C; see Figure 19 where the predicted transition temperatures for the corrosion defects are —50 °C or below. However, it is not clear if it is reasonable to apply this extra benefit unless the dimensions of the defect are accurately known. This is unlikely to be the case for defects detected by in – line inspection.

The analytic and experimental results show that existing assessment criteria can be applied even where the material has a relatively high Charpy transition temperature. For typical pipeline operating temperatures of around 0 °C a material transition temperature of around +40 °C would appear to be possible.

11.4 Complex loading and rate effects

The present investigation has considered only internal pressure loading, and single isolated defects. More complex situations such as external (biaxial) loading due to ground movement, and defect interaction, have not been considered. It is considered that the present results are likely to apply to these situations also, as the loading is similar. Failure is governed by quasi-static effects, similar to those for single defects. The Weibull stress analysis could also be applied to these situations if required.

The effect of pipe wall thickness has not been considered in detail in this project. It is known that Charpy transition temperatures may be un-conservative when applied to components thicker than the fixed Charpy specimen thickness of 10 mm. This effect is taken into account in codes such as Annex D of PD 5500 [13], the UK pressure pressure vessel code. Figure D.2 shows that a temperature shift of 10 °C is required

for every 10 mm increase in thickness above the Charpy specimen size. This suggests that small increases in thickness will not have a large effect on the limits of application of existing criteria.

As with the existing criteria for assessing corrosion defects, and indeed the NG-18 equations for cracklike defects, this work is concerned with the initiation of failure. The results suggest that the existing models may be used to predict the initation of failure in low toughness materials. However, these models do not predict the subsequent propagation behaviour after failure has initiated. This should be assessed for brittle material using the DWTT behaviour for the pipe. For many pipelines the DWTT transition temperature is above the Charpy transition temperature and so brittle fracture propagation may follow even though the initiation condition can be predicted using the ductile failure equations.

The research has not explicitly considered strain rate effects in the initiation of failure. The original research leading to the development of ASME B31G was carried out on vessels under quasi-static loading where rate effects would not occur. Subsequent test work has also been carried out in the same way. For the large majority of pipeline applications the loading will also be quasi static. However, there may be cases where there are high loading rates, such as seismic loading or transient pressure surges in liquid lines. It is also possible that a corrosion defect may “snap through” rapidly if external restraints are removed, for example when excavating a buried defect. In these cases rate effects may affect the conclusion that the existing models may be used even down to low toughness levels.

It is known that as the loading rate increases, the transition temperature will also increase, or equivalently there is a greater tendency for brittle fracture to occur. This is because the yield strength increases at higher strain rates. This increase leads to higher stresses in the plastic zone and so a greater likelihood of brittle failure. If it was assumed that the Weibull parameters m and σ_u are independent of temperature, the rate sensitivity of the brittle fracture transition could be predicted by finite element analysis if the rate sensitivity of the stress-strain curve were known.

Wilkowski et al. [14] suggest that the rate effect is equivalent to a transition temperature shift of between 33 °C and 50 °C when comparing test results from DWTT tests and quasi-static tests on through wall cracked vessels. However in this work they also identify other temperature shifts in the opposite direction. These are due to constraint differences between through wall and surface cracks and also the effects of notch acuity. They suggest that for blunt notch radii over 3 mm (1/8 inch) the temperature shift from a sharp crack is 80 °C, greater than that suggested above. They concluded: “that for corrosion flaws even in very old pipe with high Charpy transition temperature, the fractures should have failure pressures that correspond to upper-shelf behavior. The uses of limit-load solutions such as Modified ASME B31G are probably valid for such material under any conceivable normal operating conditions”.

12 CONCLUSIONS

1. This report presents an approach for removing the uncertainty in the use of existing methods for assessing corrosion defects in older, low toughness pipelines based on the Beremin approach to brittle cleavage fracture.

2. Use of the Beremin approach in conjunction with the results from ring expansion tests, vessel tests and non-linear finite element analysis has provided a method of establishing the brittle failure probability as a function of hoop stress and temperature for a variety of corrosion defects including notches, grooves and patches.

3. Effective transition temperatures have been defined as the temperature below which existing assessment criteria such as Modified ASME B31G and LPC-1 are no longer conservative. Effective transition temperatures have been evaluated for both the Modified ASME B31G and LPC-1 methods.

4. Based on typical buried pipeline operating temperatures of around 0 °C, existing assessment criteria are considered to be valid for pipelines with transition temperatures up to +40 °C.

5. It is considered that the results from ongoing investigations into the failure behavior of corrosion defects subjected to biaxial loading in modern high strength pipeline materials will remain valid for older low toughness pipelines. Similarly, rules now being developed for defect interaction are judged likely to remain valid for older low toughness pipelines.

13 RECOMMENDATIONS

1. As the pipeline temperatures experienced in the field are unlikely to be below -20 ºC, it is judged likely that existing assessment methods, such as the Modified ASME B31G and LPC-1, will remain conservative for the assessment of corrosion defects in old, low toughness pipelines.

2. It is considered that the results from ongoing investigations into the failure behaviour of corrosion defects subjected to biaxial loading in modern high strength pipeline materials will remain valid for older low toughness pipelines. Similarly, rules now being developed for defect interaction are judged likely to remain valid for older low toughness pipelines.

14 ACKNOWLEDGEMENTS

The authors wish to acknowledge the financial support from PRCI and from the US DOT. Input from the former PRCI Materials Committee, particularly Messrs Owen, Amend and Sloterdijk is also acknowledged.

15 REFERENCES

[1] Anon, ASME B31G-1991 (revision of ANSI/ASME B31G-1984): Manual for determining the remaining strength of corroded pipelines - a supplement to ASME B31 code for pressure piping, The American Society of Mechanical Engineers, New York, 1991.

[2] Kiefner, J.F. and Veith, P.H., 'A Modified Criterion for Evaluating the Remaining Strength of Corroded Pipe', Final Report on PR-3-805 to Pipeline Corrosion Supervisory Committee of the Pipeline Research Committee of the American Gas Association, Battelle, Ohio, 1989.

[3] Vieth, P. H. and Kiefner, J. F., 'RSTRENG2 User's Manual, Final report on PR-218-9205 to Corrosion Supervisory Committee, Pipeline Research Committee, American Gas Association, Kiefner & Associates, Inc., Ohio, 1993.

[4] Anon. 'Guide to Methods for Assessing the Acceptability of Flaws in Metallic Structures', BS 7910:2005, BSI, 27 July 2005

[5] Beremin F. M. 'A local criterion for cleavage fracture of a nuclear pressure vessel steel'. Met. Trans 14A, 1983, 2277-2287

[6] Wiesner C. S. 'The Local Approach to Fracture – Concepts and Applications', Abington Publishing, Cambridge, UK, 1995

[7] Pineau A. Development of the local approach to fracture over the past 25 years: theory and applications. International Journal of Fracture 2006;138:139-66.

[8] MSC/PATRAN 2001 r3, MacNeal-Schwendler Corporation, 2001.

[9] ABAQUS/Standard Version 6.4, Hibbitt, Karlsson & Sorensen Inc., 2003.

[10] Andrews R. M., Morgan G.C., Pipet D. A. and Owen R. W., 'Towards Criteria for Assessing the Remaining Strength of Corrosion Defects in Low Toughness Linepipe Materials', PRC*I* Catalog No. L51884, April 2004

[11] Wood A., Phillips G. and Andrews R. M., 'Ring Expansion Tests on 12″ Nominal Diameter Pipe at 0 °C For Gasunie', Advantica Report R8027, April 2005 (confidential to Advantica and Gasunie)

[12] Numerical Recipes in Fortran 77 : The Art of Scientific Computing', Cambridge University Press, Section 15.5 'Nonlinear Models'

[13] BSI. Unfired fusion welded pressure vessels PD 5500, Annex D. London: British Standards Institution; 2000.

[14] Wilkowski G, Rudland D, Rider D, Mincer P and Sloterdijk W: 'When Old Line Pipes Initiates Fracture in a Ductile Manner', Paper IPC2006-10326, International Pipeline Conference 2006, September 25-29 2006. ASME, New York.

APPENDIX A LOW TEMPERATURE TEST PROGRAM

The five rings HLL R7, HLL R8, HLL R9, HLL R10 and HLL R3 were all tested at low temperature using the ring expansion test configuration shown in Figure 33.

Test temperatures of –20ºC or below are thought to be below the glass transition temperature of the elastomeric seal material. In normal (room temperature) operation, the seal material is operating above its glass transition temperature and has extremely low hoop stiffness compared to the ring under test. The seal therefore expands radially, following the expansion of the ring and directly transfers the radial pressure force acting on its internal diameter to the internal diameter of the ring via the normal contact force between the two components. However, at temperatures below the glass transition temperature of the seal, the material gains significant hoop stiffness and provides a certain level of pressure containment. This prevents the ring from experiencing the pressure present in the oil reservoir. Additionally, when the pressure in the oil reservoir is of sufficient magnitude, the seal material will experience brittle fracture and allow oil to contact the ring material resulting in freezing of the oil. As a result, the method of ring expansion testing used at room temperature is not suitable for the low temperatures required for the HLL test program. To modify the test configuration for low temperature operation, a ptfe split ring of 10mm thickness has been used as a thermal barrier between the existing seal material and ring under test. This approach has been found to increase the short term (transient) temperature experienced at the seal to a value above the glass transition temperature. The split ring expands radially with the ring under test and allows transfer of the radial pressure force

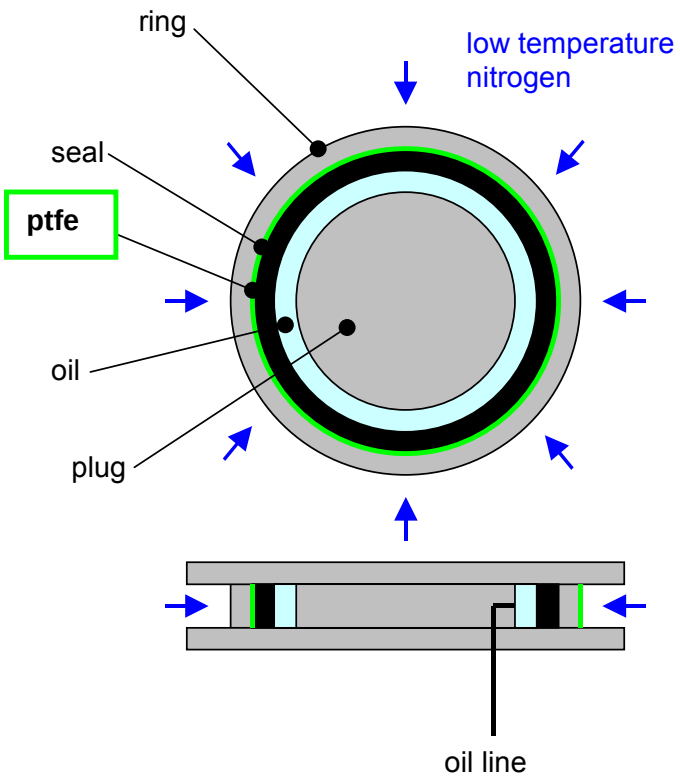

Figure 33 – HLL Low Temperature Ring Expansion Test Configuration

Figure 34 and Figure 35 show the test configuration and ptfe thermal barrier respectively.

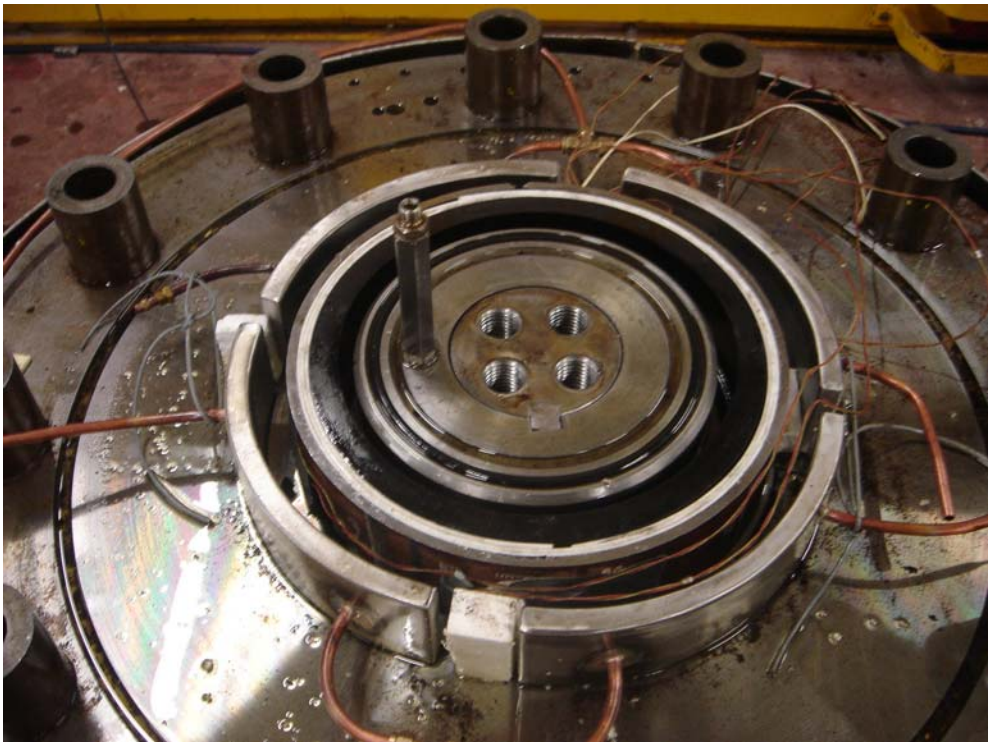

Figure 34 – Test Configuration

Figure 35 – ptfe Thermal Barrier

Figure 36 shows the ring expansion test rig in use at low temperature.

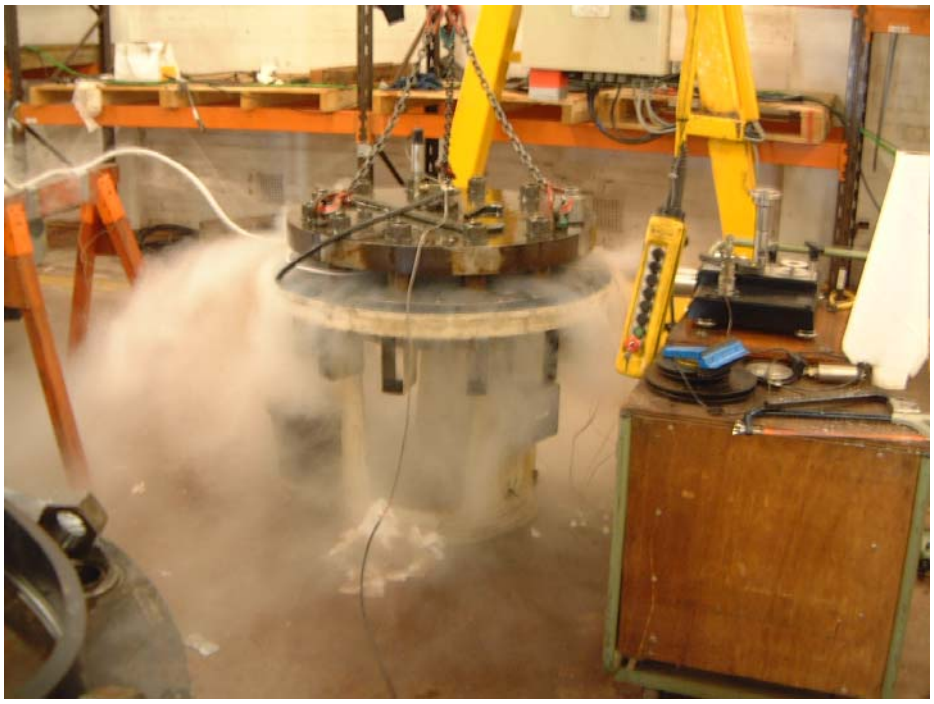

Figure 36 – Ring Expansion Test Rig During Cooling

Figure 37 and Figure 38 show an HLL notch defect following bursting.

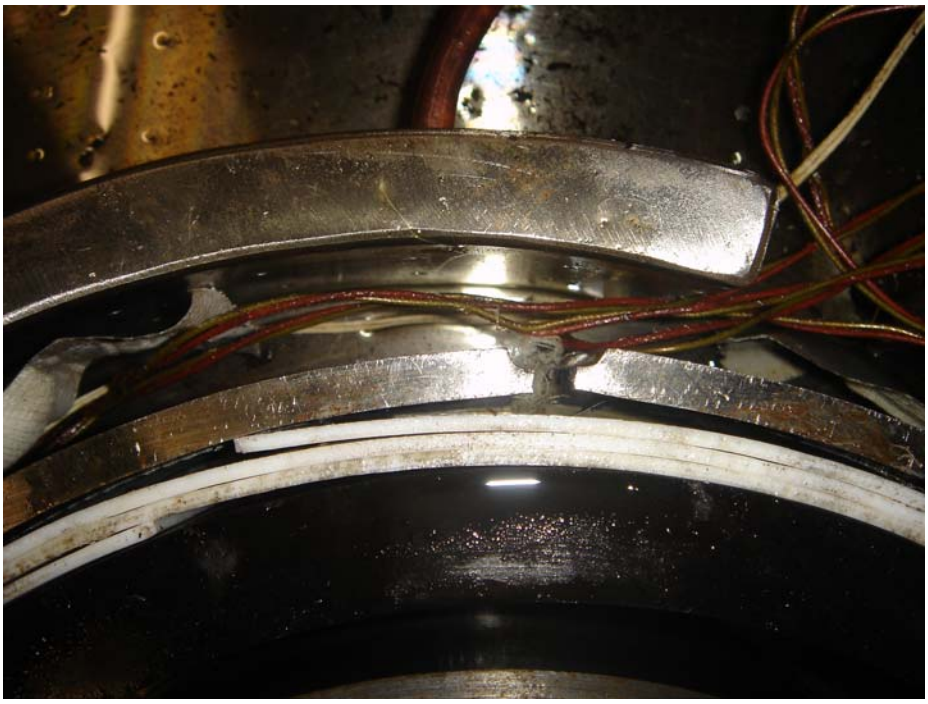

Figure 37 – HLL Notch Defect Following Bursting

Figure 38 – HLL Notch Defect Following Bursting

APPENDIX B TENSILE TEST SPECIMEN DETAILS

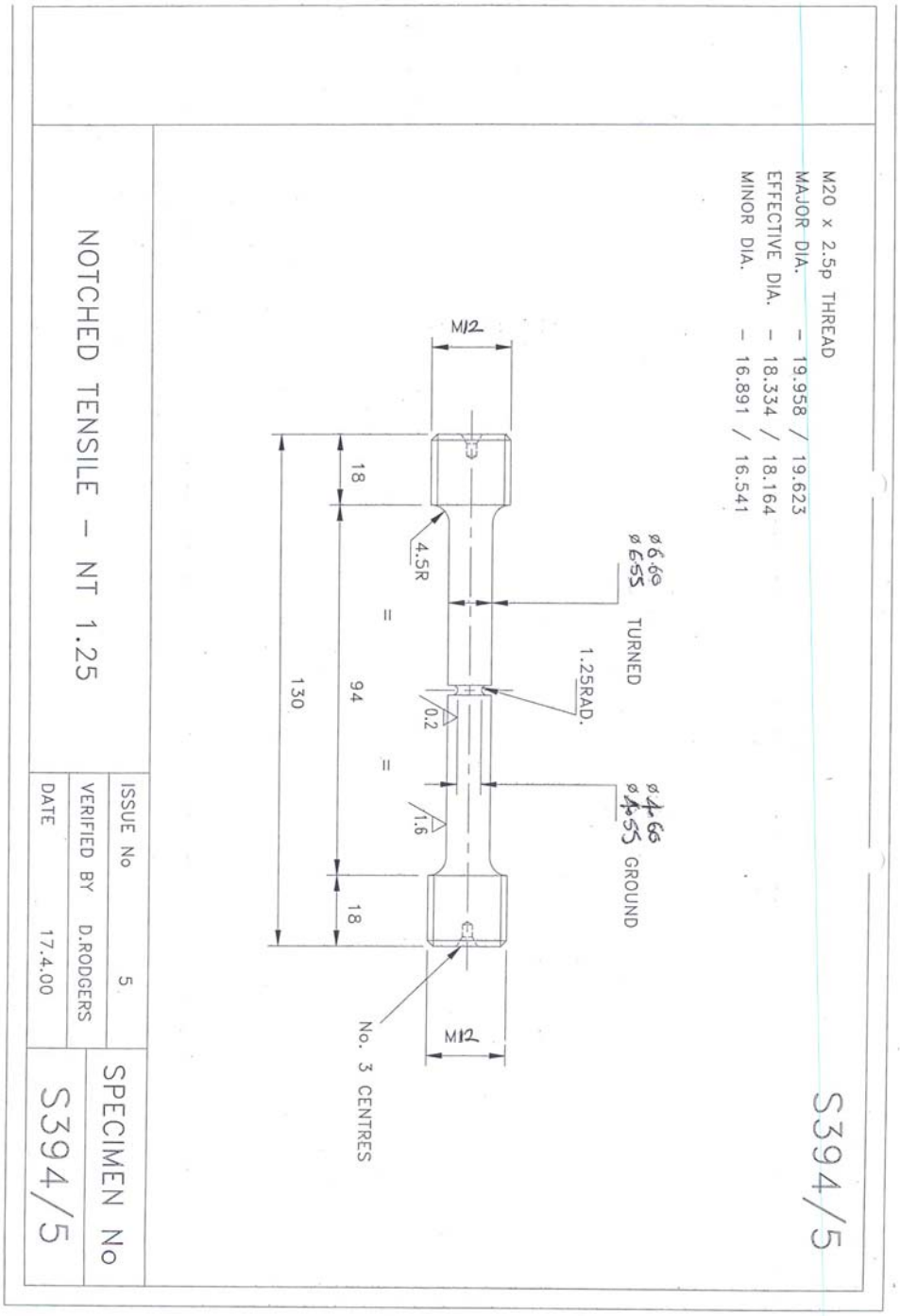

Notched Tensile Specimen

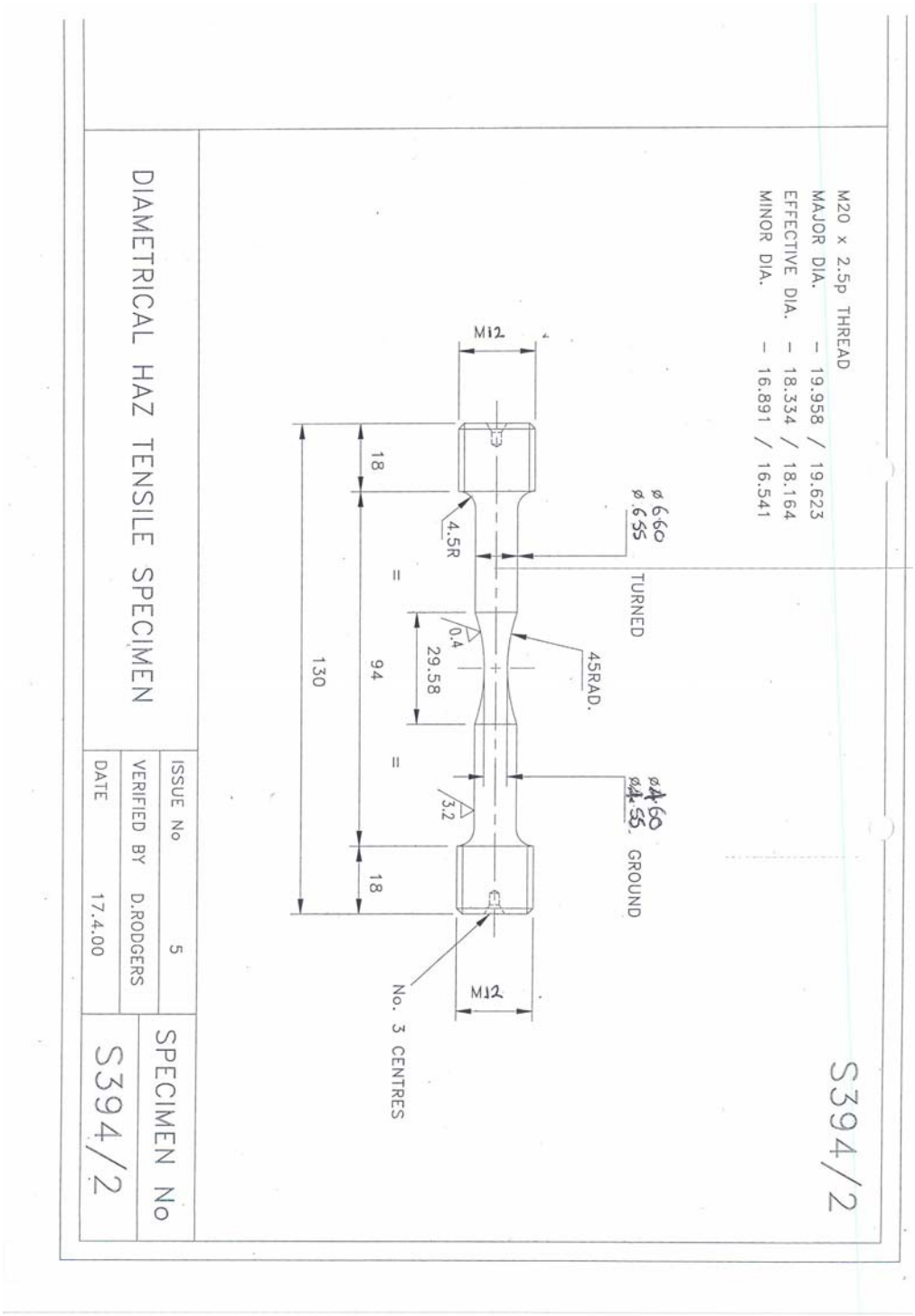

Waisted Tensile Specimen

APPENDIX C DEFECT GEOMETRY SUMMARY

ID	Pipe geometry (measured)			Defect		
	OD (mm)	t (mm)	OD/t	Test type	Description	Schematic
HJK-R1	559	8.1	69.0	Ring	33.7% notch	
HJK-R2	559	8.2	68.2	Ring	31.4% notch	
HJK-R3	559	8.1	69.0	Ring	32.1% notch	
HJK-R4	559	8.1	69.0	Ring	52.4% notch	
HJK-R5	559	8.2	68.2	Ring	50.7% notch	
HJK-R6	559	8.1	69.0	Ring	53.6% notch	
HJK-R7	559	8.1	69.0	Ring	31.6% groove	
HJK-R8	559	8.2	68.2	Ring	31.4% groove	
HJK-R9	558	8.2	68.0	Ring	31.8% groove	
HJK-R10	559	8.1	69.0	Ring	50.2% groove	
HJK-R11	559	8.1	69.0	Ring	51.7% groove	
HJK-R12	559	8.1	69.0	Ring	50.6% groove	
HJK-R13	559	8.1	69.0	Ring	31.9% patch	
HJK-R14	559	8.1	69.0	Ring	31.1% patch	
HJK-R15	559	8.1	69.0	Ring	31.4% patch	
HJK-R16	559	8.1	69.0	Ring	50.8% patch	
HJK-R17	559	8.1	69.0	Ring	51.8% patch	
HJK-R18	559	8.1	69.0	Ring	49.8% patch	

ID	Pipe geometry (measured)			Defect		
	OD (mm)	t (mm)	OD/t	Test type	Description	Schematic
HJK-V1	559	8.34	67.0	Vessel	57% notch × 125mm length	
HJK-V1 (modified)	559	8.34	67.0	Vessel	57% notch × 70mm length	
HJK-V2	559	8.28	67.5	Vessel	76% notch × 70mm length	
HJK-V2 (modified)	559	8.28	67.5	Vessel	76% notch × 125mm length	
HKR-R1	325	7	46.4	Ring	46.3% patch	
HKR-R2	326	6.8	47.9	Ring	49.6% groove	
HKR-R3	325	6.9	47.1	Ring	48.2% square groove	
HKR-R4	325	6.8	47.8	Ring	45.9% slit	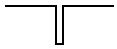
HKR-R5	325	6.9	47.1	Ring	39.7% patch	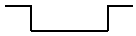
HKR-R8	325	6.9	47.1	Ring	28.0% patch	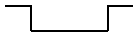
HKR-R9	325	7	46.4	Ring	58.0% patch	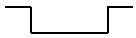
HKR-R10	325	7	46.4	Ring	75.7% patch	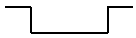
HLL-R7	326	6.9	47.3	Ring	29.4% notch	
HLL-R8	326	6.9	47.0	Ring	29.1% notch	
HLL-R9	326	6.9	46.9	Ring	47.6% notch	

ID	Pipe geometry (measured)			Defect		
	OD (mm)	t (mm)	OD/t	Test type	Description	Schematic
HLL-R10	326	6.9	47.5	Ring	62.1% notch	
HLL-R3	325	6.9	47.3	Ring	71.2% notch	

APPENDIX D WEIBULL DISTRIBUTION CALIBRATION DATA

Load inc.	Step Time	Notch Root Radial Reduction (mm)	Weibull Stress				
			m=20	m=21	m=22	m=23	m=24
1	0.02	0.0008	790.5	776.0	763.1	751.4	741.0
2	0.04	0.0100	1087.0	1061.8	1039.4	1019.5	1001.7
3	0.06	0.0269	1186.7	1159.7	1135.8	1114.5	1095.4
4	0.08	0.0434	1216.0	1188.3	1163.9	1142.1	1122.6
5	0.10	0.0594	1234.5	1206.3	1181.4	1159.3	1139.4
6	0.12	0.0748	1250.4	1221.7	1196.4	1173.9	1153.7
7	0.14	0.0898	1265.6	1236.5	1210.8	1187.8	1167.3
8	0.16	0.1044	1280.9	1251.3	1225.1	1201.8	1181.0
9	0.18	0.1187	1296.3	1266.3	1239.7	1216.0	1194.8
10	0.20	0.1326	1312.1	1281.6	1254.6	1230.6	1209.0
11	0.22	0.1463	1328.5	1297.6	1270.2	1245.7	1223.9
12	0.24	0.1596	1344.8	1313.4	1285.6	1260.8	1238.6
13	0.26	0.1727	1362.0	1330.1	1301.9	1276.7	1254.2
14	0.28	0.1856	1379.3	1347.0	1318.3	1292.8	1269.9
15	0.30	0.1983	1397.0	1364.2	1335.2	1309.3	1286.1
16	0.32	0.2110	1415.9	1382.7	1353.3	1327.1	1303.6
17	0.34	0.2236	1435.1	1401.6	1371.8	1345.3	1321.5
18	0.36	0.2362	1454.6	1420.7	1390.6	1363.8	1339.8
19	0.38	0.2489	1474.8	1440.5	1410.1	1383.0	1358.7
20	0.40	0.2616	1495.0	1460.3	1429.6	1402.2	1377.7
21	0.42	0.2744	1515.3	1480.3	1449.3	1427.7	1396.9
22	0.44	0.2875	1535.9	1500.6	1469.3	1441.4	1416.3
23	0.46	0.3006	1556.9	1521.2	1489.6	1461.1	1436.2
24	0.48	0.3140	1578.0	1542.0	1510.1	1481.7	1456.2
25	0.50	0.3277	1600.1	1563.7	1531.6	1502.9	1477.2
26	0.52	0.3416	1622.8	1586.2	1553.8	1524.9	1499.0
27	0.54	0.3559	1646.5	1609.6	1576.9	1547.8	1521.7
28	0.56	0.3705	1671.1	1633.9	1601.0	1571.8	1545.5
29	0.58	0.3855	1696.7	1659.3	1626.3	1596.9	1570.5
30	0.60	0.4009	1723.3	1685.7	1652.6	1623.0	1596.6
31	0.62	0.4168	1750.5	1712.9	1679.6	1650.0	1623.4
32	0.64	0.4332	1777.7	1739.9	1706.6	1676.9	1650.3
33	0.66	0.4500	1804.3	1766.4	1732.9	1703.1	1676.5
34	0.68	0.4673	1830.1	1792.1	1758.5	1728.6	1701.9
35	0.70	0.4849	1855.2	1817.0	1783.3	1753.3	1726.4
36	0.72	0.5029	1789.4	1841.0	1807.1	1777.0	1750.1
37	0.74	0.5213	1902.7	1864.2	1830.1	1799.9	1772.8
38	0.76	0.5399	1925.1	1886.4	1852.2	1821.8	1794.6
39	0.78	0.5587	1946.7	1907.8	1873.4	1842.9	1815.5
40	0.80	0.5778	1967.4	1928.3	1893.8	1863.1	1835.6
41	0.82	0.5970	1987.4	1948.1	1913.4	1882.5	1854.9
42	0.84	0.6163	2006.8	1967.3	1932.4	1901.3	1873.6
43	0.86	0.6358	2025.8	1986.0	1950.9	1919.7	1891.7

Load inc.	Step Time	Notch Root Radial Reduction (mm)	Weibull Stress				
			m=20	m=21	m=22	m=23	m=24
44	0.88	0.6554	2044.4	2004.4	1969.1	1937.7	1909.6
45	0.90	0.6751	2063.0	2022.8	1987.3	1955.7	1927.4
46	0.92	0.6950	2081.8	2041.4	2005.6	1973.8	1945.4
47	0.94	0.7150	2100.9	2060.2	2024.3	1992.3	1963.7
48	0.96	0.7351	2120.5	2079.7	2043.5	2011.3	1982.5
49	0.98	0.7553	2140.9	2099.9	2063.5	2031.2	2002.2
50	1.00	0.7758	2162.2	2121.0	2084.4	2051.9	2022.8

APPENDIX E RING EXPANSION DEFECT RESULTS SUMMARY

ID	Original Test Temperature ºC	5% (95%) Failure Probability Transition Temperature ºC		Defect		
		Mod ASME B31G	LPC-1	Description	Schematic	k_t
HJK-R1	-20	-20.1	-22.4	33.7% notch		3.40
HJK-R2	0	-27.9	-29.0	31.4% notch		3.30
HJK-R3	+20	-27.4	-28.7	32.1% notch		3.31
HJK-R4	-20	-20.5 (-52.6)	--25.3 (-56.2)	52.4% notch		4.85
HJK-R5	0	-8.9 (-52.8)	-20.5 (-56.2)	50.7% notch		4.71
HJK-R6	+20	-21.6 (-52.4)	-26.3 (-56.2)	53.6% notch		5.01
HJK-R7	-20	-27.8	-28.9	31.6% groove		3.32
HJK-R8	0	-27.7	-28.8	31.4% groove		3.29
HJK-R9	+20	-27.3	-28.4	31.8% groove		3.31
HJK-R10	-20	-25.3	-29.3	50.2% groove		4.32
HJK-R11	0	-26.2	-30.3	51.7% groove		6.15
HJK-R12	+20	-25.4	-29.4	50.6% groove		4.36
HJK-R13	-20	<-60	<-60	31.9% patch		2.18

ID	Original Test Temperature ºC	5% (95%) Failure Probability Transition Temperature ºC		Defect		
		Mod ASME B31G	LPC-1	Description	Schematic	k_t
HJK-R14	0	<-60	<-60	31.1% patch		2.14
HJK-R15	+20	<-60	<-60	31.4% patch		2.16
HJK-R16	-20	-54.2	-59.3	50.8% patch		3.27
HJK-R17	0	-54.0	-59.3	51.8% patch		3.33
HJK-R18	+20	<-60	-59.0	49.8% patch		3.20
HJK-V1	+7.4	NA	NA	57% notch × 125mm length		NA
HJK-V1 (modified)	NA	-38.9	NA	57% notch × 70mm length		NA
HJK-V2	+7.5	-43.7	-41.0	76% notch × 70mm length		NA
HJK-V2 (modified)	NA	NA	NA	76% notch × 125mm length		NA
HKR-R1	-1.6	<-60	<-60	46.3% patch		2.40
HKR-R2	-4.4	-35.9	-38.3	49.6% groove		3.24
HKR-R3	-3	-35.3	-37.1	48.2% square groove		5.32
HKR-R4	-3.9	NA (-21.1)	NA (-22.5)	45.9% slit	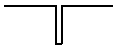	12.99
HKR-R5	-5	-46.7	-46.9	39.7% patch		4.64
HKR-R8	-1.7	-51.2	-50.0	28.0% patch	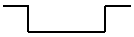	3.80

ID	Original Test Temperature ºC	5% (95%) Failure Probability Transition Temperature ºC		Defect		
		Mod ASME B31G	LPC-1	Description	Schematic	k_t
HKR-R9	-2.4	-48.8	-52.6	58.0% patch	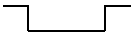	4.47
HKR-R10	-9.2	-59.0	<-60	75.7% patch		1.69
HLL-R7	-20	-46.7	-39.9	29.4% notch		1.51
HLL-R8	-60	-46.1	-39.7	29.1% notch		1.50
HLL-R9	-20	-29.1 (-59.3)	-30.8 NA	47.6% notch		2.23
HLL-R10	-60	-26.3	-31.3	62.1% notch		2.93
HLL-R3	-60	-45.7	-52.7	71.2% notch		2.82

APPENDIX F 5% / 95% FAILURE PROBABILITY GRAPHS

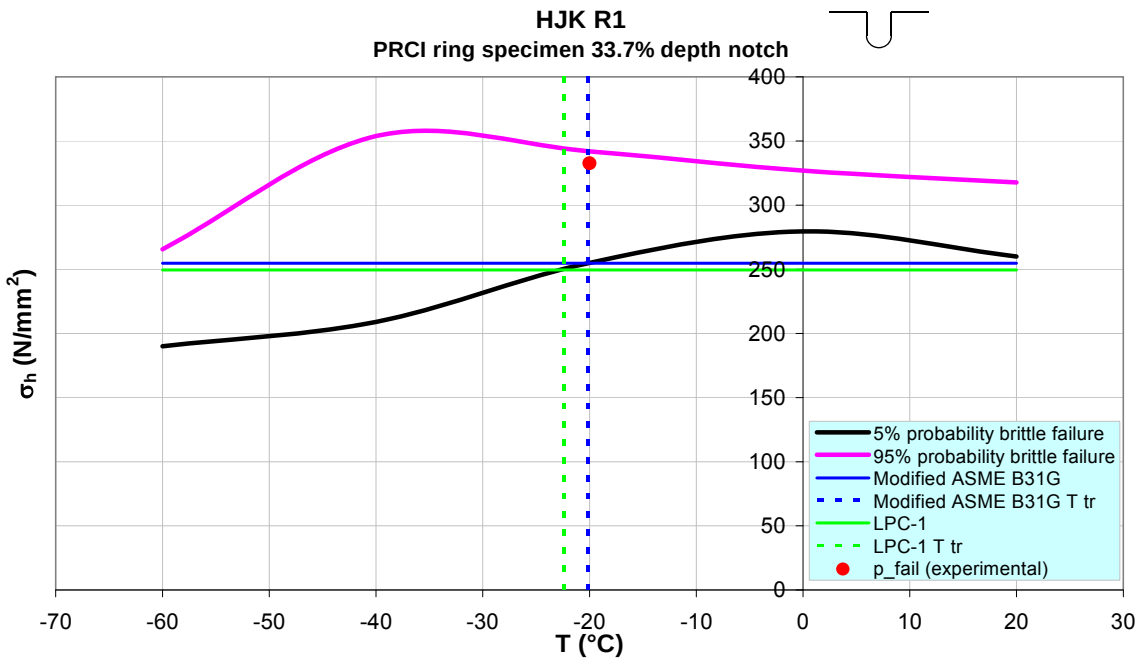

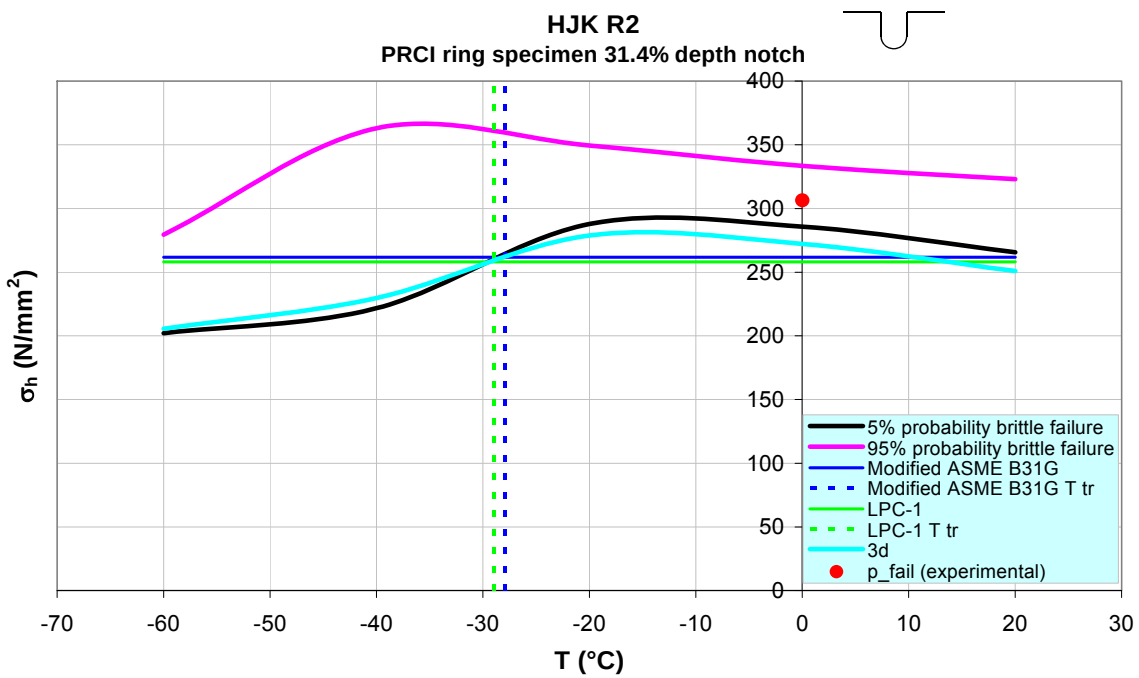

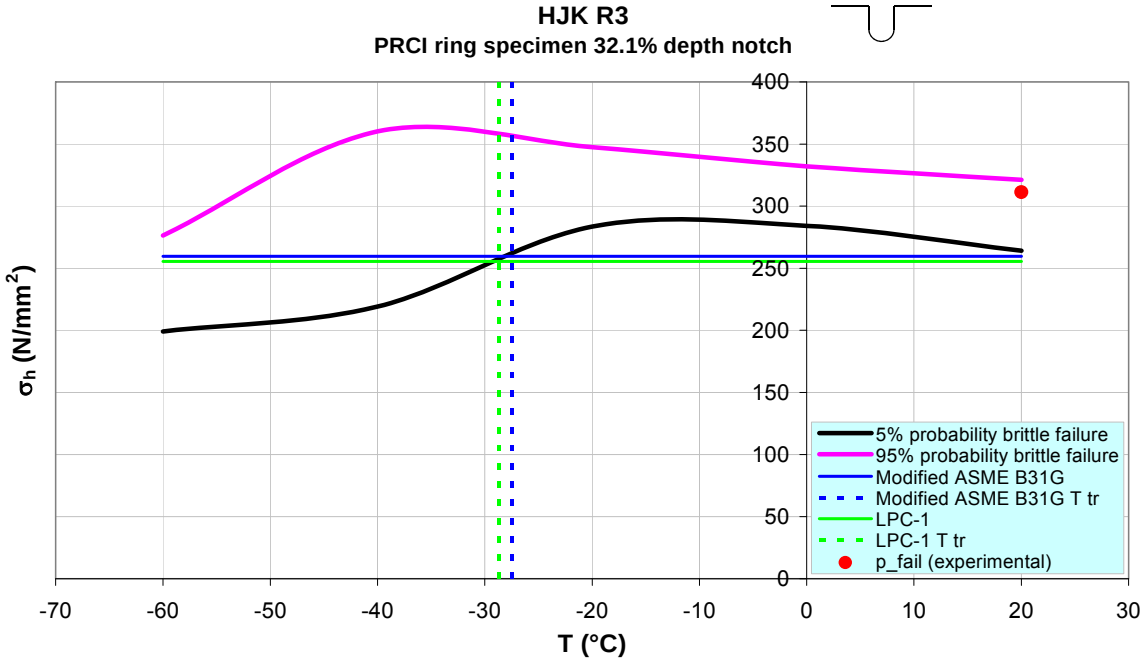
HJK R3
PRCI ring specimen 32.1% depth notch
σh (N/mm2)
T (°C)
400
350
300
250
200
150
100
50
0
-70
-60
-50
-40
-30
-20
-10
0
10
20
30
5% probability brittle failure
95% probability brittle failure
Modified ASME B31G
Modified ASME B31G T tr
LPC-1
LPC-1 T tr
p_fail (experimental)

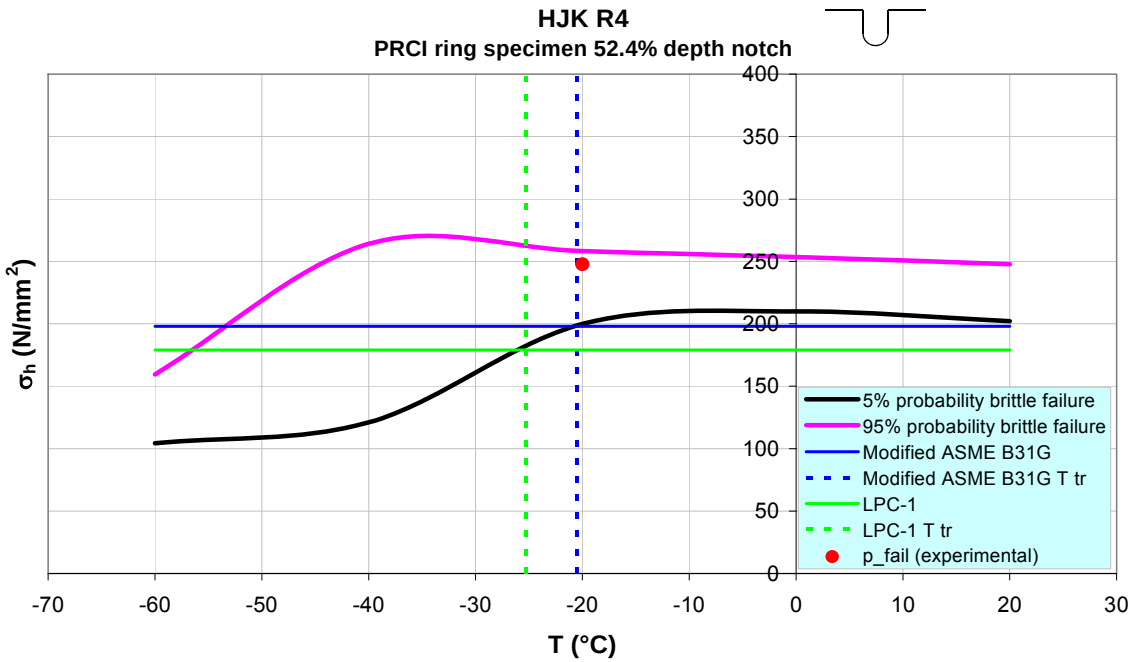
HJK R4
PRCI ring specimen 52.4% depth notch
σh (N/mm2)
T (°C)
400
350
300
250
200
150
100
50
0
-70
-60
-50
-40
-30
-20
-10
0
10
20
30
5% probability brittle failure
95% probability brittle failure
Modified ASME B31G
Modified ASME B31G T tr
LPC-1
LPC-1 T tr
p_fail (experimental)

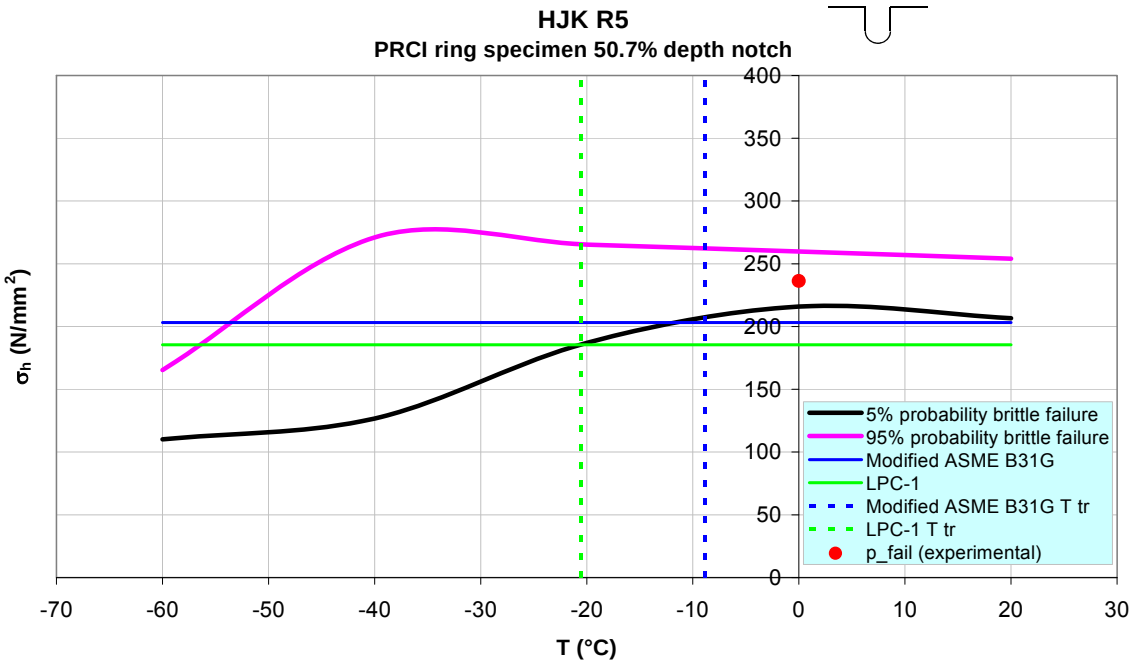
HJK R5
PRCI ring specimen 50.7% depth notch
σh (N/mm2)
T (°C)
400
350
300
250
200
150
100
50
0
-70
-60
-50
-40
-30
-20
-10
0
10
20
30
5% probability brittle failure
95% probability brittle failure
Modified ASME B31G
LPC-1
Modified ASME B31G T tr
LPC-1 T tr
p_fail (experimental)

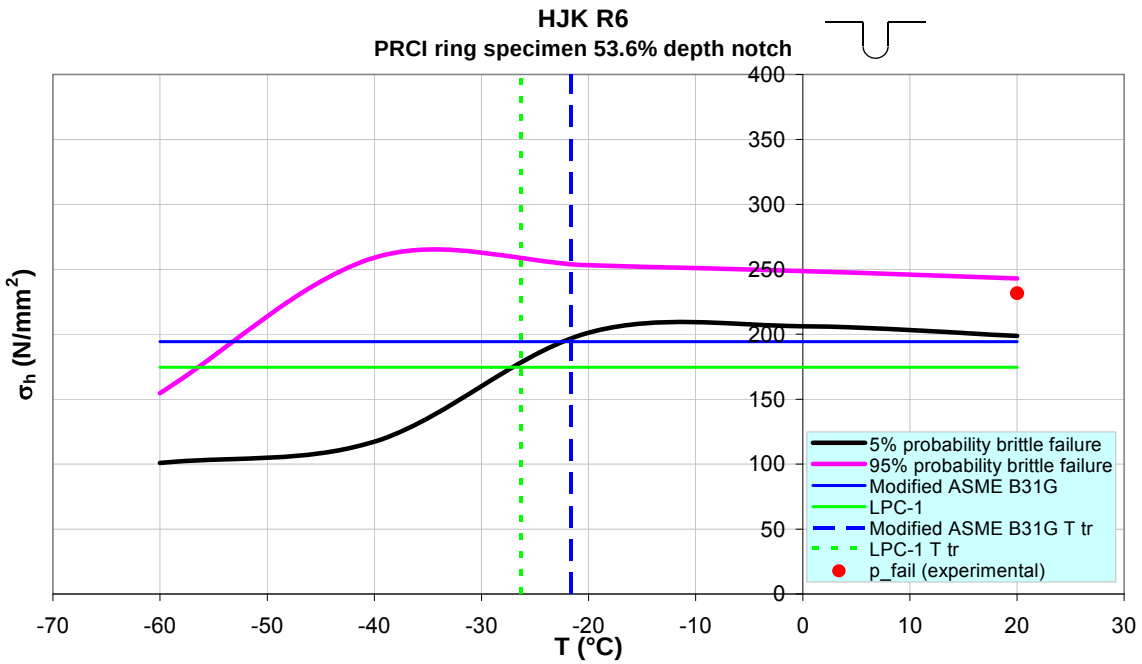
HJK R6
PRCI ring specimen 53.6% depth notch
σh (N/mm2)
T (°C)
400
350
300
250
200
150
100
50
0
-70
-60
-50
-40
-30
-20
-10
0
10
20
30
5% probability brittle failure
95% probability brittle failure
Modified ASME B31G
LPC-1
Modified ASME B31G T tr
LPC-1 T tr
p_fail (experimental)

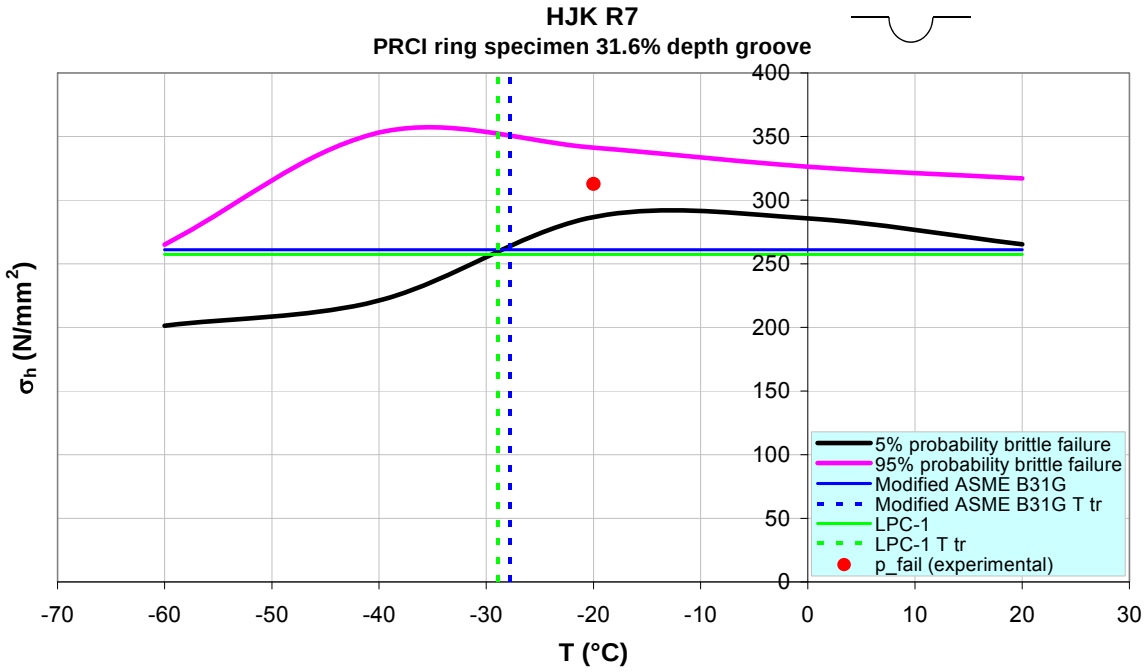
HJK R7
PRCI ring specimen 31.6% depth groove
σh (N/mm2)
T (°C)
400
350
300
250
200
150
100
50
0
-70
-60
-50
-40
-30
-20
-10
0
10
20
30
5% probability brittle failure
95% probability brittle failure
Modified ASME B31G
Modified ASME B31G T tr
LPC-1
LPC-1 T tr
p_fail (experimental)

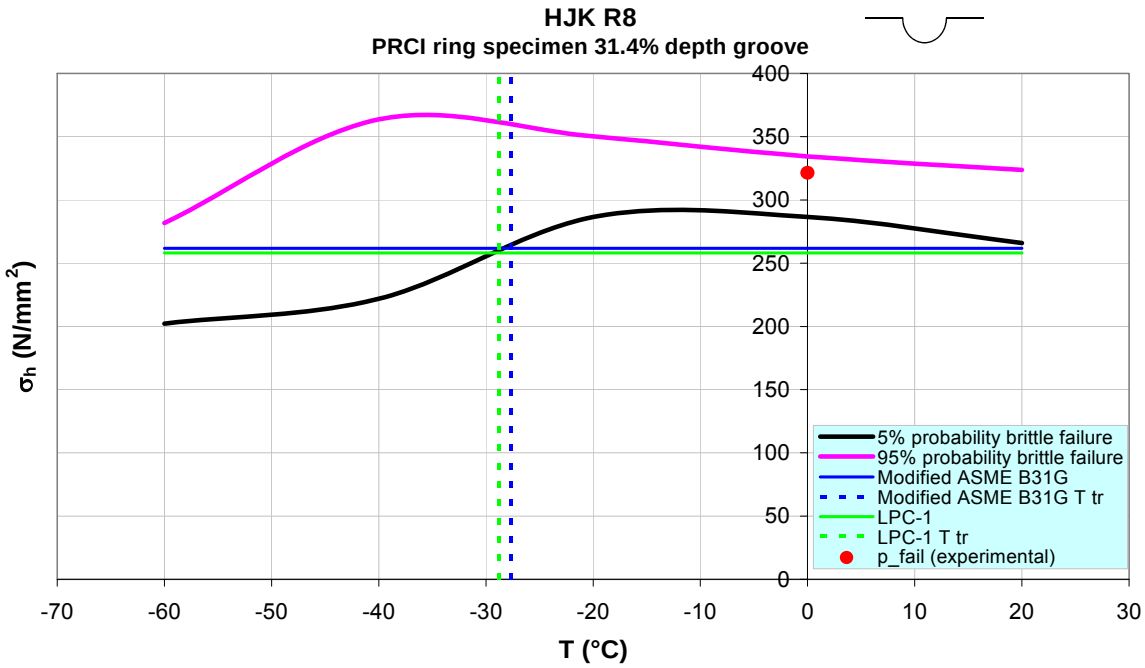
HJK R8
PRCI ring specimen 31.4% depth groove
σh (N/mm2)
T (°C)
400
350
300
250
200
150
100
50
0
-70
-60
-50
-40
-30
-20
-10
0
10
20
30
5% probability brittle failure
95% probability brittle failure
Modified ASME B31G
Modified ASME B31G T tr
LPC-1
LPC-1 T tr
p_fail (experimental)

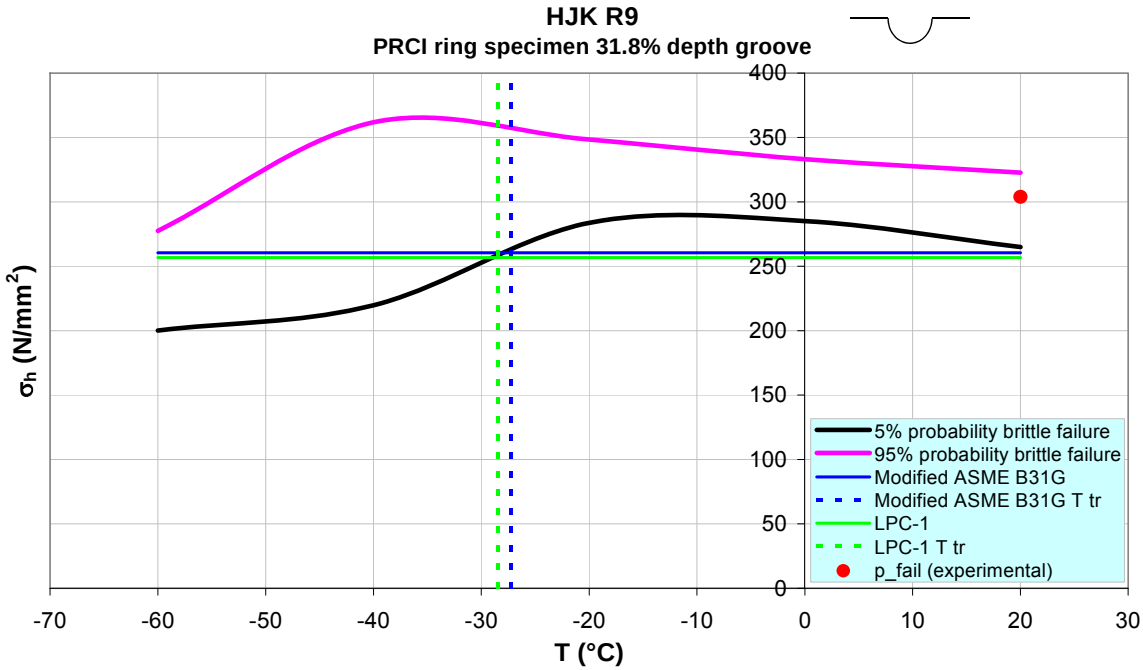
HJK R9
PRCI ring specimen 31.8% depth groove
σh (N/mm2)
T (°C)
400
350
300
250
200
150
100
50
0
-70
-60
-50
-40
-30
-20
-10
0
10
20
30
5% probability brittle failure
95% probability brittle failure
Modified ASME B31G
Modified ASME B31G T tr
LPC-1
LPC-1 T tr
p_fail (experimental)

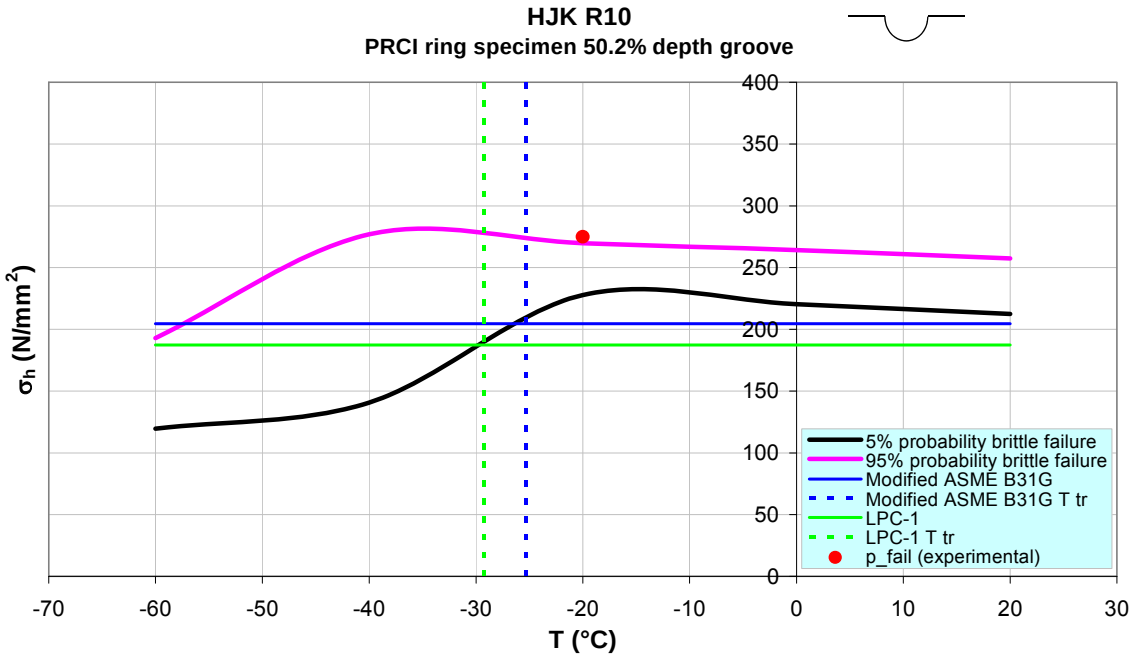
HJK R10
PRCI ring specimen 50.2% depth groove
σh (N/mm2)
T (°C)
400
350
300
250
200
150
100
50
0
-70
-60
-50
-40
-30
-20
-10
0
10
20
30
5% probability brittle failure
95% probability brittle failure
Modified ASME B31G
Modified ASME B31G T tr
LPC-1
LPC-1 T tr
p_fail (experimental)

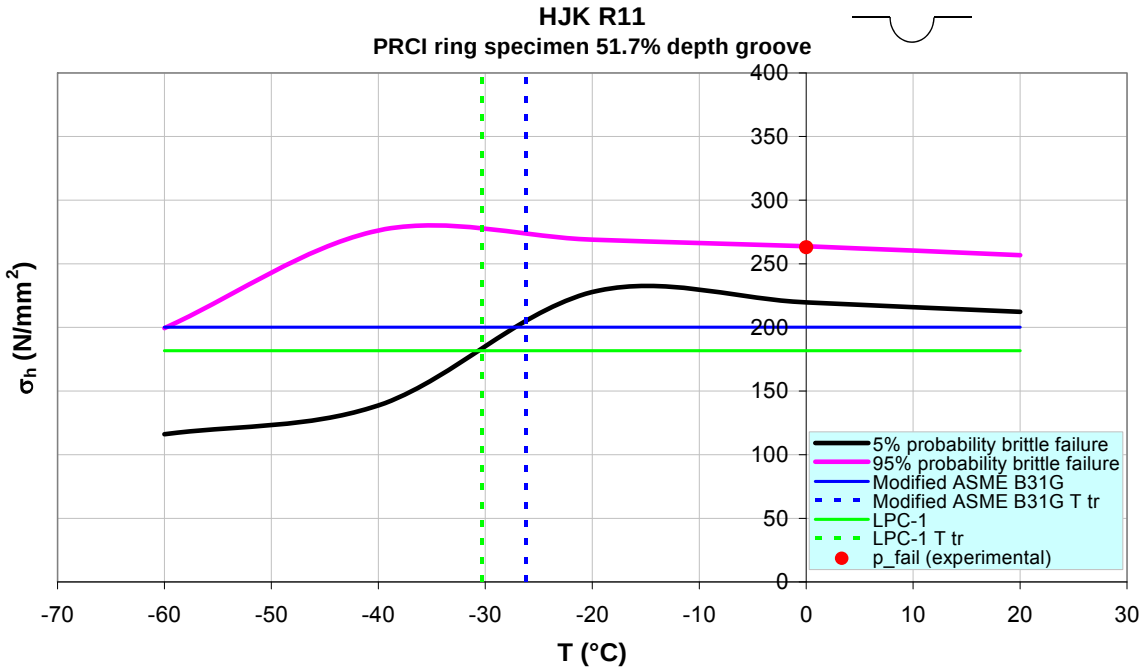
HJK R11
PRCI ring specimen 51.7% depth groove
σh (N/mm2)
T (°C)
400
350
300
250
200
150
100
50
0
-70
-60
-50
-40
-30
-20
-10
0
10
20
30
5% probability brittle failure
95% probability brittle failure
Modified ASME B31G
Modified ASME B31G T tr
LPC-1
LPC-1 T tr
p_fail (experimental)

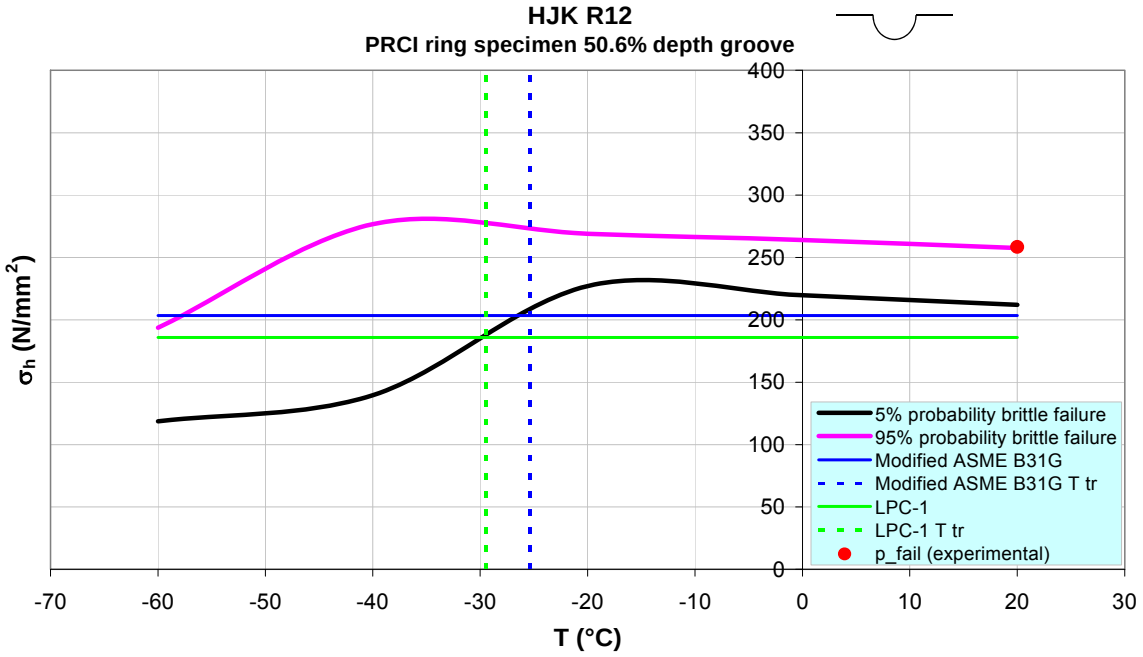
HJK R12
PRCI ring specimen 50.6% depth groove
σh (N/mm2)
T (°C)
400
350
300
250
200
150
100
50
0
-70
-60
-50
-40
-30
-20
-10
0
10
20
30
5% probability brittle failure
95% probability brittle failure
Modified ASME B31G
Modified ASME B31G T tr
LPC-1
LPC-1 T tr
p_fail (experimental)

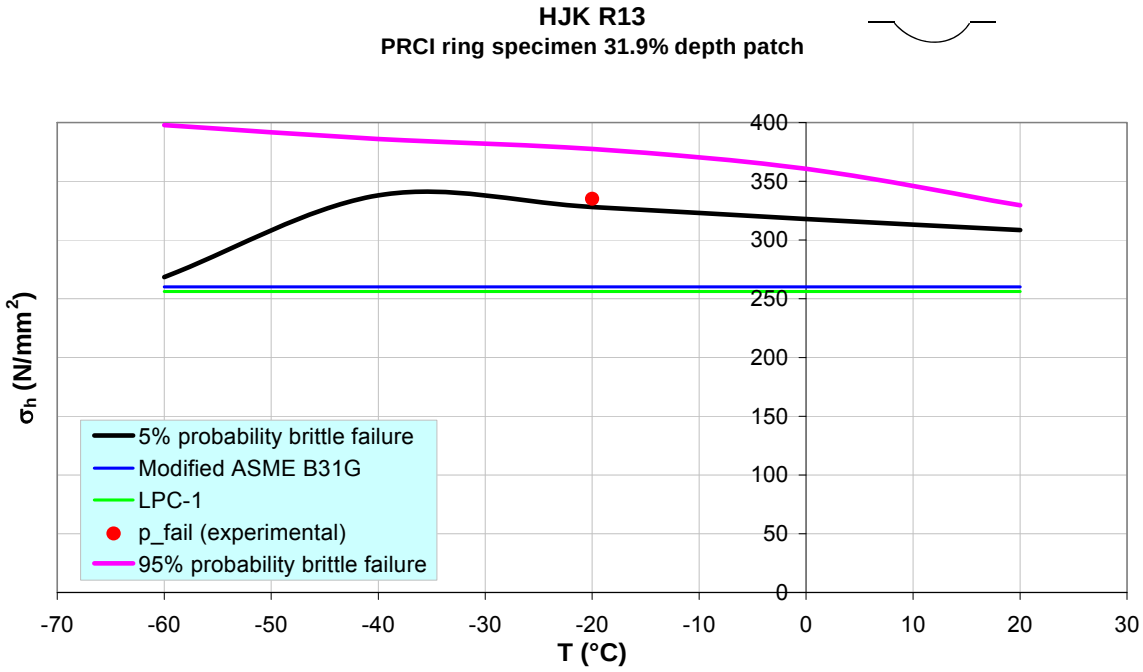
HJK R13
PRCI ring specimen 31.9% depth patch
σh (N/mm2)
T (°C)
5% probability brittle failure
Modified ASME B31G
LPC-1
p_fail (experimental)
95% probability brittle failure
400
350
300
250
200
150
100
50
0
-70
-60
-50
-40
-30
-20
-10
0
10
20
30

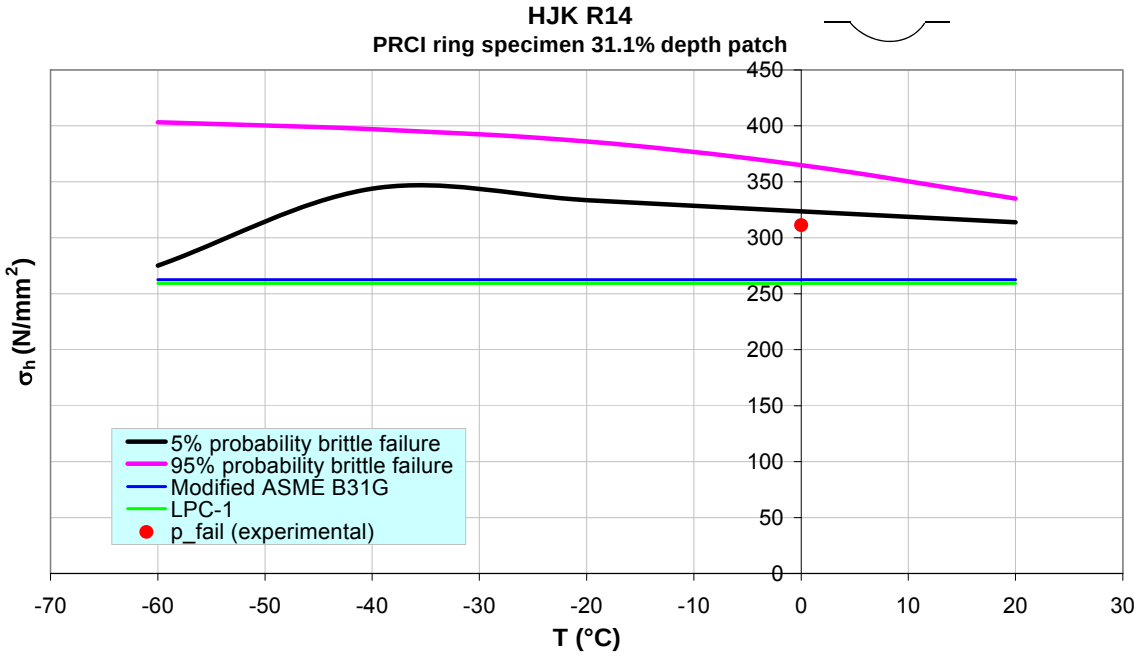
HJK R14
PRCI ring specimen 31.1% depth patch
σh (N/mm2)
T (°C)
5% probability brittle failure
95% probability brittle failure
Modified ASME B31G
LPC-1
p_fail (experimental)
450
400
350
300
250
200
150
100
50
0
-70
-60
-50
-40
-30
-20
-10
0
10
20
30

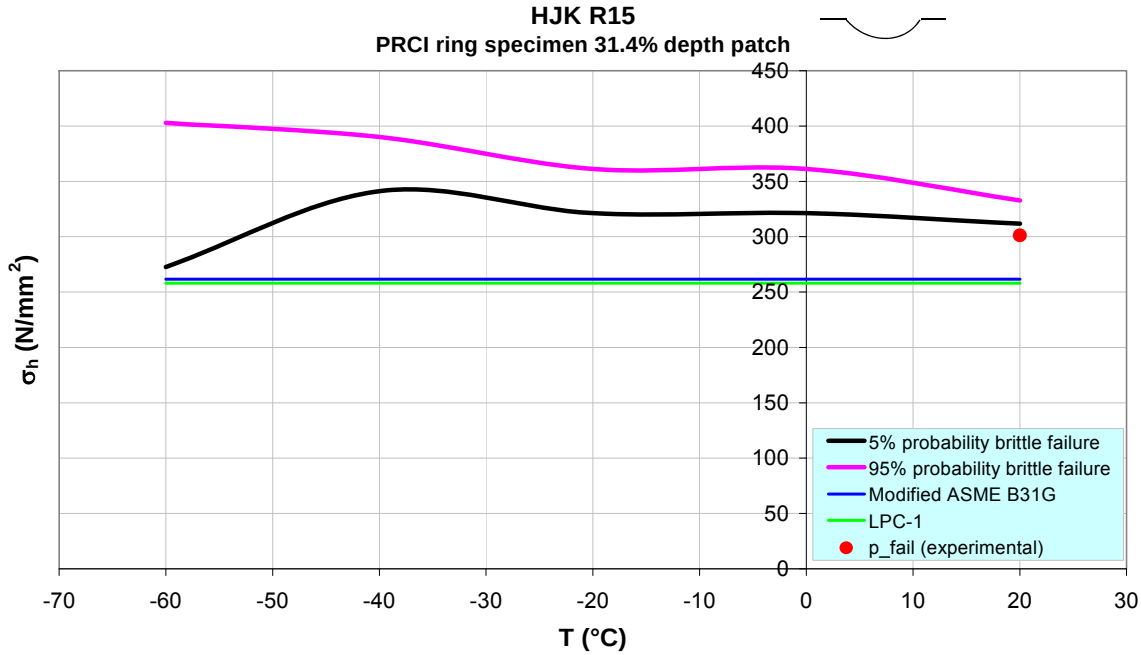
HJK R15
PRCI ring specimen 31.4% depth patch
σh (N/mm2)
T (°C)
450
400
350
300
250
200
150
100
50
0
-70
-60
-50
-40
-30
-20
-10
0
10
20
30
5% probability brittle failure
95% probability brittle failure
Modified ASME B31G
LPC-1
p_fail (experimental)

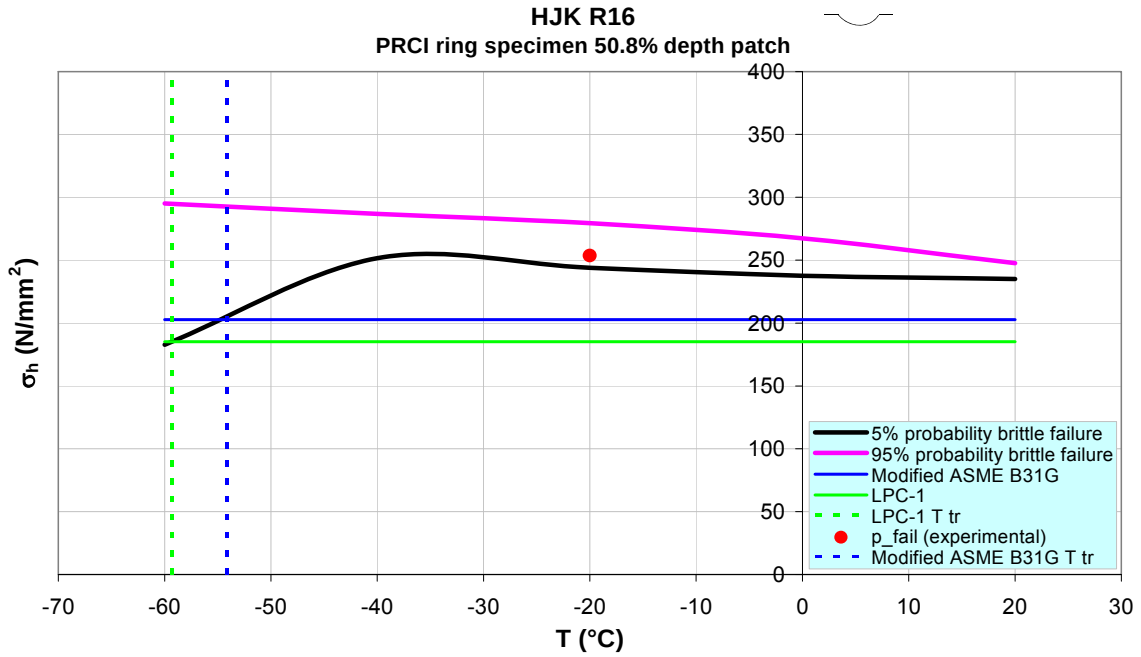
HJK R16
PRCI ring specimen 50.8% depth patch
σh (N/mm2)
T (°C)
400
350
300
250
200
150
100
50
0
-70
-60
-50
-40
-30
-20
-10
0
10
20
30
5% probability brittle failure
95% probability brittle failure
Modified ASME B31G
LPC-1
LPC-1 T tr
p_fail (experimental)
Modified ASME B31G T tr

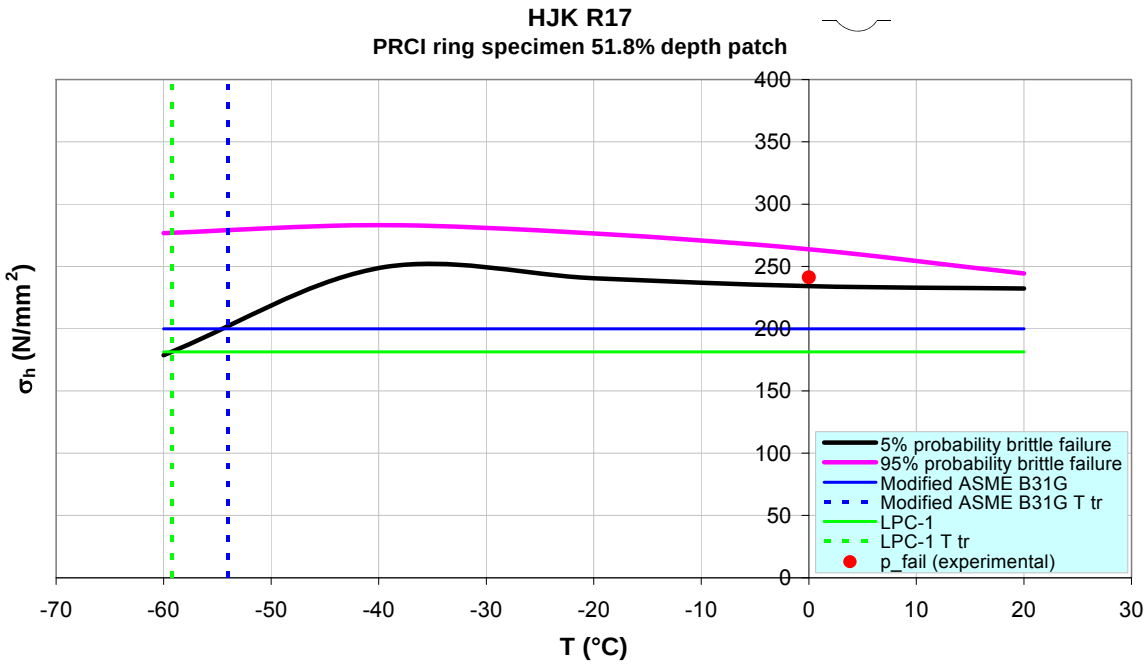
HJK R17
PRCI ring specimen 51.8% depth patch
σh (N/mm2)
T (°C)
400
350
300
250
200
150
100
50
0
-70
-60
-50
-40
-30
-20
-10
0
10
20
30
5% probability brittle failure
95% probability brittle failure
Modified ASME B31G
Modified ASME B31G T tr
LPC-1
LPC-1 T tr
p_fail (experimental)

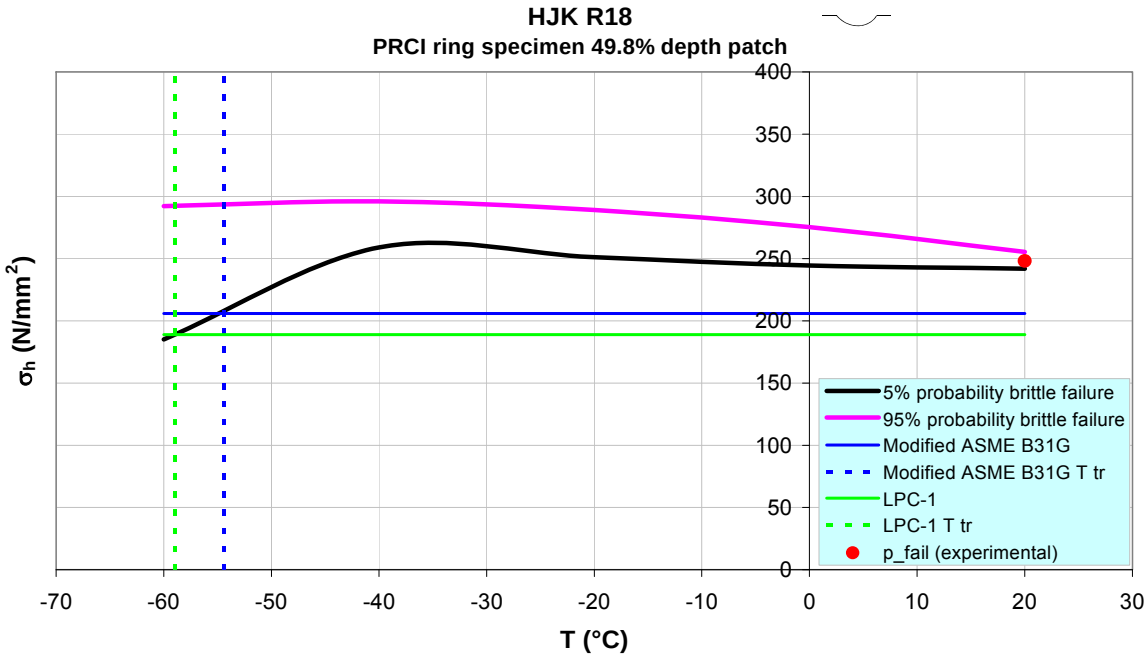
HJK R18
PRCI ring specimen 49.8% depth patch
σh (N/mm2)
T (°C)
400
350
300
250
200
150
100
50
0
-70
-60
-50
-40
-30
-20
-10
0
10
20
30
5% probability brittle failure
95% probability brittle failure
Modified ASME B31G
Modified ASME B31G T tr
LPC-1
LPC-1 T tr
p_fail (experimental)

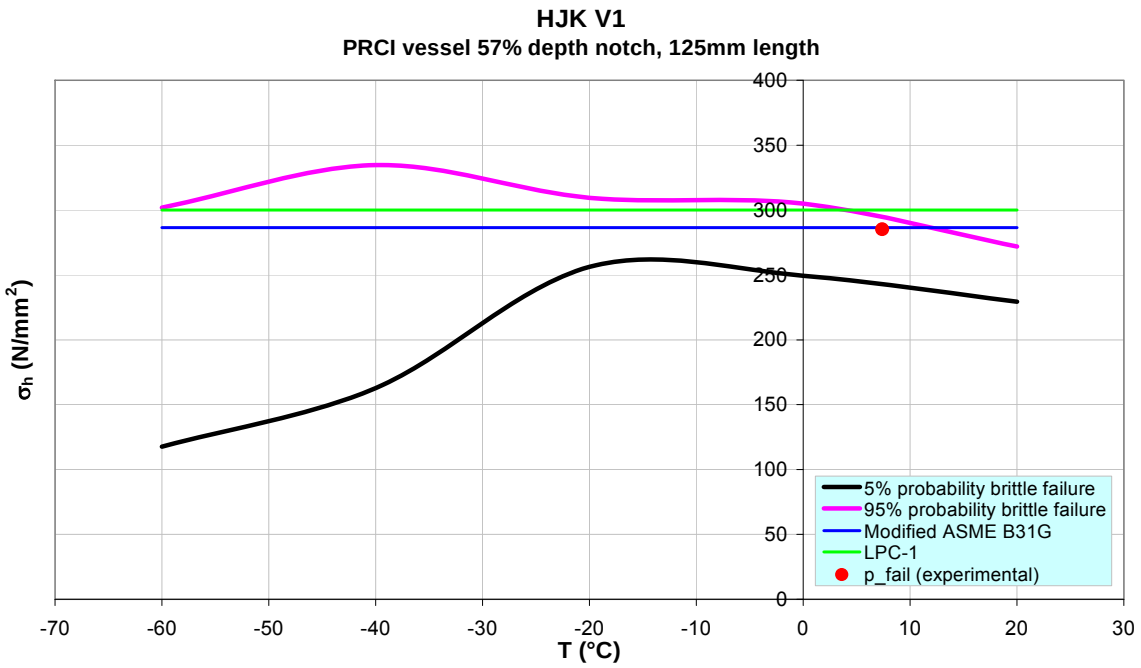
HJK V1
PRCI vessel 57% depth notch, 125mm length
σh (N/mm2)
T (°C)
400
350
300
250
200
150
100
50
0
-70
-60
-50
-40
-30
-20
-10
0
10
20
30
5% probability brittle failure
95% probability brittle failure
Modified ASME B31G
LPC-1
p_fail (experimental)

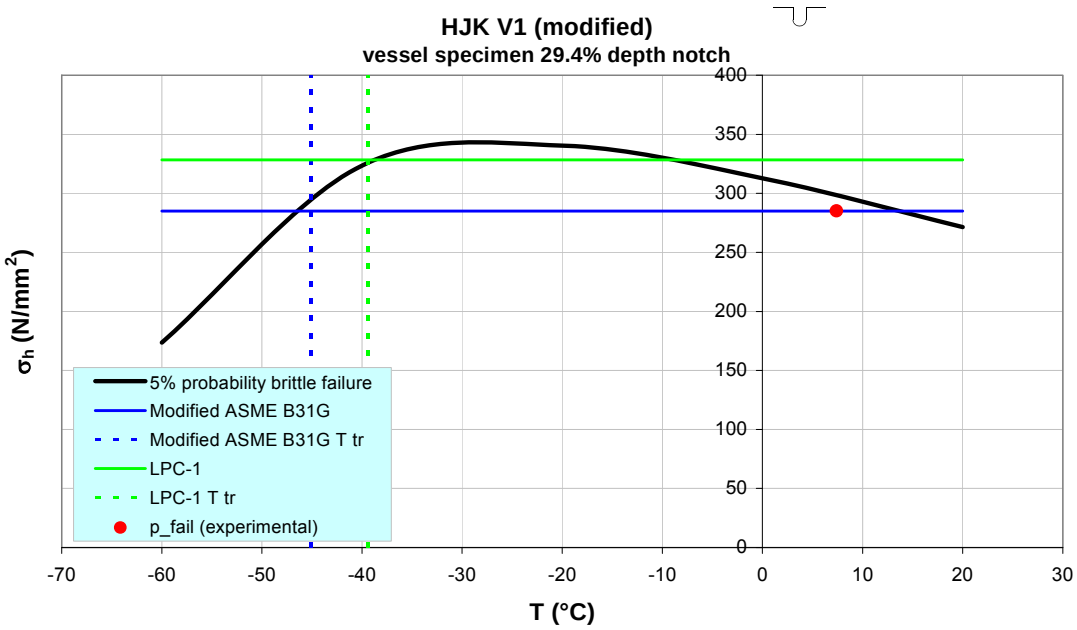
HJK V1 (modified)
vessel specimen 29.4% depth notch
σh (N/mm2)
T (°C)
400
350
300
250
200
150
100
50
0
-70
-60
-50
-40
-30
-20
-10
0
10
20
30
5% probability brittle failure
Modified ASME B31G
Modified ASME B31G T tr
LPC-1
LPC-1 T tr
p_fail (experimental)

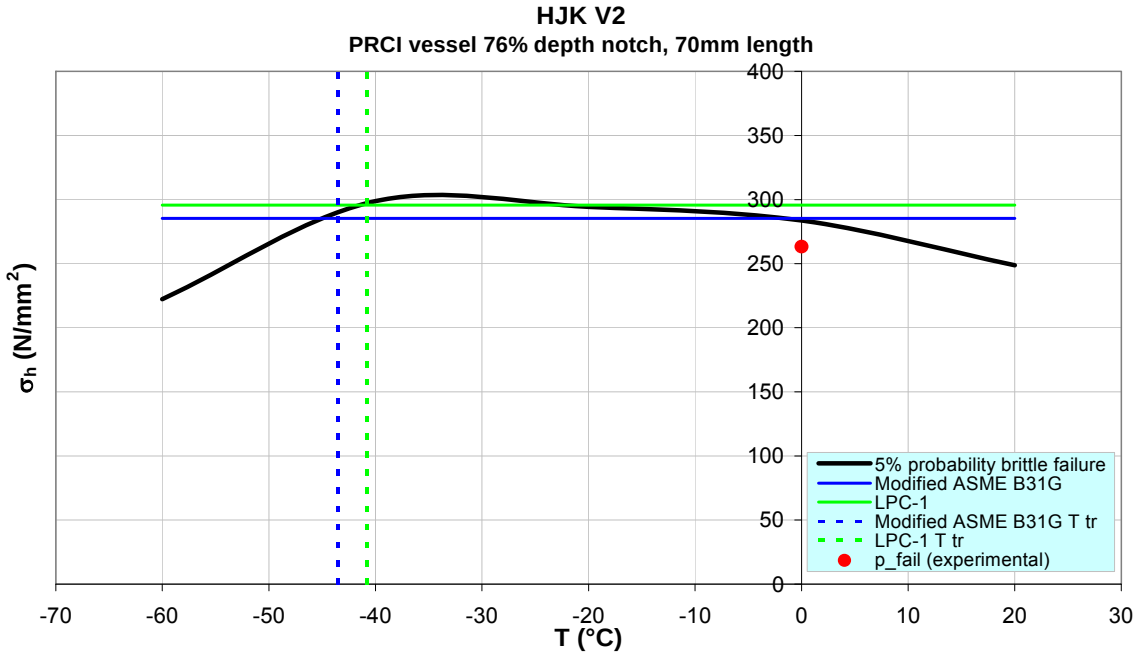
HJK V2
PRCI vessel 76% depth notch, 70mm length
σh (N/mm2)
T (°C)
400
350
300
250
200
150
100
50
0
-70
-60
-50
-40
-30
-20
-10
0
10
20
30
5% probability brittle failure
Modified ASME B31G
LPC-1
Modified ASME B31G T tr
LPC-1 T tr
p_fail (experimental)

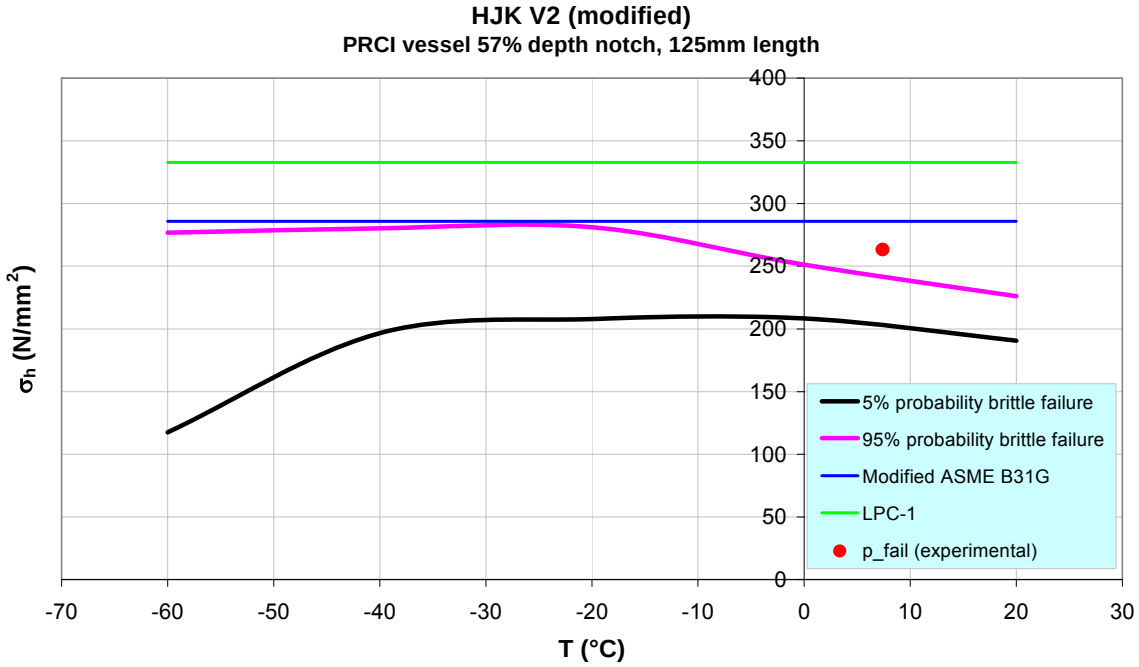
HJK V2 (modified)
PRCI vessel 57% depth notch, 125mm length
σh (N/mm2)
T (°C)
400
350
300
250
200
150
100
50
0
-70
-60
-50
-40
-30
-20
-10
0
10
20
30
5% probability brittle failure
95% probability brittle failure
Modified ASME B31G
LPC-1
p_fail (experimental)

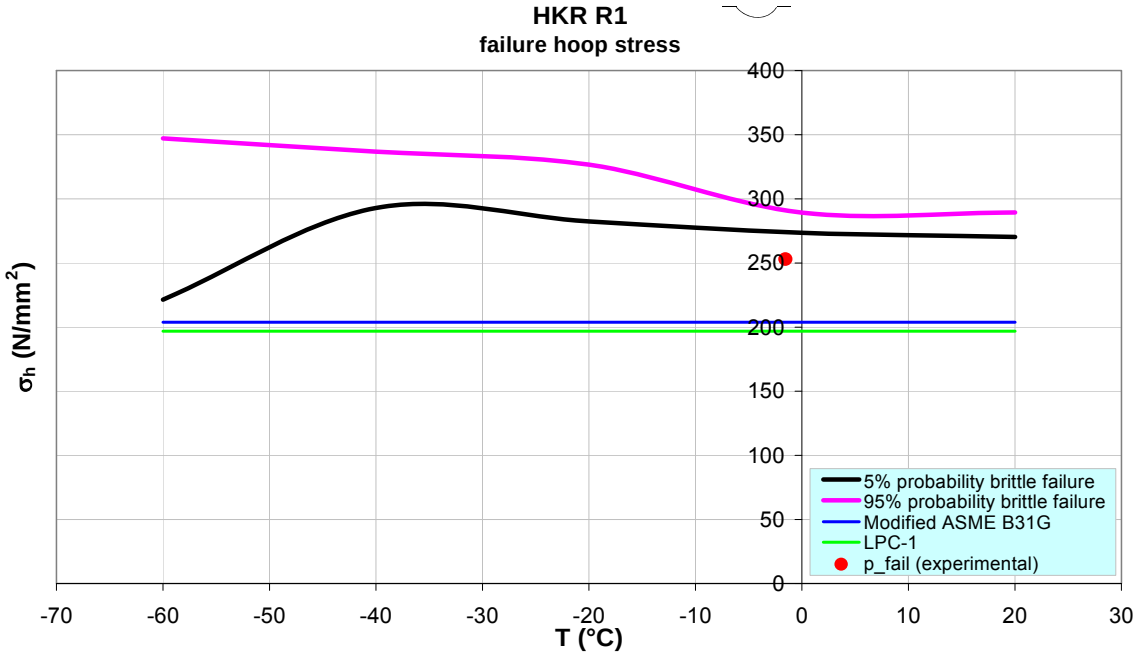
HKR R1
failure hoop stress
σh (N/mm2)
T (°C)
400
350
300
250
200
150
100
50
0
-70
-60
-50
-40
-30
-20
-10
0
10
20
30
5% probability brittle failure
95% probability brittle failure
Modified ASME B31G
LPC-1
p_fail (experimental)

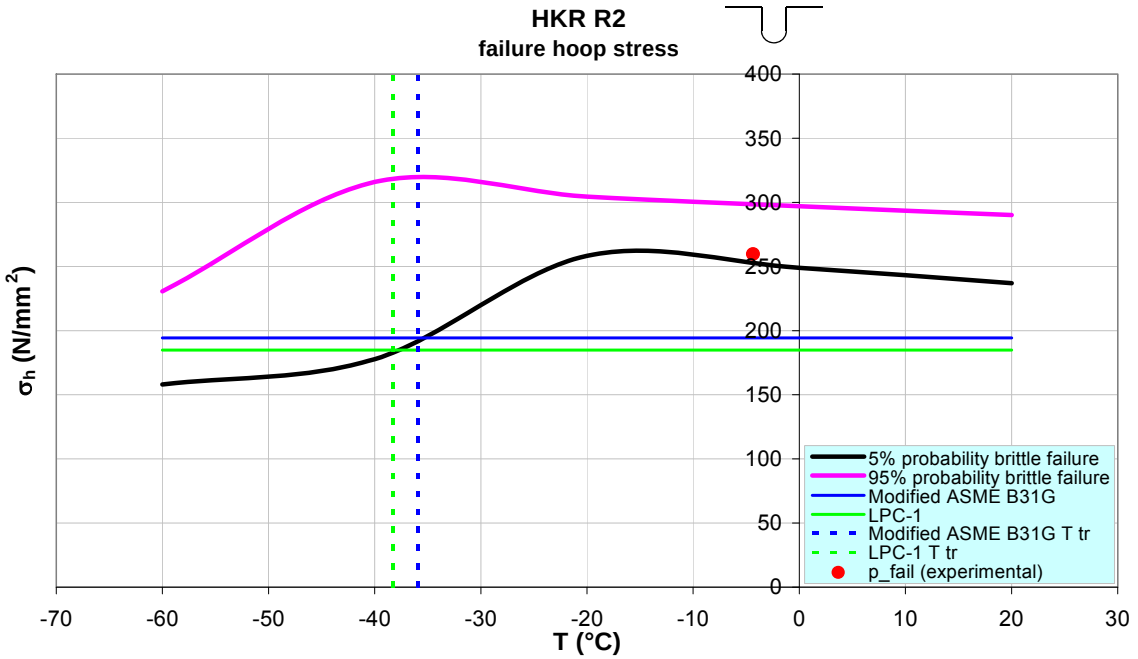
HKR R2
failure hoop stress
σh (N/mm2)
T (°C)
400
350
300
250
200
150
100
50
0
-70
-60
-50
-40
-30
-20
-10
0
10
20
30
5% probability brittle failure
95% probability brittle failure
Modified ASME B31G
LPC-1
Modified ASME B31G T tr
LPC-1 T tr
p_fail (experimental)

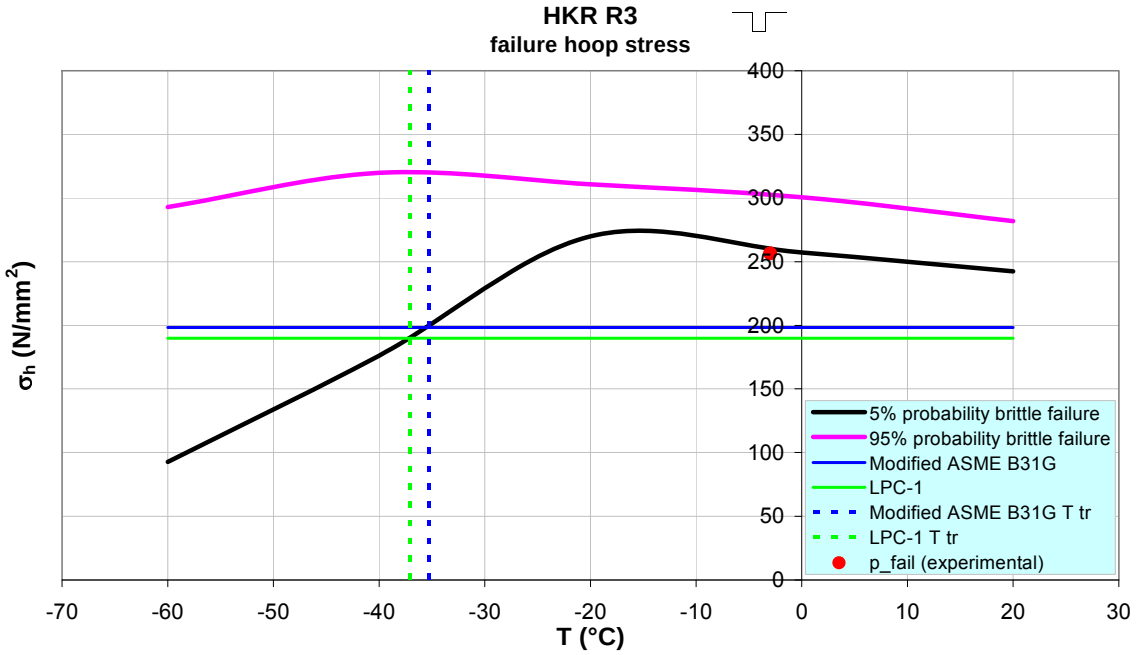
HKR R3
failure hoop stress
σh (N/mm2)
T (°C)
400
350
300
250
200
150
100
50
0
-70
-60
-50
-40
-30
-20
-10
0
10
20
30
5% probability brittle failure
95% probability brittle failure
Modified ASME B31G
LPC-1
Modified ASME B31G T tr
LPC-1 T tr
p_fail (experimental)

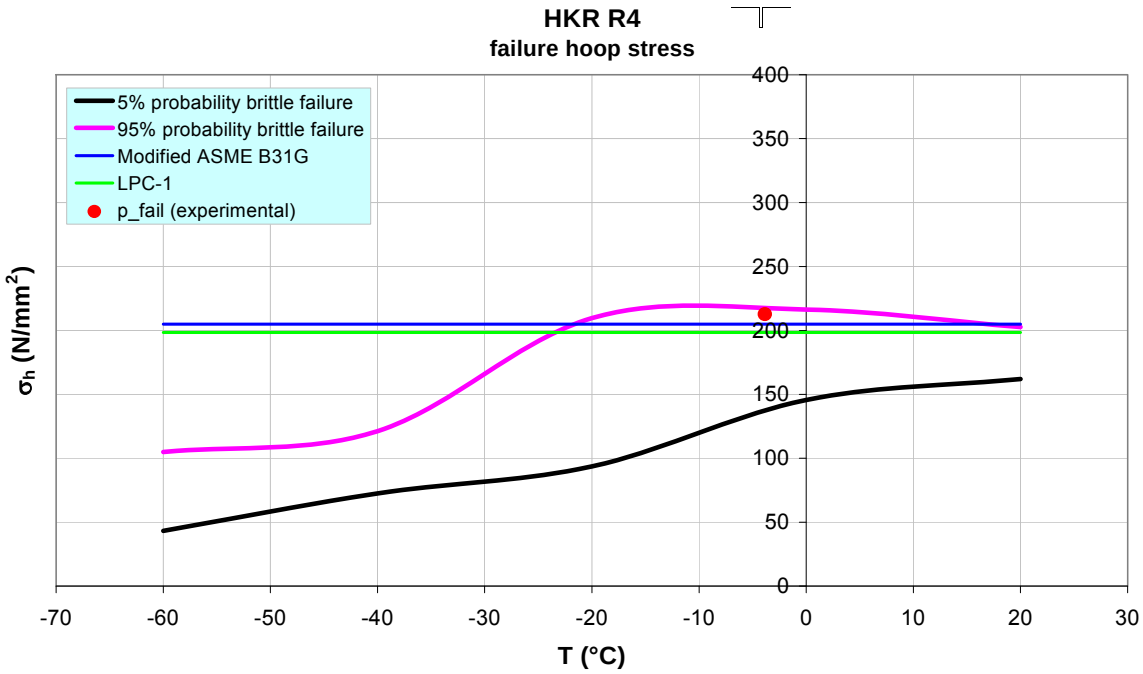
HKR R4
failure hoop stress
σh (N/mm2)
T (°C)
400
350
300
250
200
150
100
50
0
-70
-60
-50
-40
-30
-20
-10
0
10
20
30
5% probability brittle failure
95% probability brittle failure
Modified ASME B31G
LPC-1
p_fail (experimental)

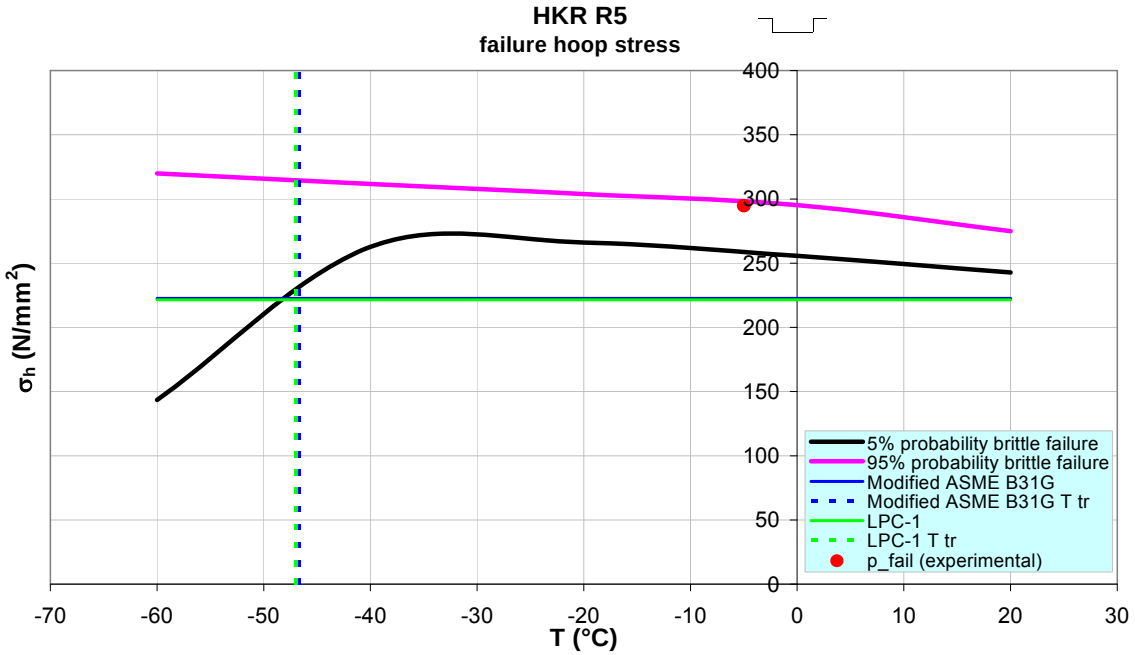
HKR R5
failure hoop stress
σh (N/mm2)
T (°C)
400
350
300
250
200
150
100
50
0
-70
-60
-50
-40
-30
-20
-10
0
10
20
30
5% probability brittle failure
95% probability brittle failure
Modified ASME B31G
Modified ASME B31G T tr
LPC-1
LPC-1 T tr
p_fail (experimental)

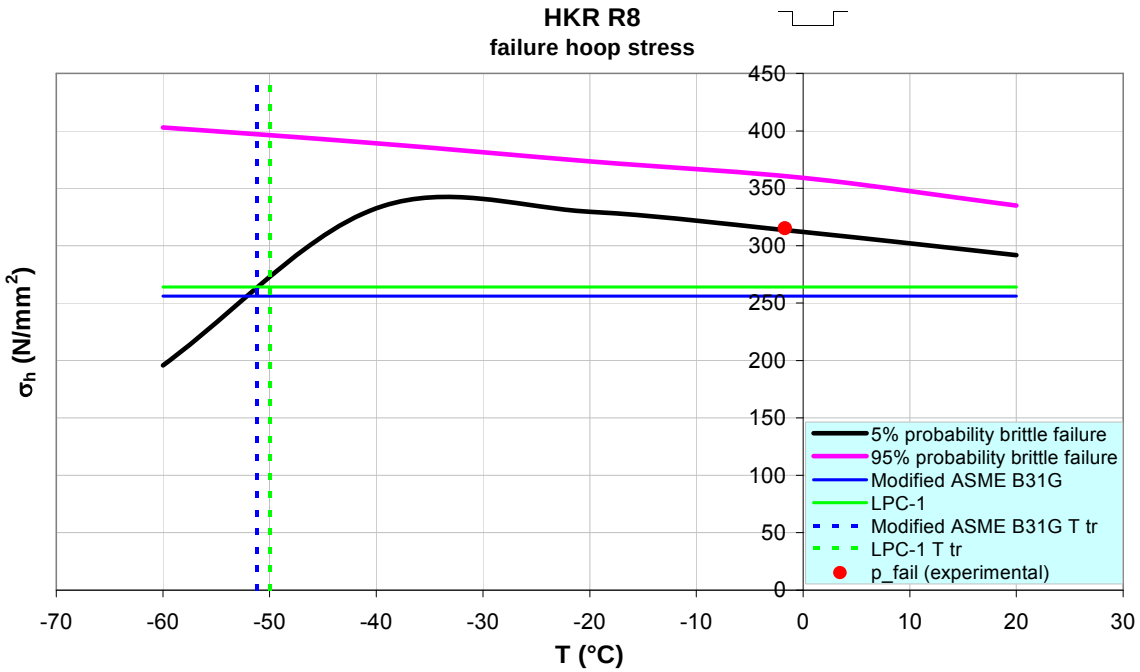
HKR R8
failure hoop stress
σh (N/mm2)
T (°C)
450
400
350
300
250
200
150
100
50
0
-70
-60
-50
-40
-30
-20
-10
0
10
20
30
5% probability brittle failure
95% probability brittle failure
Modified ASME B31G
LPC-1
Modified ASME B31G T tr
LPC-1 T tr
p_fail (experimental)

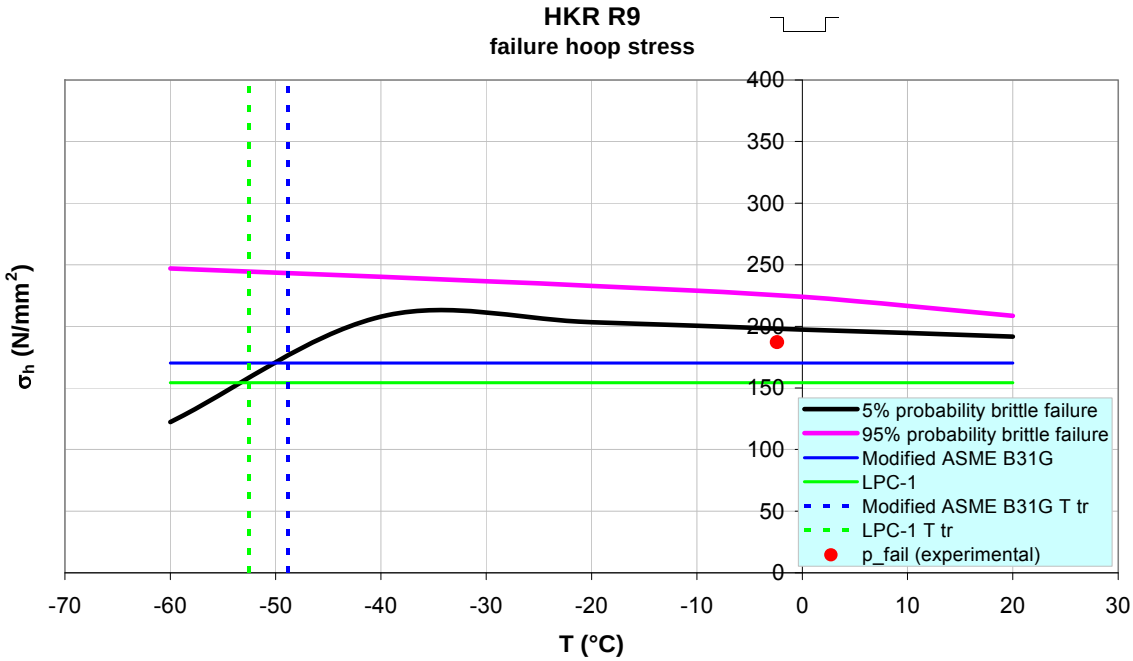
HKR R9
failure hoop stress
σh (N/mm2)
T (°C)
400
350
300
250
200
150
100
50
0
-70
-60
-50
-40
-30
-20
-10
0
10
20
30
5% probability brittle failure
95% probability brittle failure
Modified ASME B31G
LPC-1
Modified ASME B31G T tr
LPC-1 T tr
p_fail (experimental)

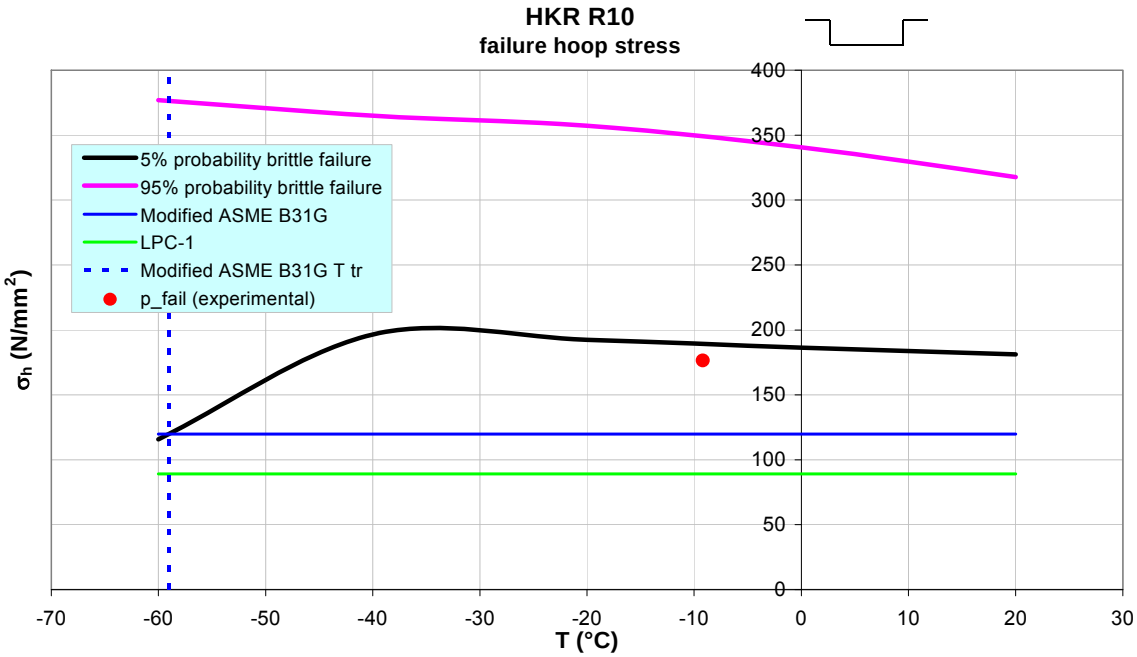
HKR R10
failure hoop stress
σh (N/mm2)
T (°C)
400
350
300
250
200
150
100
50
0
-70
-60
-50
-40
-30
-20
-10
0
10
20
30
5% probability brittle failure
95% probability brittle failure
Modified ASME B31G
LPC-1
Modified ASME B31G T tr
p_fail (experimental)

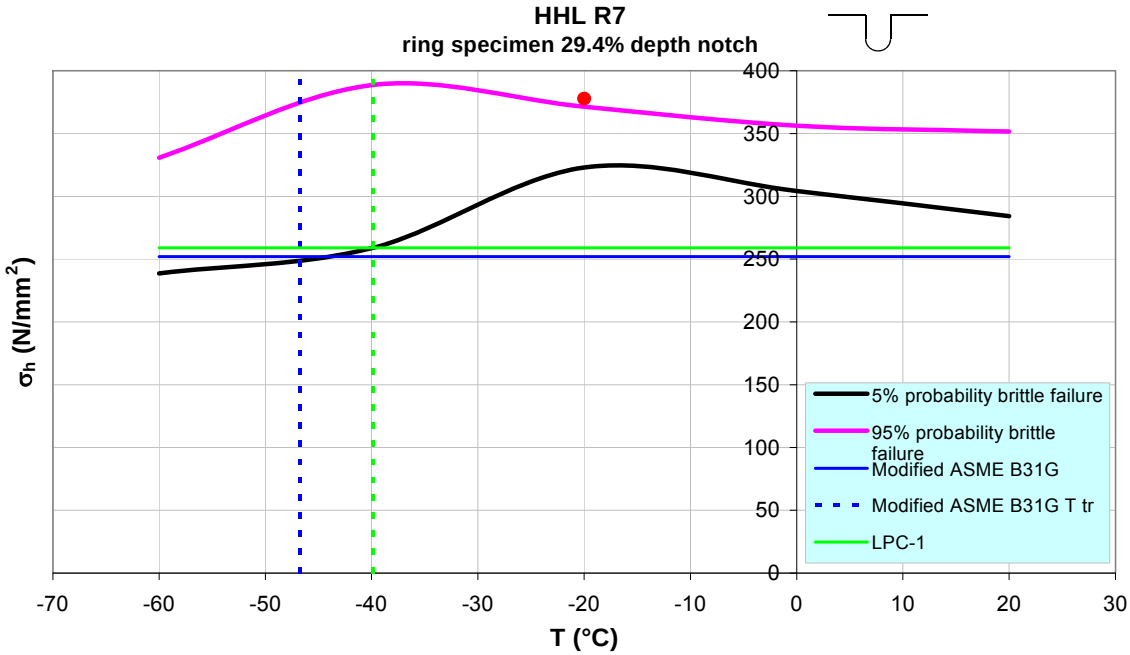
HHL R7
ring specimen 29.4% depth notch
σh (N/mm2)
T (°C)
400
350
300
250
200
150
100
50
0
-70
-60
-50
-40
-30
-20
-10
0
10
20
30
5% probability brittle failure
95% probability brittle failure
Modified ASME B31G
Modified ASME B31G T tr
LPC-1

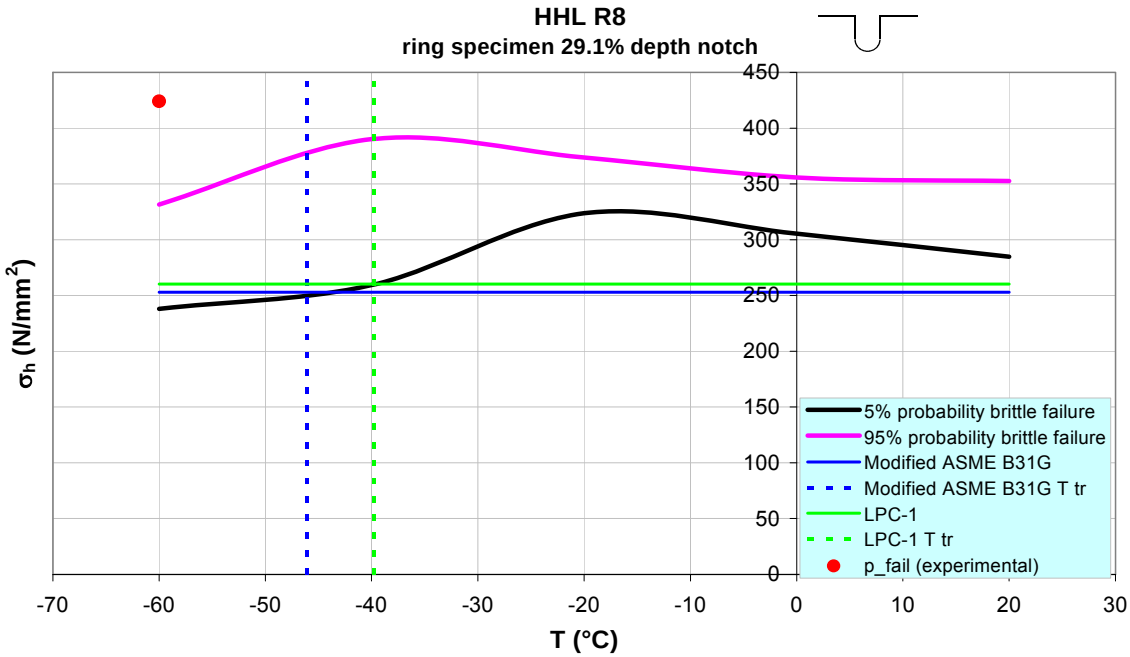
HHL R8
ring specimen 29.1% depth notch
σh (N/mm2)
T (°C)
450
400
350
300
250
200
150
100
50
0
-70
-60
-50
-40
-30
-20
-10
0
10
20
30
5% probability brittle failure
95% probability brittle failure
Modified ASME B31G
Modified ASME B31G T tr
LPC-1
LPC-1 T tr
p_fail (experimental)

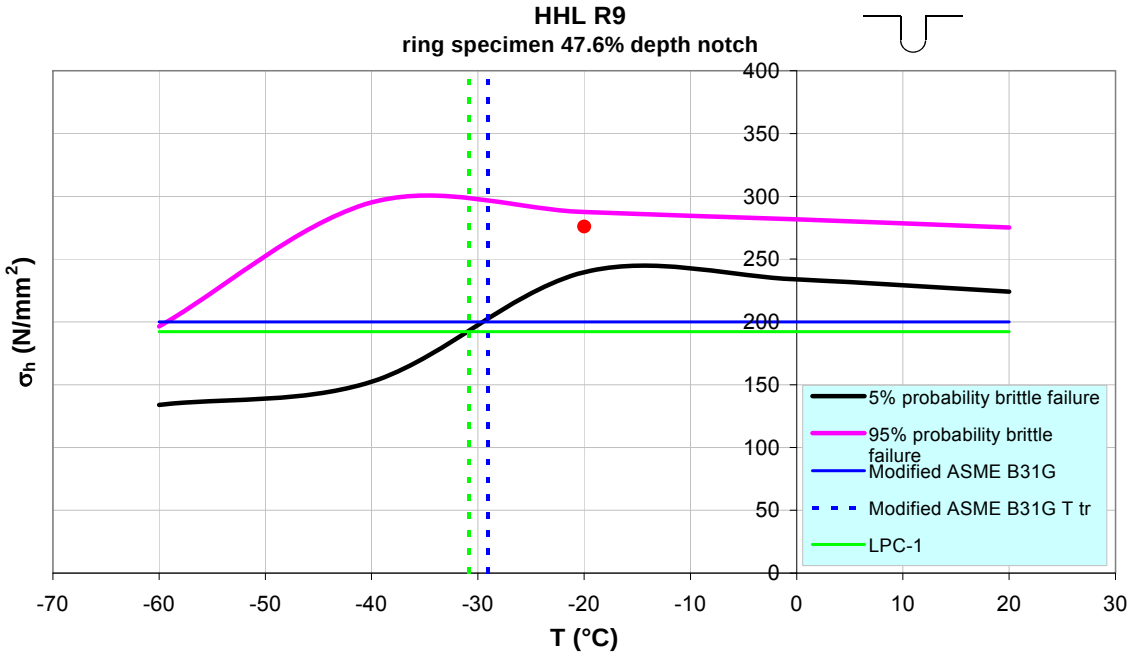
HHL R9
ring specimen 47.6% depth notch
σh (N/mm2)
T (°C)
400
350
300
250
200
150
100
50
0
-70
-60
-50
-40
-30
-20
-10
0
10
20
30
5% probability brittle failure
95% probability brittle failure
Modified ASME B31G
Modified ASME B31G T tr
LPC-1

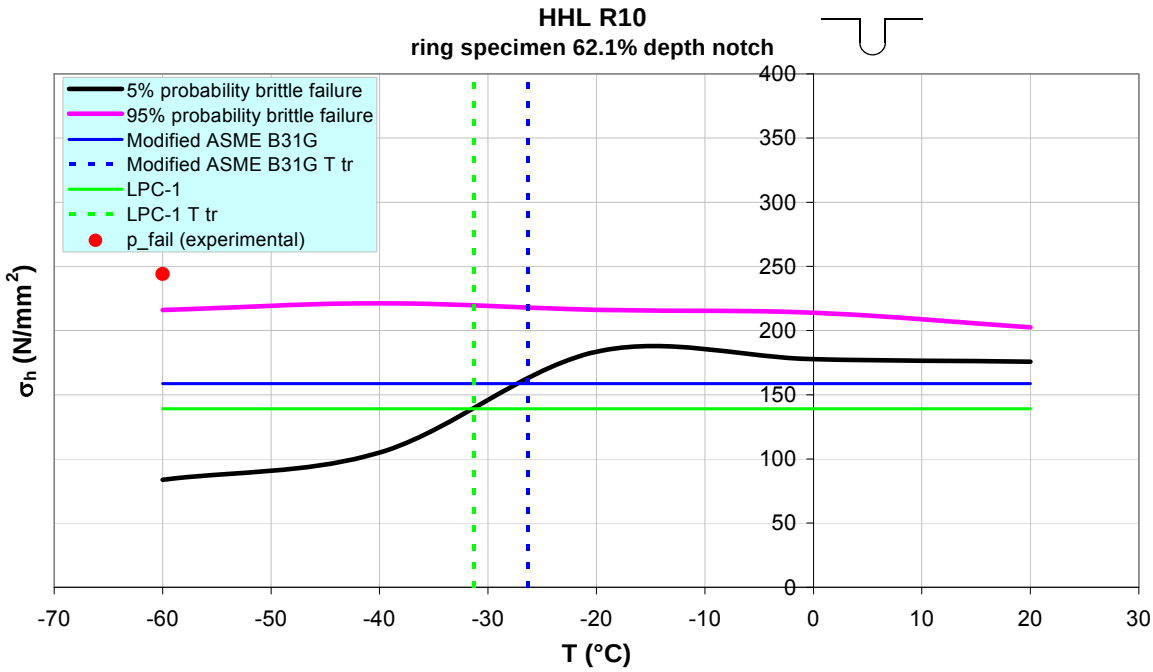
HHL R10
ring specimen 62.1% depth notch
σh (N/mm2)
T (°C)
400
350
300
250
200
150
100
50
0
-70
-60
-50
-40
-30
-20
-10
0
10
20
30
5% probability brittle failure
95% probability brittle failure
Modified ASME B31G
Modified ASME B31G T tr
LPC-1
LPC-1 T tr
p_fail (experimental)

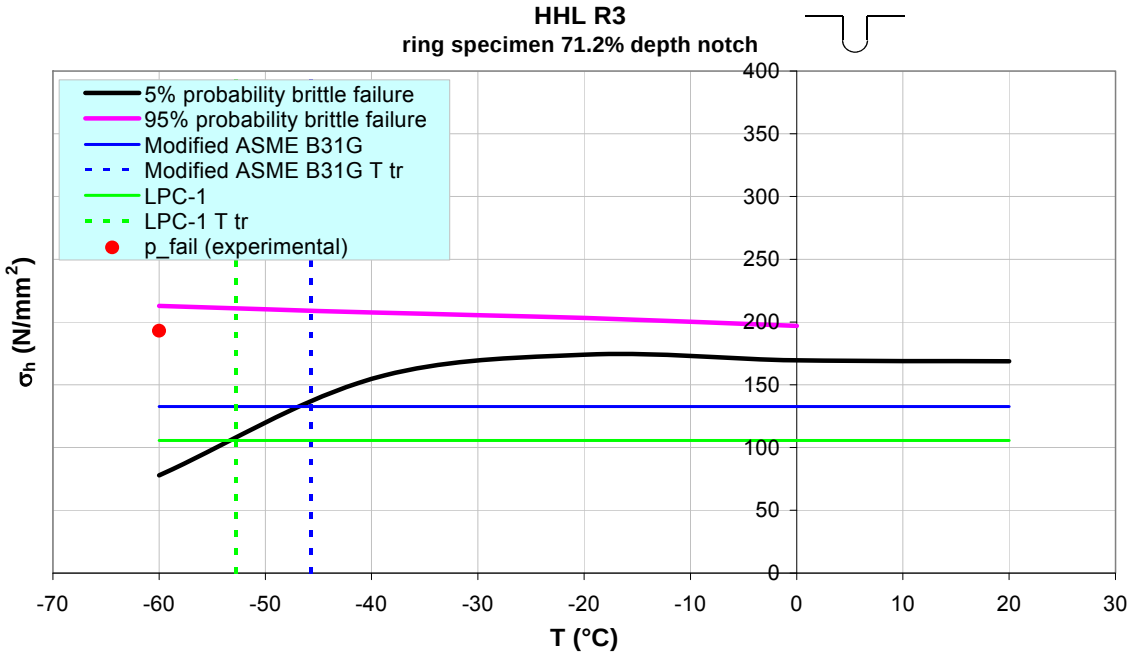
HHL R3
ring specimen 71.2% depth notch
5% probability brittle failure
95% probability brittle failure
Modified ASME B31G
Modified ASME B31G T tr
LPC-1
LPC-1 T tr
p_fail (experimental)
σh (N/mm2)
T (°C)
400
350
300
250
200
150
100
50
0
-70
-60
-50
-40
-30
-20
-10
0
10
20
30

APPENDIX G PROCEDURE FLOWCHART

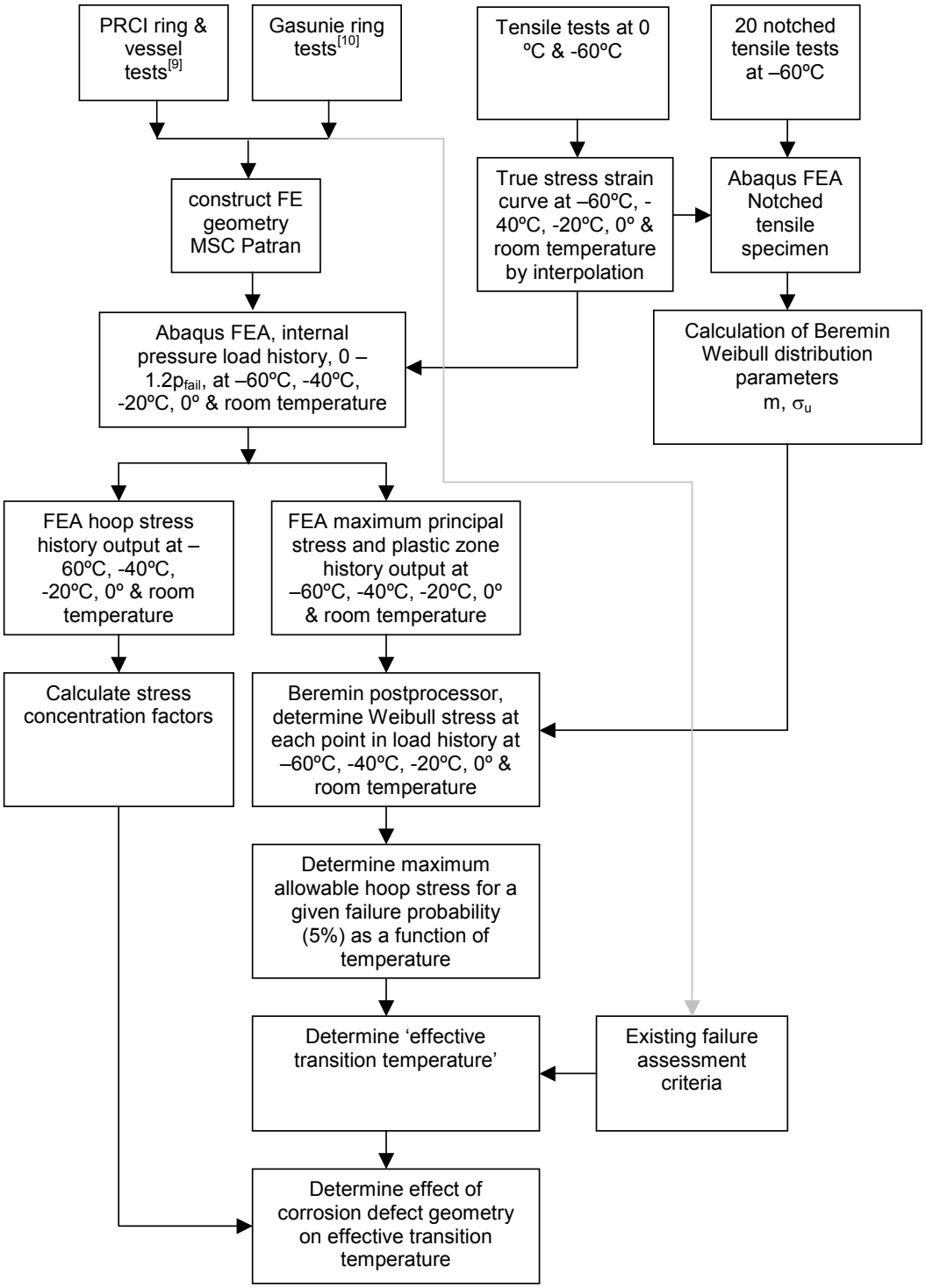
PRCI ring & vessel tests[9]
Gasunie ring tests[10]
Tensile tests at 0 ºC & -60ºC
20 notched tensile tests at –60ºC
construct FE geometry MSC Patran
True stress strain curve at –60ºC, -40ºC, -20ºC, 0º & room temperature by interpolation
Abaqus FEA Notched tensile specimen
Abaqus FEA, internal pressure load history, 0 – 1.2p_fail, at –60ºC, -40ºC, -20ºC, 0º & room temperature
Calculation of Beremin Weibull distribution parameters m, σ_u
FEA hoop stress history output at –60ºC, -40ºC, -20ºC, 0º & room temperature
FEA maximum principal stress and plastic zone history output at –60ºC, -40ºC, -20ºC, 0º & room temperature
Calculate stress concentration factors
Beremin postprocessor, determine Weibull stress at each point in load history at –60ºC, -40ºC, -20ºC, 0º & room temperature
Determine maximum allowable hoop stress for a given failure probability (5%) as a function of temperature
Determine 'effective transition temperature'
Existing failure assessment criteria
Determine effect of corrosion defect geometry on effective transition temperature

APPENDIX H THE MODIFIED ASME B31G AND LPC-1 METHODS

The Modified ASME B31G Method

The Modified ASME B31G (0.85dL) failure equation is defined by Equation B2 and Equation B3 where, $\bar{\sigma} = \sigma_{smys} + 10{,}000$ (units: lb/in^2). As the material grades were unknown in the present project, the measured values of yield strength have been used.

$$P_f = \frac{2\bar{\sigma}}{\left(\frac{D}{t}\right)}\left[\frac{1-0.85\left(\frac{d}{t}\right)}{1-0.85\left(\frac{d}{t}\right)\frac{1}{\sqrt{1+0.6275\left(\frac{L}{\sqrt{Dt}}\right)^2-0.003375\left(\frac{L}{\sqrt{Dt}}\right)^4}}}\right] \qquad \text{(B2)}$$

$$\text{for } \left(\frac{d}{t}\right) \le 0.8\,;\ \frac{L}{\sqrt{Dt}} \le 7.071$$

$$P_f = \frac{2\bar{\sigma}}{\left(\frac{D}{t}\right)}\left[\frac{1-0.85\left(\frac{d}{t}\right)}{1-0.85\left(\frac{d}{t}\right)\frac{1}{\left[3.3+0.032\left(\frac{L}{\sqrt{Dt}}\right)^2\right]}}\right] \qquad \text{for } \left(\frac{d}{t}\right) \le 0.8\,;\ \frac{L}{\sqrt{Dt}} > 7.071 \qquad \text{(B3)}$$

In the case of ring expansion defects, the length is effectively set to infinity and Equation B2 reduces to Equation B4. However, it should be noted that use of the Modified ASME B31G method for infinitely long corrosion defects is inappropriate, see Advantica Report 6781, Issue 6.0.

$$P_f = \frac{2\bar{\sigma}}{\left(\frac{D}{t}\right)}\left(1-0.85\left(\frac{d}{t}\right)\right) \qquad \text{(B4)}$$

LPC-1 Method

The LPC-1 failure equation is defined by Equation B4 where $\bar{\sigma} = \sigma_{smts}$. As the material grades were unknown, the measured values of ultimate tensile strength have been used and f has been set to 0.9.

$$P_f = \frac{2f\bar{\sigma}}{\left(\frac{D}{t}-1\right)}\left[\frac{1-\left(\frac{d}{t}\right)}{1-\left(\frac{d}{t}\right)\frac{1}{\sqrt{1+0.31\left(\frac{L}{\sqrt{Dt}}\right)^2}}}\right] \qquad \text{for } \left(\frac{d}{t}\right) \le 0.85\text{; all lengths} \qquad \text{(B5)}$$

In the case of ring expansion defects, the length is effectively set to infinity and Equation B5 reduces to Equation B6.

$$P_f = \frac{2f\bar{\sigma}}{\left(\frac{D}{t}-1\right)}\left(1-\left(\frac{d}{t}\right)\right) \qquad \text{(B6)}$$

ID	Experiment		Mod ASME B31G		LPC-1	
	Failure Pressure (bar)	Failure Hoop Stress (N/mm^2)	Failure Pressure (bar)	Failure Hoop Stress (N/mm^2)	Failure Pressure (bar)	Failure Hoop Stress (N/mm^2)
HJK-R1	96.4	331.2	73.8	254.7	72.3	249.5
HJK-R2	89.9	307.8	76.8	261.7	75.7	258.2
HJK-R3	90.2	310.7	75.2	259.6	74.0	255.5
HJK-R4	71.9	247.4	57.5	198.0	52.0	179.1
HJK-R5	69.3	237.6	59.6	203.1	54.4	185.5
HJK-R6	67.1	231.2	56.4	194.3	50.7	174.6
HJK-R7	90.8	311.7	75.8	261.1	74.7	257.4
HJK-R8	94.3	321.6	76.8	261.7	75.7	258.2
HJK-R9	89.3	304.7	76.6	260.5	75.4	256.7
HJK-R10	79.7	274.3	59.3	204.6	54.3	187.4
HJK-R11	76.2	260.0	58.7	200.1	53.3	181.8

ID	Experiment		Mod ASME B31G		LPC-1	
HJK-R12	74.9	257.5	59.0	203.4	53.9	185.9
HJK-R13	97.1	334.6	75.4	260.2	74.3	256.2
HJK-R14	90.2	309.4	76.1	262.6	75.1	259.2
HJK-R15	87.3	301.4	76.0	261.7	74.9	258.1
HJK-R16	73.5	253.7	58.9	202.8	53.7	185.1
HJK-R17	69.9	239.8	58.6	199.8	53.2	181.4
HJK-R18	71.9	246.2	60.4	205.9	55.4	188.9
HJK-V1	89.5	285.2	85.3	285.8	89.4	299.5
HJK-V1 (modified)	NA	NA	98.9	331.5	106.3	356.3
HJK-V2	87.6	263.3	84.3	284.6	87.4	294.9
HJK-V2 (modified)	NA	NA	66.5	224.6	63.5	214.2
HKR-R1	109.0	253.0	83.8	203.7	80.9	196.9
HKR-R2	108.4	259.8	79.8	194.3	75.8	184.8
HKR-R3	108.9	256.5	82.4	198.3	78.9	190.0
HKR-R4	89.0	212.7	85.1	204.9	82.4	198.4
HKR-R5	125.2	294.9	96.6	222.6	96.0	221.3
HKR-R8	133.8	315.1	107.3	256.0	110.7	264.1
HKR-R9	80.6	187.1	74.2	170.3	67.2	154.2
HKR-R10	47.1	109.3	50.9	119.8	37.9	89.2
HLL-R7	159.7	377.8	106.5	252.0	109.5	259.0
HLL-R8	180.5	424.1	107.6	252.9	110.7	260.1
HLL-R9	117.7	276.0	85.3	200.0	82.0	192.3
HLL-R10	102.8	244.0	66.8	158.6	58.6	139.0
HLL-R3	81.6	193.1	56.1	132.6	44.6	105.7

Units

The analyses were carried out and have been reported in SI units, with the exception of pressures which are reported in bar. Conversion factors for the units used in this report are given below:

25.4 mm = 1 inch

1 N/mm^2 ≡ 1 MPa = 145.04 psi

1 N/mm^2 = 10 bar

1 °C = 5/9(°F-32)